The Thesis Committee for Afnan Alnahdi
Certifies that this is the approved version of the following Thesis:

Design of Single and Multi-Well Surfactant-Polymer EOR Tests in a Viscous Oil Reservoir

APPROVED BY
SUPERVISING COMMITTEE:

Kishore K. Mohanty, Supervisor

Matthew T. Balhoff

Design of Single and Multi-Well Surfactant-Polymer EOR Tests in a Viscous Oil Reservoir

by

Afnan Alnahdi

Thesis

Presented to the Faculty of the Graduate School of

The University of Texas at Austin

in Partial Fulfillment

of the Requirements

for the Degree of

Master of Science in Engineering

The University of Texas at Austin

August 2020

Dedication

To my loving family and parents, Sabah and Majdi, to my siblings, and to my friends.

Acknowledgements

I would like to express my genuine appreciation and gratitude to my advisor, Dr. Kishore Mohanty, for his guidance and patience throughout my graduate journey. He has been extremely generous with his time and advice. Every discussion with him has been an immensely enriching and insightful experience, and I am honored to work with him. I would also like to extend my gratitude to Dr. Matthew Balhoff, for his time and valuable feedback on my thesis.

Special thanks to Haishan Luo, for assisting me and always answering my questions. His help and feedback have been greatly valuable to my work. I would also like to thank Ali Goudarzi, for sharing with me his expertise in using UTCHEM software. Many thanks extended to my research group colleagues; Krishna Panthi, for his help with answering research questions and sharing his experimental coreflood data, and Haofeng Song, for also sharing his experimental work with me. Their collaboration was pivotal to my work.

I would also like to thank my sponsor, Saudi Aramco, for their extraordinary support to my education. Many thanks to Messmore Barb, Joanna Castillo and UT-PGE staff; Amy Stewart, Jessica Yeager and John Cassibry for their help.

Finally, I am particularly grateful to my family, especially my parents, whom I'll always be indebted to. Their endless support and encouragement motivate me to always do better.

Abstract

Design of Single and Multi-Well Surfactant-Polymer EOR Tests in a Viscous Oil Reservoir

Afnan Alnahdi, M.S.E

The University of Texas at Austin, 2020

Supervisor: Kishore K. Mohanty

Surfactant-polymer (SP) flooding is a well-established enhanced oil recovery (EOR) technique that has been extensively evaluated in the laboratory and field pilot scales. The efficacy of the SP process is manifested in its ability to combine the mechanisms of surfactant and polymer methods: mobilization of the discontinuous oil ganglia using surfactant and sweep enhancement of the polymer injection. Modeling of these advanced processes, with adequate upscaling from laboratory to pilot scale, is vital for field implementation design and success.

The objective of this work is to conduct a thorough design of field SP pilot tests in a highly viscous sandstone reservoir. The design starts from history matching coreflood experiments, followed by an upscaling to a single well test, an interwell tracer test and finally a multi-well SP pilot test. Using the numerical simulator CMG-STARS, the workflow begins with constructing and matching key physico-chemical parameters from 8 core floods. Then these parameters are used with the reservoir description to simulate

single-well chemical tracer test (SWCT), inter-well tracer test (IWTT) and multi-well SP pilot test. A sector model including 5-spot pattern was used in the pilot simulation studies. The design process of the tests entailed conducting several sensitivities pertaining to polymer type, concentration, SP slug size, well rates and injection production ratio (IPR), tracer concentrations and amounts, and pore volumes injected.

A successful history match was achieved with coreflood experiments. The developed surfactant and polymer models were then used in the SWCT, IWTT and SP pilot models. SP slug size and tracer push volume were the key parameters for the interpretation of SWCT. Injected tracer amount was the most fundamental variable in the design of the IWTT. Based on sensitivity results, design parameters were recommended for each test. To provide recovery-maximizing testing strategy for the SP pilot design, optimization of various parameters including IPR, SP slug size, and polymer concentration was used. As a result, an incremental recovery of 22% was achieved. If new information is acquired from field implemented IWTT, it can provide valuable information about the reservoir characteristics that could further augment the SP pilot design.

Table of Contents

List of Tables

List of Figures

Chapter 1: Introduction

1.1 Research Objective

Despite the recent emergence of renewable energy, oil demand and supply of energy has been unwavering. To meet the demand, enhanced oil recovery EOR processes are deemed necessary, especially to maintain reserves and compensate the declining recovery from maturing fields. A typical ultimate recovery from a reservoir that has undergone primary and secondary recovery is 35% (Lake *et al.,* 2014). That is, 65% of the original oil is left behind, which is an enormous potential. Among the different EOR methods, the chemical methods may be the best candidate to exploit the remaining oil due to their proven efficiency and versatility, as well as feasibility and cost (Gbadamosi *et al.,* 2019). The efforts in assessing chemical enhanced oil recovery (cEOR) processes have been longstanding, the interest of cEOR have thrived during the 1980s due to the high oil prices and technical progress (Gbadamosi *et al.,* 2019).

Chemical flooding, especially surfactant-polymer (SP) flooding which is the subject of this work, involves the injection of a surfactant to mobilize the trapped oil coupled with polymer injection for mobility control. The goal of SP is to capitalize on the different mechanisms of surfactant and polymer methods and combine them for better recovery. The mechanisms comprise of IFT reduction by surfactant and mobility ratio modification by increasing the viscosity with the use of polymer and altering relative permeabilities.

The advanced processes and mechanisms of the chemical methods necessitated the development of advanced simulators to capture the various physiochemical processes and interactions. UTCHEM, developed by The University of Texas, and CMG-STARS, developed by the Computer Modeling Group are two of the widely used software for

modeling chemical flooding. Both of these are discussed herein, but mainly CMG-STARS. This work highlights the holistic design process of SP flood pilot starting from history matching the corefloods experiments for a viscous oil sandstone reservoir. The objective of this work is to capture the physico-chemical parameters by firstly matching the coreflood, and then evaluate different scenarios and parameter sensitivities to provide design recommendation for a single well chemical test SWCT, interwell tracer test IWTT, and finally SP pilot test.

1.2 CHAPTERS DESCRIPTIONS

This thesis is comprised of 6 chapters. Chapter 2 provides background and literature review of mechanisms of surfactant, polymer and SP flooding, and it also discusses the models of SP flood available in UTCHEM and CMG-STARS. Chapter 3 presents the data preparation and conversion from lab to model and discusses the history matching process of the corefloods. Chapter 4 introduces the single well chemical test and presents the simulation studies for the design of the test. Chapter 5 provides an introduction and brief literature review of the interwell tracer test including residence time distribution RTD analysis, and presents simulation studies and results for the IWTT, followed by simulation sensitivity and results for the design of the SP pilot. Chapter 6 highlights the main findings of the simulation studies conducted on the SWCT, IWTT and SP pilot and thereby provide design recommendations.

Chapter 2: Literature Review

In this chapter the literature relevant to chemical EOR is discussed.

2.1 BACKGROUND

2.1.1 Polymer Methods

The sole objective of polymer flooding is to provide better volumetric sweep efficiencies than conventional waterflooding. During waterflooding, oil can be left behind for two reasons: trapped oil due to capillary forces, creating residual oil saturation, or bypassed oil as a result of unfavorable mobility ratio and heterogeneity (large scale layering and large-scale sand channeling). Polymer methods emerged as a remedy for the inefficiency of water flooding, as they can provide better mobility control to water and reduce the amount of bypassed oil. A better mobility control requires mobility ratio (M) enhancement. Better mobility ratio (defined shortly) could be achieved by increasing the water viscosity and reducing aqueous phase permeability. Polymers can increase the solution viscosity 2-20 times with concentrations of only few hundred parts per million or ppm (Sorbie, 1991). On the other hand, the effect of permeability reduction on mobility ratio is less substantial than viscosity increase in the case of high permeability formations (Lake *et al*., 2014).The mobility ratio is defined as the ratio of the mobility of the displacing fluid to the mobility of the displaced fluid (Craig, 1971), i.e.,

$$M = \frac{\lambda_{displacing}}{\lambda_{displaced}} = \frac{k_{displacing} * \mu_{displaced}}{k_{displaced} * \mu_{displacing}} \qquad (2.1.1)$$

where λ is mobility, k is permeability and μ is the viscosity. The mobility ratio is a critical factor that determines the stability of the displacement process. For a mobility ratio of M>1, the flow becomes unstable; viscous fingers of water grow and bypass a lot of oil. As areal

and vertical sweeps decrease with higher mobility ratios (Green and Willhite, 2018), a mobility ratio less than unity is desired.

Polymer floods cause crossflow due to vertical permeability contrast in layered reservoirs. In the case of polymer injection, the zone behind the polymer slug exhibits higher pressures (in higher permeability layers because the polymer flows through them first), the pressure difference induces some polymer flow from high permeability to low permeability layers, while vice versa for the oil flow ahead of the slug. This happens only when we assume there are no vertical barriers between the layers. Therefore, polymer flooding plays a critical role in mitigating heterogeneities (Sorbie, 1991).

The forces that govern the fluid flow in porous medium are the pressure gradient exerted by the displacing phase, buoyancy force, and capillary pressure force. To displace residual oil, the viscous to capillary forces ratio needs to be modified, this ratio is represented by a dimensionless quantity defined as the capillary number (N_c). Moore and Slobod (1956) and other authors recognized the relationship between oil mobilization and the ratio of viscous to capillary forces, this ratio defined as the capillary number (Stegemeier, 1976; Chatzis and Morrow, 1984; Pope *et al.*, 2000):

$$N_C = \frac{k\Delta P}{\sigma L} \tag{2.1.2}$$

where k is the permeability, σ the interfacial tension between displacing and displaced fluids, and $\frac{\Delta P}{L}$ is the pressure gradient exerted by the displacing phase. Trapping number (N_T) is a general form of capillary number that includes pressure gradient, buoyancy and capillary pressure, defined as (Jin, 1995):

$$N_T = \frac{|\,\vec{\vec{k}}(\vec{\nabla}\Phi + g(\rho_{\ell'} - \rho_{\ell})\vec{\nabla}D)|}{\sigma_{\ell'\ell}} \tag{2.1.3}$$

where $\nabla\Phi$ is the flow potential gradient, g is gravity acceleration, ρ_ℓ, $and\ \rho_\ell$ are the densities of the displacing and displaced fluids, respectively, and D is the depth. When buoyancy forces are ignored, different forms of capillary number are available in literature; when Darcy's law is used to convert the pressure gradient to velocity, it yields to the following simpler definition (Foster, 1973; Du Prey, 1973, Erlich *et al.*, 1974, Lake *et al.,* 2014):

$$N_C = \frac{u\,\mu}{\sigma} \tag{2.1.4}$$

where u is the Darcy's velocity. A typical value of N_c in water flood is in the order of 10^{-6}, in order to mobilize the oil, this number must be increased by several orders of magnitude, a typical polymer flood achieves up to one order of magnitude increase in N_c which is not sufficient in displacing the oil. Therefore, comes the notion of polymer inability to reduce the residual oil saturation alone unless accompanied by interfacial tension altering agents such as surfactants. However, recent studies on viscoelastic polymers showed that polymers can reduce the residual oil saturation (Huh and Pope 2008; Sheng 2011, Qi *et al.*, 2017); nevertheless, a comprehensive understanding of the mechanism of viscoelastic polymers is not yet established.

2.1.2 Surfactant Methods

The surfactant, or the surface-active agent, has two different functional groups; the head, which exhibits great affinity to water (hydrophilic) and the hydrocarbon tail, which does not show affinity to water (hydrophobic). The amphiphilic nature of the surfactant allows it to be present at the oil-water interface interacting with some of the oil and water molecules (Rosen, 1978). Surfactants can be classified into four categories based on their ionic nature: anionic, nonionic, cationic and zwitterionic (Ottewill, 1984). The two most used types in EOR applications are the anionic and nonionic surfactants; the anionic

surfactant is primarily used because it exhibits favorable properties such as low adsorption (on sandstones) and stability. The cationic surfactants are not favorable because of their high adsorption to the rock surface due to their charge. The nonionic surfactants are generally used as cosurfactants as they have good tolerability to salinity because they are not charged, but they often do not reduce the IFT as effectively as anionic surfactants (Green and Willhite, 2018). The surfactant used in the work of this thesis is of a nonionic nature.

Surfactant/oil/brine solutions are greatly affected by the salinity of the brine, surfactant type, concentration, hydrocarbon properties and temperature. Understanding microemulsion phase behavior is the first crucial step in designing surfactant EOR applications. A microemulsion is "a stable, translucent micellar solution of oil, water that may contain electrolytes, and one or more amphiphilic compounds" (Healy and Reed, 1974, Introduction, para.2). At low salinity, the system separates into excess oil phase and water-external microemulsion phase that contains the water, surfactant and some solubilized oil, this phase environment is referred to as Winsor type I (Winsor, 1954) or type II (-) (Nelson and Pope, 1978). At high salinity, the systems separate into water excess phase and oil-external microemulsion phase that contains oil, surfactant and some solubilized water, this phase environment is referred to as Winsor type II or type II (+). At some intermediate salinity range, the systems separate into an excess oil phase, excess water phase and middle phase microemulsion. **Figure 2-1** shows the three types of microemulsion phases. The phase environment of the system described in this thesis is Winsor type I.

The mechanisms of oil recovery in surfactant flooding can be categorized based on their impact on the following: fractional flow and phase behavior (Larson *et al.,*1982). The fractional flow is affected by IFT reduction and wettability alterations. The amphiphilic

nature of the surfactant allows it to adsorb to the oil-water interface interacting with some of the oil and water molecules, such that the hydrophilic head is oriented towards the water and the tail towards the oil, resulting in a significant reduction in the interfacial tension. As discussed in section 2.1.1, increasing the capillary number by orders of magnitude and exceeding the critical capillary number can reduce the residual oil saturation. Achieving significant increase in the capillary number is relatively easier by weakening the capillary force (IFT) as compared to increasing the viscous force (pressure gradient). As the IFT is reduced, the capillary forces acting on the trapped oil are weekend allowing the mobilization of the oil. This mobilization of oil impacts the relative permeability curves of the fractional flow, resulting in higher fractional flow of oil (ratio of volumetric flow rate of oil to total volumetric flow rate). A desired IFT is in the order of 10^{-3} mN/m (Lake *et al.,* 2014) referred to as optimal IFT that is present in optimal salinity conditions. To elaborate on the meaning of optimal, it is important to address solubilization ratios: in Winsor type I and type III microemulsion phases, the oil solubilization ratio is defined as the volume of oil to the volume of surfactant in that phase:

$$S_{oil/me} = \frac{C_{oil/me}}{C_{surf/me}} \tag{2.1.5}$$

Similarly, for type II and type III microemulsion phases, the water solubilization ratio is defined as:

$$S_{surf/me} = \frac{C_{water/me}}{C_{surf/me}} \tag{2.1.6}$$

Huh (1979) introduced IFT equation as a function of solubilization ratios:

$$\sigma_{i/me} = \frac{0.3}{S_{i/me}{}^{2}} \tag{2.1.7}$$

where *i* represents the respective phase. There is a particular salinity where both IFT values (between *i* phase and microemulsion phase) are equal; this salinity is referred to as optimal salinity. Other authors define optimal salinities in terms of equal

solubilization ratios (Healy *et al.*, 1976) or equal contact angles (Reed and Healy, 1984). However, all three definitions yield similar results (Lake *et al.*, 2014).

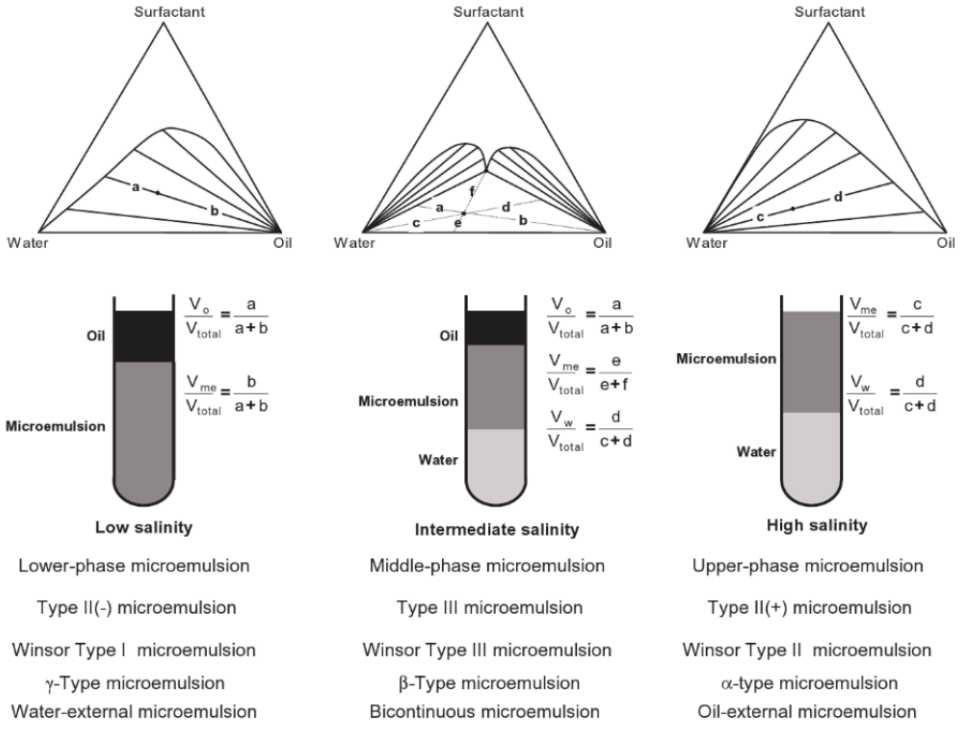

Figure 2-1: Schematic Representation of The Three Phase Systems (Sheng, 2013)

Wettability alteration is another mechanism of oil recovery. During wettability alteration, the oil is driven out of the matrix by spontaneous imbibition of water, consequently changing the wettability from oil wet to water or mixed wet. Mixed wettability conditions might be favorable as data showed that maximum recovery was obtained at these conditions (Lorenz *et al.,* 1974). Changing the wettability can entail fluids redistribution from small pores to large pores and vice versa (Lake *et al.,* 2014). This redistribution affects the relative permeabilities and hence the fractional flow. Since our work investigates a water-wet sandstone, wettability reversal is not considered.

Oil solubilization and swelling are also mechanisms that are related to the phase behavior. The solubilization of oil in the microemulsion causes mobilization of the dissolved oil. The water solubilized in microemulsion phase in type II causes oil swelling by reducing the amount of oil that may be entrapped in the pore space (Larson *et al.,*1982). Several more investigations on surfactant mechanisms are discussed in literature (Hirasaki *et al.,* 2011), and they may be beyond the scope of the work discussed in this thesis. However, the main mechanism that are of interest to our work are the reduction of IFT and to a lesser degree, oil solubilization.

2.1.3 Surfactant Polymer (SP) Flood

The combination of polymer and surfactant can yield to an even better oil recovery. The goal of using surfactant is to mobilize discontinuous oil ganglia; the coalescence of detrapped oil drops result in what is referred to as an oil bank. However, surfactant alone is not efficient without a good mobility control and is therefore less likely to be injected alone (Sheng, 2013). Unstable floods coupled with heterogeneity can cause fingering, early chemical/water breakthroughs, and emulsions production, resulting in poor sweep and recovery. In order to have a stable displacement, the oil bank should move faster than the chemical slug front; the mobility of the oil bank must be higher than or equal to the mobility of the SP flood. Thus, the viscosity of the chemical solution is supposed to be higher than the viscosity of the oil to offset the effect of the increased relative permeability of water. That is because when IFT is lowered by surfactant, N_c increases, which consequently increases the relative permeabilities. Therefore, the use of polymer to increase viscosity yields a stable oil bank.

2.1.4 Chemical Flood Simulation

With the rising interest in enhanced oil recovery applications, several simulators have been developed in the industry to model the advanced processes like chemical floods. The capabilities of these simulators have improved over the years to capture various physiochemical mechanisms, and model the phase behavior changes of micellar fluids, including multi-phase and multi-components variations and transport in heterogeneous porous media and properties.

Numerous chemical flood simulators are available commercially including Computer Modeling Group (CMG) software, and UTCHEM, developed at The University of Texas. The above-mentioned software will be the focus of the upcoming two sections; the coreflood matching was initially constructed using UTCHEM due to its availability and industry's utilization in SP flooding. As the field's model constructed by the operator company was provided in CMG, it was decided to switch to CMG for convenience and consistency. For the sake of brevity, the review in the next sections will focus on the description of the polymer and surfactant models.

2.2 UTCHEM OVERVIEW

UTCHEM is a compositional, multi-component, three-dimensional, 4 phase (aqueous, oleic, microemulsion, gas) simulator. It was first developed by Pope and Nelson in 1978 for one-dimensional and homogeneous system and captured the complex changes of phase behavior and interfacial tension in correlation with surfactant concentration, salinity, and solubilization ratio. It also modeled the changes of polymer viscosity due to the polymer concentration and solution salinity. Other significant physiochemical interactions such as cation exchange and adsorption were also included (Pope and Nelson, 1978; UTCHEM Technical Documentation, 2019). Bhuyan *et al.* in 1990 presented more

general numerical simulation that incorporated other geochemical reactions pertaining to alkaline and micellar-polymer flooding (Bhuyan *et al.*, 1990). UTCHEM also has the ability to model wettability alteration, relative permeability changes with trapping number, biological reactions, tracers, molecular diffusion and others.

2.2.1 Modeling of Polymer:

2.2.1.1 Electrolytes and Polymer Concentration dependence on Polymer Viscosity

UTCHEM models polymer viscosity at low shear rate as a function of polymer concentration, salinity and hardness using Flory-Huggins equation (Flory, 1953):

$$\mu_p^0 = \mu_w(1 + \left(A_{p1}C_{4\ell} + A_{p2}C_{4\ell}^2 + A_{p3}\, C_{4\ell}^3\right)C_{SEP}^{sp} \qquad (2.2.1)$$

where μ_w is the water viscosity, $C_{4\ell}$ is the concentration of polymer in the aqueous phase, A_{p1-3} are the model matching parameters, sp is a model parameter that reflects the salinity dependence of polymer; it is the slope of the normalized polymer viscosity $\frac{(\mu_p - \mu_w)}{\mu_w}$vs. salinity on a log-log scale, C_{SEP} is the effective salinity of the polymer given by the following:

$$C_{SEP} = \frac{C_{anion} + \left(\beta_p - 1\right)C_{divalent_{cation}}}{C_{water}} \qquad (2.2.2)$$

where $C_{anion}, C_{divalent_{cation}}, C_{water}$ are the concentrations of monovalent anions, calcium and water in the aqueous phase, respectively. β_p is an input parameter that reflects the effect of calcium and it is measured in the laboratory.

2.2.1.2 Polymer Rheology

UTCHEM models the dependence of shear rate on viscosity using Carreau's model and Meter's equation. Meter equation is as shown below (Meter and Bird, 1964):

$$\mu_p = \mu_w + \frac{\mu_p^0 - \mu_w}{1 + \left(\frac{\dot{\gamma_{eq}}}{\dot{\gamma}_{\frac{1}{2}}}\right)^{P_\alpha - 1}} \tag{2.2.3}$$

Where $\dot{\gamma}_{\frac{1}{2}}$ is the half shear rate; viscosity equals the average of μ_w and μ_p^0 at low shear rates. P_α and $\dot{\gamma}_{\frac{1}{2}}$ are input matching parameters, $\dot{\gamma_{eq}}$ is the equivalent shear rate and is modeled by the modified Blake-Kozeny capillary bundle equation (Lin, 1981; Sorbie, 1991):

$$\dot{\gamma_{eq}} = \frac{\dot{\gamma_c}|u_\ell|}{\sqrt{\bar{k}\, k_{r\ell}\phi\, S_\ell}} \tag{2.2.4}$$

Where $\dot{\gamma_c}$ is equal to 3.97 C and it is a coefficient that represents the non-ideal effects such as pore walls. A Typical value for C is 6 (Cannella et al., 1988).

UTCHEM offers another option that utilizes a recently developed unified viscosity model UVM which incorporates the Newtonian, shear thinning and shear thickening behaviors of polymers in porous media (Delshad *et al.*, 2008). The apparent polymer viscosity consists of two parts: shear-viscosity-dominant part and elongational-viscosity-dominant part:

$$\mu_{app} = \mu_{shear} + \mu_{elongational} \tag{2.2.5}$$

Carreau's model is used to calculate the shear thinning viscosity:

$$\mu_{shear} = \mu_w + \mu_p^0 - \mu_w \left[1 + \left(\dot{\lambda}_{eff}\right)^2\right]^{\frac{n_1 - 1}{2}} \tag{2.2.6}$$

Where μ_p^0 is the polymer viscosity at low shear rate and is calculated using Flory-Huggins equation in **Eqn. 2.2.1**. n_1 is UVM parameter for shear thinning, and λ is a calculated parameter related to the polymer concentration:

$$\lambda = \beta_1 \exp\left(\beta_2 C_p\right) \tag{2.2.7}$$

β_{1-2} are model input parameters measured in the laboratory. The shear thickening behavior is calculated as follows:

$$\mu_{elongational} = \mu_{max} + \left\{1 - \exp\left[-\left(\lambda_2 \tau \dot{\gamma}_{eff}\right)^{n_2 - 1}\right]\right\} \quad (2.2.8)$$

n_2 is UVM parameter for shear thinning μ_{max} viscosity is calculated based on empirical laboratory findings:

$$\mu_{max} = \mu_w\left(AP_{11} + AP_{22} ln C_p\right) \quad (2.2.9)$$

$$\tau = \tau_0 + \tau_1 C_p \quad (2.2.10)$$

Where AP_{11} , AP_{22}, τ_0 , $\tau_1$are shear thickening model input parameters obtained by viscosity measurements, and τ is the relaxation time. $\dot{\gamma}_{eff}$ is in-situ shear rate, and is calculated as the following for a single-phase flow (Cannella *et al.*, 1988)

$$\dot{\gamma}_{eff} = C\left(\frac{3n+1}{4n}\right)^{\frac{n}{n-1}} \frac{4\,|\overrightarrow{u_w}|}{\sqrt{8\bar{k}\phi}} \quad (2.2.11)$$

Where μ is the Darcy velocity (q/A), *n* is determined from the slope of the linear portion of a log-log plot of the polymer viscosity vs. shear rate. *C* is the shear rate correction factor that reflects the non-ideal effects and it depends on the porosity and the permeability. The correlation was extended to incorporate multi-phase flow effects by representing the equation in terms of relative permeability instead of absolute value:

$$\dot{\gamma}_{eff} = C\left(\frac{3n+1}{4n}\right)^{\frac{n}{n-1}} \frac{4\,|\overrightarrow{u_w}|}{\sqrt{8\bar{k}k_{rw}\phi S_w}} \quad (2.2.12)$$

2.2.1.3 Polymer Adsorption

UTCHEM uses Langmuir-type isotherm to model polymer adsorption, and describes the adsorption as a function of concentration, permeability and salinity. The polymer can adsorb by two mechanisms: trapping in small pores and adsorbing on the solid surface:

$$\widehat{C_4} = \min\left(\widetilde{C_4}, \frac{a_4\left(\widetilde{C_4} - \widehat{C_4}\right)}{1 + b_4\left(\widetilde{C_4} - \widehat{C_4}\right)}\right) \quad (2.2.13)$$

Where $\widehat{C_4}$ is the adsorbed polymer concentration, $\widetilde{C_4}$ is the overall polymer concentration in mobile and stationary phases, the concentrations are normalized by the water concentration, and a_4 and b_4 are polymer adsorption parameters. The minimum concentration is taken so that the adsorbed polymer does not exceed the total polymer concentration. The permeability impact on adsorption is demonstrated as follows:

$$a_4 = (a_{41} + a_{42}C_{SEP})\left(\frac{k_{ref}}{k}\right)^{0.5} \tag{2.2.14}$$

Where k_{ref} is the reference permeability at which the adsorption measurement took place. C_{SEP} is the effective salinity described by **Eqn. 2.2.2** a_{41} and a_{42} are input matching parameters, that could be used to match the laboratory measurement data.

2.2.1.4 Permeability Reduction

Adsorbed polymer reduces the brine permeability, coupled with increase viscosity of polymeric solution, the mobility ratio is reduced. The impact of this is reflected by the resistance factor R_{F}, which is a measure of mobility reduction due to polymer injection.

$$R_F = \frac{\lambda_w}{\lambda_p} = \frac{\frac{k_w}{\mu_w}}{\frac{k_p}{\mu_p}} \tag{2.2.15}$$

The ratio k_w/k_p represents the reduction of effective permeability to brine to that of polymer, the ratio is denoted by R_{k} .The residual resistance factor R_{RF} is the ratio of mobility before and after polymer injection. So, it reflects the lastingness of the permeability reduction including after the polymer injection has stopped, and after the polymer has passed through the porous media . UTCHEM models the permeability reduction as the following, and is assumed to be irreversible:

$$R_k = 1 + \frac{\left(R_{k_{max}} - 1\right)b_{rk}C_{4\ell}}{1 + b_{rk}C_{4\ell}} \tag{2.2.16}$$

Where $R_{\mathrm{k_{max}}}$

$$R_{kmax} = \min\left\{\left[1 - \frac{c_{rk}\left(A_{P1}C_{SEP}^{sp}\right)^{\frac{1}{3}}}{\left(\frac{\sqrt{k_x k_y}}{\phi}\right)^{\frac{1}{2}}}\right], 10\right\} \quad (2.2.17)$$

Where b_{rk}, c_{rk} , A_{P1} are input parameters

2.2.1.5 Inaccessible Pore Volume

The large molecular weight of polymers hinders it from passing through smaller pores, causing a reduction in porosity. This phenomenon is modeled in UTCHEM by multiplying the porosity by effective pore volume of polymer:

$$IPV = \phi_{polymer} * PV \quad (2.2.18)$$

where

$$\phi_{polymer} = \phi * \frac{apparent\ porosity\ for\ polymer}{actual\ porosity} \quad (2.2.19)$$

2.2.2 Modeling of Surfactant:

2.2.2.1 Phase Behavior and Binodal Curve

Description of the binodal curve and tie lines is required to represent the phase behavior of the solution of surfactant/oil/water with respect to salinity. The phase behavior model in UTCHEM uses Hand's rule [Hand,1939] and is based on the work by Pope and Nelson [1978], Prouvost *et al*. [1984; 1985; 1986], Satoh [1984], and Camilleri *et al.* [1987a, 1987b, 1987c]. The following equations are used in the UTCHEM simulator:

- **Hand's Model:**

The formulation of the binodal curve using Hand's rule is assumed to be the same in all phase environments:

$$\frac{C_{3l}}{C_{2l}} = A\left(\frac{C_{3l}}{C_{1l}}\right)^{B} \quad (2.2.20)$$

Where *A*, *B* are empirical parameters, the current formulation in UTCHEM uses *B* = -1, representing a symmetrical binodal curve. The subscripts 1,2 and 3 refer to water, oil, and surfactant, respectively. Given that the minimum and maximum salinity for type III systems are measured in the lab and added as an input, parameter *A* related to height of binodal curve is estimated as follows:

$$A_m = \left(\frac{2C_{3max,m}}{1 - C_{3max,m}} \right)^2 \tag{2.2.21}$$

Where m =0,1 and 2 represent low, optimal and high salinity respectively, therefore A_0, A_1 ,A_2 are estimated.

- Maximum Height of Binodal Curve:

$$C_{3Max} = \frac{\sqrt{A_0}}{2+\sqrt{A_0}} \qquad at\ C_{SE} = 0$$

$$C_{3Max} = \frac{\sqrt{A_1}}{2+\sqrt{A_1}} \qquad at\ C_{SE} = 1$$

$$C_{3Max} = \frac{\sqrt{A_2}}{2+\sqrt{A_2}} \qquad at\ C_{SE} = 2$$

Where C_{SE} = effective salinity

- **Salinity Effect:**

A is then calculated, depending on the phase environment. For Type II- ($C_{SE} < C_{SEOP}$) where C_{SEOP} = the optimum effective salinity and, and is linearly interpolated as:

$$A = (A_0 - A_1)\left(1 - \frac{C_{SE}}{C_{SEOP}}\right) + A_1 \tag{2.2.22}$$

And for Type II+ ($C_{SE} > C_{SEOP}$)

$$A = (A_2 - A_1)\left(\frac{C_{SE}}{C_{SEOP}} - 1\right) + A_1 \tag{2.2.23}$$

- **Phase Composition:**

After *A* is calculated, surfactant concentration is calculated at different oil concentrations. Depending on phase environment, the solution of Hand's equation (for type II- and type II +):

$$C_{33} = \frac{1}{2}(-A\ C_{23} + \sqrt{(A\ C_{23})^2 + 4\ A\ C_{23}\ (1 - C_{23})} \quad (2.2.24)$$

$$C_{13} = 1 - C_{23} - C_{33} \quad (2.2.25)$$

Solution of Hand 's equation (for type III), where *M* refers to the invariant point, the phase compositions of type III are:

$$C_{3M} = \frac{1}{2}(-A\ C_{2M} + \sqrt{(A\ C_{2M})^2 + 4\ A\ C_{2M}\ (1 - C_{2M})} \quad (2.2.26)$$

$$C_{2M} = \frac{2\ a\ (4 - A) - \sqrt{[2\ a\ (4 - A) + A]^2 - 16\ a^2(4 - A)}}{2(4 - A)} \quad (2.2.27)$$

$$C_{1M} = 1 - C_{2M} - C_{3M} \quad (2.2.28)$$

Where the coordinates of invariant point (*M*) are calculated as a function of effective salinity, where C_{SEL} = lower effective salinity limit, C_{SEU}= upper effective salinity limit:

$$a = \frac{C_{SE} - C_{SEL}}{C_{SEU} - C_{SEL}} \quad (2.2.29)$$

$$Cos60^0 = \frac{a - C_{2M}}{C_{3M}} \quad (2.2.30)$$

- **Effective Salinity Model:**

$$C_{SE} = \frac{C_{51}}{(1 - \beta_6 F_6^S)(1 + \beta_7 F_7^S\ )\big(1 + \beta_T (T - T_o)\big)} \quad (2.2.31)$$

where $\beta_6, \beta_7\ , and\ \beta_T$ are input parameters and are related to effect of divalent cations (i.e. calcium and magnesium), cosolvent-alcohol, and temperature respectively, F_6 is fraction of total cations bound to surfactant micelles , F_7:

$$F_7 = \frac{total\ volume\ of\ alchohol\ associated\ with\ surfactant}{total\ volume\ of\ surfactatn\ psuedocomponent} \quad (2.2.32)$$

2.2.2.2 Interfacial Tension IFT

Depending on the user's preference, either Healy and Reed's (1974) or Huh's (1979) correlations will be used. As for Healy and Reed's, the interfacial tension can be calculated with respect to solubilization parameters once the phase compositions are

known. Similarly for Huh's, the interfacial tension is related to solubilization ratio in Chun-Huh's equation.

Chun Huh equation:

$$\sigma_{\ell 3} = \frac{c}{{R_{\ell 3}}^2} \quad for\ \ell = 1{,}2 \tag{2.2.33}$$

where c is typically 0.3, and subscript 3 refers to the microemulsion phase. The Hirasaki (1981) modification, F_ℓ is introduced to Huh's:

$$\sigma_{\ell 3} = \sigma_{ow} e^{-aR_{\ell 3}} + \frac{F_\ell c}{{R_{\ell 3}}^2}\left(1 - e^{\left(-a{R_{\ell 3}}^3\right)}\right) \tag{2.2.34}$$

where a is a constant that is approximately equal to 10, and F_ℓ is defined as:

$$F_\ell = \frac{1 - e^{-\sqrt{con_\ell}}}{e^{-\sqrt{2}}} for\ \ell = 1{,}2 \tag{2.2.35}$$

2.2.2.3 Microemulsion ME Viscosity

UTCHEM uses three models to model the microemulsion viscosities: an original model used by UTCHEM, Dashti and Delshad model (Dashti, 2014), and Tagavifar and Pope model (Tagavifar, 2014; Tagavifar *et al.*, 2016). The original model calculates the microemulsion viscosity as a function of composition and liquid phase viscosities. The Dashti and Delshad model calculates the microemulsion viscosity as a function of salinity, where the model is not continuous across the three phase environments. Rather, a correlation is constructed for each phase type using the salinity boundaries for type III phase. Tagavifar and Pope model incorporates the dependence of shear rate on microemulsion viscosity.

Briefly, only show the original model is shown as follows:

$$\mu_3 = C_{13}\mu_w e^{\alpha_1(C_{23}+C_{33})} + C_{23}\mu_o e^{\alpha_2(C_{13}+C_{33})} + C_{33}\alpha_3 e^{(\alpha_4 C_{13}+\alpha_5 C_{23})} \tag{2.2.36}$$

Where μ_w and μ_o are water and oil phase viscosities, respectively, and the water viscosity is replaced by polymer viscosity in the presence of polymer. And α are input parameters determined by matching the lab viscosity measurements at different compositions.

2.2.2.4 Surfactant Adsorption

Similarly as used in polymer adsorption, Langmuir-type isotherm is used to model surfactant adsorption, and it describes the adsorption as a function of concentration, permeability and salinity, and $\widehat{C_3}$ is the adsorbed surfactant concentration, $\widetilde{C_3}$ is the overall surfactant concentration in mobile and stationary phases:

$$\widehat{C_3} = \min\left(\widetilde{C_3}, \frac{a_3\left(\widetilde{C_3} - \widehat{C_3}\right)}{1 + b_3\left(\widetilde{C_3} - \widehat{C_3}\right)}\right) \tag{2.2.37}$$

$$a_3 = (a_{31} + a_{32}C_{SEP})\left(\frac{k_{ref}}{k}\right)^{0.5} \tag{2.2.38}$$

2.3 CMG OVERVIEW

CMG-STARS is a three phase, multi-component, 3-dimensional and compositional advanced chemical simulator developed by the Computer Modeling Group. It is one of the most widely used simulators for chemical and thermal processes. CMG-STARS has the capabilities of modeling various processes of thermal recovery, chemical flooding, geomechanics, solid migration and others. Its many features include user-defined flexible components in any fluid or non-fluid phase, user defined chemical reactions, phase equilibrium functions. CMG-STARS can model polymer flood, effect of salinity on polymer viscosity, adsorption, retention, capillary number, IFT reduction, permeability reduction, dispersion and diffusion, inaccessible pore volume, geochemical reaction i.e. hydrolysis and other related phenomena. CMG-STARS does not include a distinct

microemulsion ME phase similar to UTCHEM but modeling ME is available in CMG-GEM component simulator (CMG-STARS Manual, 2019)

2.3.1 Modeling of Polymer:

2.3.1.1 Electrolytes and Polymer Concentration dependence on Polymer Viscosity

CMG-STARS models the salinity effect for polymer solution as the following:

$$\mu_p = \mu_p^0 \left(\frac{X_{salt}}{X_{\min}} \right)^{sp} \quad for\ X_{salt} > X_{min} \tag{2.3.1}$$

$$\mu_p = \mu_p^0 \quad for\ X_{salt} < X_{min} \tag{2.3.2}$$

Given that the salinity component affecting viscosity is defined, $X_{\min}$ is the salinity component fraction (mass /molar) below which the viscosity is independent of salinity. sp is the slope of polymer viscosity vs. salinity (salinity/ minimum salinity) on log-log scale. X_{salt} is the salinity component fraction (mass/molar). μ_p^0 is the viscosity of the polymer defined by the user in the input viscosity table. If the salinity component is actually represented by more than one component (i.e., multiple cationic components), X_{salt} is replaced by equivalent salinity X_{eq}, this is to account for divalent ions that may have greater impact on the viscosity than the monovalent ions, therefore the equivalent salinity is the weighted salinity of all components. Where i represents the cation component number, β_{vs_i} is the coefficient of equivalent salinity:

$$X_{eq} = \sum_{i=1}^{all\ cations} \beta_{vs_i} X_i \tag{2.3.3}$$

The resultant polymer viscosity, μ_p , is then used in the calculations of phase viscosity using the non-linear mixing rule function described in the next section.

2.3.1.2 Polymer Rheology

CMG-STARS models the dependence of shear rate (or velocity) on polymer viscosity on two ways: the user can provide tabulated data of shear rate (or velocity) vs. polymer viscosity; if velocity is used then conversion to shear rate using Darcy's velocity is required (will be shown shortly in this section), and this is a flexible option .The other option can specify if the non-Newtonian fluid (polymer) is shear thinning, shear thickening or a combination of both. If the shear thinning option used, the calculation for the apparent polymer viscosity is as the following:

$$\mu_{app} = \mu_{1,p} \quad for \;\; u_1 < u_{1_{lower}} \tag{2.3.4}$$

$$\mu_{app} = \mu_{1,p} \left[\frac{u_1}{u_{1_{lower}}}\right]^{n_{thin}-1} \quad for\, u_{1_{lower}} < u_1 < u_{1_{upper}} \tag{2.3.5}$$

$$\mu_{app} = \mu_{1,o} \quad for\, u_1 > u_{1_{upper}} \tag{2.3.6}$$

where $\mu_{1,p}$ is the viscosity at low shear rate, or the upper boundary viscosity, and $\mu_{1,o}$ is the viscosity that is equal to the Newtonian viscosity, or the viscosity of the phase in the absence of non-Newtonian fluid (polymer), and n_{thin} is the power law exponent in the viscosity shear thinning equation. For the shear thickening polymer:

$$\mu_{app} = \mu_{1,p} \quad for \;\; u_1 < u_{1_{lower}} \tag{2.3.7}$$

$$\mu_{app} = \mu_{1,max} \left[\frac{u_1}{u_{1_{max}}}\right]^{n_{thick}-1} \quad for\, u_{1_{lower}} < u_1 < u_{1_{max}} \tag{2.3.8}$$

$$\mu_{app} = \mu_{1,max} \quad for\, u_1 > u_{1_{upper}} \tag{2.3.9}$$

where $\mu_{1,p}$ in this case is the viscosity in the lower shear thickening region, that is equal to the phase viscosity in the absence of polymer. $\mu_{1,max}$ is the viscosity of the upper region of the shear thickening region, and n_{thick} is the power law exponent in the viscosity shear thinning equation. If both shear thinning and shear thickening options are used, the polymer viscosity is then the sum of both power law relations:

$$\mu_{app} = \mu_{app\,thin} + \mu_{app\,thick} \tag{2.3.10}$$

$$\mu_{app} = \mu_{1,p} \quad for\ u_1 < u_{1_{lower}} \tag{2.3.11}$$

$$\mu_{app} = \mu_{app\,thin} + \mu_{app\,thick} \quad for\ u_{1_{lower}} < u_1 < u_{1_{max}} \tag{2.3.12}$$

$$\mu_{app} = \mu_{1,max} \quad for\ u_1 > u_{1_{upper}} \tag{2.3.13}$$

For the conversion from Darcy's velocity to porous medium equivalent shear rate, the following the modified Blake-Kozeny capillary bundle equation is used (Lin, 1981; Sorbie, 1991) (similar to **Eqn. 2.2.11** used in UTCHEM):

$$\dot{\gamma_{eq}} = \frac{\dot{\gamma_{fac}}|u_\ell|}{\sqrt{\bar{k}\, k_{r\ell}\phi\, S_\ell}} \tag{2.3.14}$$

Where $\dot{\gamma_{fac}}$ is given by:

$$\dot{\gamma_{fac}} = C\left(\frac{3n+1}{4n}\right)^{\frac{n}{n-1}} \tag{2.3.15}$$

The default value of $\dot{\gamma_{fac}}$ used in CMG-STARS is 4.8, that represents a typical value for *C*=6 (Cannella *et al.,* 1988) and *n*=0.5.

To model the liquid phase viscosities in the presence of a non-Newtonian fluid, CMG-STARS utilizes non-linear mixing function for liquid viscosity:

$$\ln(\mu) = \sum\nolimits_{i=S} f_i(X_i).\ln(\mu_i) + N.\sum\nolimits_{i\neq S} X_i \ln(\mu_i) \tag{2.3.16}$$

$$N = \frac{1 - \sum_{i=S} f_i(X_i)}{\sum_{i\neq S} X_i} \tag{2.3.17}$$

where the *X* represents the component (polymer) molar fraction, function *f(x)* performs as a weighting factor for each molar fraction. The index S represents the set of nonlinear components (in this case it is polymer only). The *N* is a normalizing factor. The nonlinear logarithmic function *f(x)* uses 11 entries to define the component viscosity at 11 evenly distributed concentrations between the minimum and maximum concentrations of polymer. The model is set to yield an exponential increase in solution viscosity with increase in polymer concentration.

2.3.1.3 Polymer Adsorption

CMG-STARS models adsorption either by providing tabulated data of adsorption vs. adsorbing component concentration, or by using the following Langmuir isotherm expression:

$$ad = \frac{(tad_1 + tad_2 * Xnacl) * ca}{(1 + tad_3 * ca)} \tag{2.3.18}$$

where tad_1 and tad_3 are the first and second parameters, respectively, in Langmuir expression for the adsorption isotherm. Parameter tad_2 introduces the salinity dependence and has a unit of gmol/m^3. XNACL is the salinity of the brine, and *ca* is the mole fraction of the adsorbing component (i.e., surfactant, polymer).

2.3.1.4 Permeability Reduction

The permeability reduction factor for the water phase in CMG-STARS is modeled as the following:

$$RKW = \frac{1 + (RRF - 1) * AD(C,T)}{ADMAXT} \tag{2.3.19}$$

The calculation for each phase is done similarly. The *RRF* is the residual resistance factor. $AD(C,T)$ is the adsorption in the isotherm at a given concentration and temperature, defined in previous section. *ADMAXT* is the maximum adsorption capacity in the adsorption isotherm. Therefore, the reduced permeability for each block in water phase is given by (same calculation for other phases):

$$AKW(I) = \frac{AK(I) * krw}{RKW(I)} \tag{2.3.20}$$

The I represents the grid block number, $K(I)$ is the block permeability is a given input parameter that is measured in the lab. The accessible pore volume is also given as an input.

2.3.2 Modeling of Surfactant:

2.3.2.1 IFT and Fluid Phase Equilibrium

CMG-STARS allows the user to explicitly provide the relationship between surfactant concentration and IFT using tabulated data of lab measurements. The simulator does not model the surfactant phase behavior in detail such as UTCHEM, however it allows for components partitioning between phases through phase equilibrium ratios, defined as the *K*-values. The user can provide these *K*-values as a function of temperature, concentration and pressure. To define this, CMG-STARS uses Hand's tie lines option described by van Quy *et al.* (1972) and Young and Stephenson (1983). The Hand's rule assumes that all tie-lines intersect at one point in a ternary system (van Quy *et al.* ,1972; Young, L.C. and Stephenson, 1983; CMG-STARS Manual, 2019). A normalized composition variable is defined as:

$$u = \frac{Z_3}{AZ_2 + B} \tag{2.3.21}$$

$A\ u$ and $B\ u$ are slope and intersect corresponding to a specific over-all (or global) compositions ($Z_3, Z_2,$ and Z_1), reshaping the previous relationship gives:

$$Z_3 = A(u)Z_2 + B(u) \tag{2.3.22}$$

The composition variable u, ranges from zero to 1. The *K*-value is therefore defined as:

$$k_i^{BA} = \frac{composnent\ i\ composition\ in\ phase\ B}{component\ i\ composition\ in\ phase\ A} \tag{2.3.23}$$

Figure 2-2 below illustrates the Hand's rule in ternary diagram.

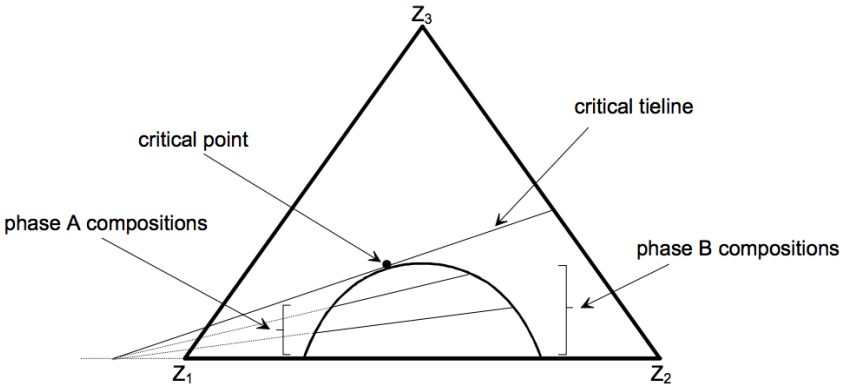

Figure 2-2:Hand's Tie-Lines in Ternary Diagram (CMG-STARS Technical Manual, 2019)

2.3.2.2 Surfactant Adsorption

The same Langmuir expression described under the polymer adsorption section is used for surfactant adsorption definition.

2.4 COMPARISON BETWEEN UTCHEM AND CMG-STARS

For brevity, the summary of UTCHEM and CMG-STARS models described in the previous two sections are focused solely on selected polymer and surfactant properties that are the main contributors to the work described in this thesis. The key differences between the two simulators are the following:

- Polymer viscosity models: UTCHEM uses Meter's equation described in **Eqn. 2.2.3** to model the change in polymer viscosity with respect to shear rate, it also uses a unified viscosity model UVM which incorporates the Newtonian, shear thinning and shear thickening behaviors of polymers in porous media using Carreau's model. CMG-STARS utilizes different power law relations to describe the polymer viscosity and uses it in a non-linear mixing function to calculate the final liquid phase viscosity.

- Surfactant phase behavior and IFT: Using Hand's equation, UTCHEM describes the phase behavior of a surfactant in three phase environments (Type I, Type II and Type III) with respect to salinity, concentration and composition. Which allows it to calculate the IFT using either Healy and Reed's (1974) or Huh's (1979) correlations. In CMG-STARS, the effect of salinity on phase behavior is not included, however it has the capability to model components partitioning between phases through phase equilibrium ratios, defined as the *K*-values which are dependent on temperature, concentration and pressure. Unlike UTCHEM, the values of IFT in CMG-STARS and their dependence on surfactant concentration are user inputs.
- Electrolytes and polymer viscosity: The effects of salinity and hardness on polymer viscosity are incorporated in both simulators but they utilize different models. UTCHEM uses Flory-Huggins equation (Flory, 1953) to describe the polymer viscosity with respect to concentration and salinity and hardness. CMG-STARS incorporates the impact of salinity and hardness by using equivalent salinity expression as described in **section 2.3.1**.
- Polymer and Surfactant Adsorptions: Both simulators use Langmuir-type equation to describe the relationship between adsorption and salinity concentration, and permeability. The effect of hardness on adsorption is included in UTCHEM, but not CMG-STARS.
- Microemulsion phase: UTCHEM models a distinct microemulsion ME phase. CMG-STARS does not have this option.

Table 2-1 below summarizes the differences in key properties models in UTCHEM and CMG-STARS. Goudarzi *et al*. (2013;2016) conducted a comparison between different chemical EOR simulators (UTCHEM , CMG-STARS and Eclipse), **Table 2-2** shows

Goudarzi's comparison of polymer and surfactant models in UTCHEM and CMG-STARS, with our slight modification to the effect of hardness on viscosity.

Properties	UTCHEM	CMG-STARS
Polymer Viscosity Calculation	○ Flory Huggins' equation, which includes effect of concentration, salinity and hardness on the polymer viscosity. ○ The reduction in polymer viscosity by shear rate is modeled by Meter's eqn. ○ Carreau's model is used in a unified viscosity model calculation that incorporates Newtonian and Non-Newtonian fluids.	○ Model allows to specify type of fluid, shear thinning, thickening, mixed using power law relations, or input viscosity vs shear rate table. ○ The tabulated data is used to calculate component viscosities. ○ Final phase viscosity is calculated using mixing rule. ○ The effect of salinity and hardness on polymer is included
Adsorption	○ Uses Langmuir adsorption that includes polymer concentration salinity, hardness and permeability.	○ Langmuir adsorption isotherm for composition and temperature dependent adsorption and permeability.
IFT calculations	○ UTCHEM calculates IFT based on oil solubilization ratios, implementing Chun Huh's and Healy or Reed's correlation.	○ For modeling surfactant, the user provides surfactant concentration vs IFT table, temperature dependency is optional
Microemulsion	○ UTCHEM calculates microemulsion phase viscosity, includes the effect of oil, water and surfactant concentrations.	○ Does not include a distinct ME phase

Table 2-1:Summary of Polymer and Surfactant Models Comparison Between UTCHEM and CMG-STARS

Polymer Module	UTCHEM	CMG-STARS
Viscosity vs. polymer conc.	✓	✓
Viscosity vs. shear rate	✓	✓
Adsorption	✓	✓
Permeability reduction	✓	✓
Inaccessible pore volume	✓	✓
Effect of salinity on viscosity and adsorption	✓	✓
Effect of hardness on viscosity*	✓	✓
Effect of hardness on adsorption and permeability reduction	✓	Not included
Surfactant Module	**UTCHEM**	**CMG-STARS**
ME viscosity	✓	Not included
Interfacial tension	✓	Included (tabular format)
Phase behavior	✓	Not included
Surfactant adsorption	✓	✓

Table 2-2: Goudarzi's *et al. (*2016) Comparison of Polymer and Surfactant Models in UTCHEM and CMG-STARS (with slight addition) *The addition to the comparison

2.5 Brief Fluid And Reservoir Description

Reservoir A is a high temperature unconsolidated sandstone reservoir. The temperature of the reservoir is 70° C with permeability ranging from 500-9000 mD and porosity ranging from 13-31%. Despite the good reservoir permeability and porosity, the recovery from the reservoir is challenging due to the high viscous nature of oil, with viscosity of approximately 300 cP. and oil gravity of 15° API. Oil has a density of 0.95 g/ml and is acidic with a TAN of 1.5 mg KOH/gm of oil. The formation brine composition constitutes of 8600 PPM NaCl and 9670 of total dissolved salts. The field has undergone

primary recovery and it currently exhibits high water cut. Considering the nature of the viscous oil, examination of enhanced oil recovery techniques was deemed necessary. Phase-I of the surfactant-polymer flood study entailed screening of different surfactant formulations and evaluate their efficacy with coreflood experiments. Based on the results of phase I, two surfactant formulations were recommended. The goal of Phase-II, described in this thesis, is to conduct simulation studies to design an SP pilot for the reservoir.

Chapter 3: Model Calibration Using Coreflood History Matching

This chapter describes the setup of the coreflood models, key physico-chemical parameters and results of the coreflood history matching process. The inferred key parameters derived by the history matching will lay the basis for the pilot scale models.

3.1 Model Grids Set Up

22 coreflood experiments were conducted on the subjected reservoir, 8 of them were chosen for history matching. The 8 corefloods cover a diverse range of different surfactant types, polymer concentrations, permeabilities, and core types. All experiments are conducted at reservoir temperature 70º C. The viscosity of the oil at reservoir temperature ranges 330-370 cP. **Table 3-1** shows a brief description of the modeled corefloods. More details about the coreflood chemical injection and recovery are presented in **Table 3-5**.

Coreflood No.	Core Type	Surfactant	Polymer Conc. ppm	Permeability, Darcy	Flood Nature/Process
1	Sandpack	Phenol-7PO-15EO	8000	28.45	Tertiary/SP+P
2	Sandpack	Phenol-7PO-15EO	8000	12.50	Tertiary/SP+P
4	Sandpack	C9-11-8EO	8000	8.23	Tertiary/SP+P
5	Bentheimer Core	C9-11-8EO	8000	1.58	Tertiary/SP+P
6	Sandpack	C9-11-8EO	9000	12	Secondary/SP+P
7	Sandpack	C9-11-8EO	9000	7.70	Tertiary/SP+P
9	Sandpack	C9-11-8EO	5000	5.6	Tertiary/SP+P
8	2D Cell	C9-11-8EO	9000	9.47	Tertiary/SP+P

Table 3-1: Summary of the 8 Modeled Corefloods

The chemical formulations used are (i) 1 wt.% nonionic surfactant C9-11-8EO (Shell) with 0.5-0.8 wt.% of Flopaam 3630s (SNF) or (ii) 1 wt.% nonionic surfactant Phenol-7PO-15EO (Harcros-Venus) with 0.5-0.8 wt.% of Flopaam 3630s (SNF). The permeability

range is 1.5-28 Darcy. The experiments are conducted in Sandpack, Bentheimer Core and 2D Cell.

All the 1-D coreflood models are set up with multiple grid blocks in the flow direction (z-direction: vertical) 1x1x50 with 2 wells. The injector well is at the bottom grid and producer well is at the top grid. For the 2D cell, the 2 wells orientations are vertical, with 20x1x20 number of grids. All corefloods are assumed to be homogeneous and isotropic. More details are shown in **Table 3-2** and **Table 3-3** which summarize the grids construction and main physical properties for the 1D floods and the 2D cell, respectively. **Figure 3-1** shows the grids setup for the 1D core (left) and 2D cell (right).

Parameter	Value	Remark
Number of grid blocks	1x1x50	
Flow Direction	Vertical	
Grid thickness, Δx, cm	1.8	Constant Size
Grid thickness, Δy, cm	1.8	Constant Size
Grid thickness, Δz, cm	1.22	Constant Size
Number of wells	2	Bottom injector and top producer
Porosity, ∅	Constant Value	Dependent on core porosity value
Permeability, x direction	Constant Value	Dependent on core permeability value
Permeability, y direction	1, Ratio y/x perm	Dependent on x-direction perm
Permeability, z direction	1, Ratio z/x perm	Dependent on x-direction perm

Table 3-2: Basic Grids Setup and Physical Properties for the 1D Corefloods

Property	Value
Number of grid blocks	20*1*20
Grid thickness, *D*x, cm	1.27
Grid thickness, *D*y, cm	1.6
Grid thickness, *D*z, cm	0.635
Orientation	2D Horizontal
Permeability, D	9.47
Porosity, ∅	36

Table 3-3: 2D Cell Grids Setup and Main Properties

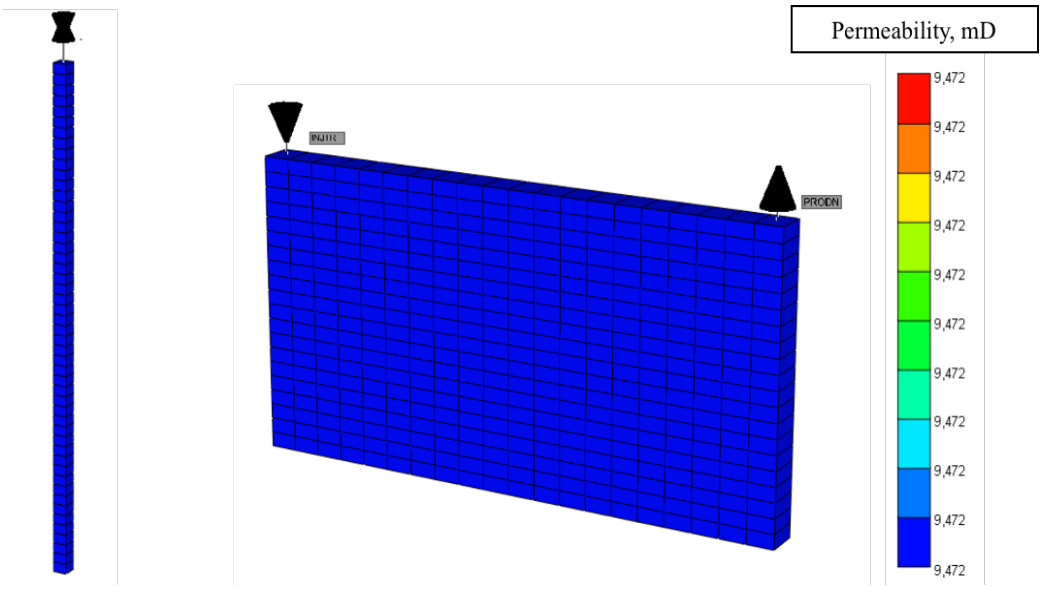

Figure 3-1:Grids Setup for the 1D cores (Left) and 2D cell (Right)

3.2 Model Key Parameters

Data preparation is the first and most critical step in history matching SP corefloods; this step involves gathering all the required lab measurement data for the simulation and accurately convert them from lab to simulation units. The goal is to use the history match to derive the simulation key parameters for the chemical processes' models, which will lay the basis for the pilot scale models. The key parameters/models discussed in this section are; surfactant, polymer, adsorption, relative permeability curve and capillary desaturation curve.

3.2.1 Polymer Model

The available data related to the polymer HPAM 3630 behavior from lab measurement include: water composition, viscosity vs. shear rate, viscosity at low shear rate at concentrations (9000 PPM,8000 PPM, 5000 PPM). These data will be used in the model directly or used for interpretation. As was shown from **section 2.4,** CMG-STARS and UTCHEM use different set of parameters to model the polymer rheology. All the

history matching was conducted using CMG-STARS; one coreflood (Coreflood No.1) matching was conducted using both UTCHEM and CMG-STARS for comparison. The model setup for this experiment using UTCHEM and CMG-STARS is shown. The viscosity of 8000 PPM HPAM3630 at low shear rate was matched using matching parameters for UTCHEM by the Flory-Huggins (1953) **Eqn.2.2.1**.

$$\mu_p^0 = \mu_w(1 + \left(A_{p1}C_{4\ell} + A_{p2}C_{4\ell}^2 + A_{p3}\, C_{4\ell}^3\right)C_{SEP}^{sp}$$

The matched point is shown in **Figure 3-2**:

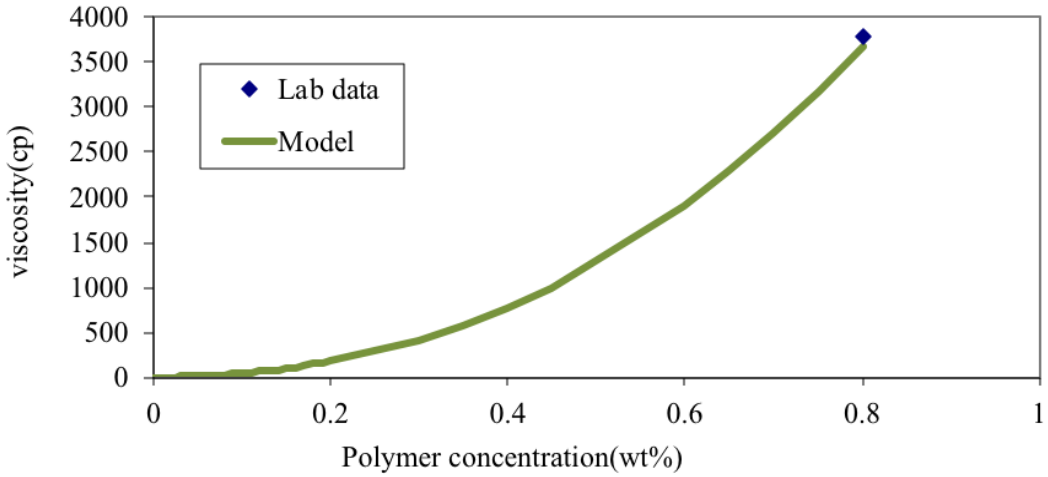

Figure 3-2: Viscosity vs. Polymer Concentration; Model vs. Lab data at 0.8 wt.% Polymer Concentration

The parameters for calculating the polymer viscosity at zero shear rate (A_{p1} , A_{p2}, A_{p3}) were then assumed by matching the lab data (single point of 8000 ppm polymer viscosity) to the model. The effective salinity, C_{SEP} is determined using the background salinity. The formation brine and softened brine compositions are shown in **Table 3-4.** Converting from lab unit to UTCHEM units of salinity (meg/ml), the background monovalent salinity and hardness are therefore 0.147 meq/ml and 0.0138, respectively.

Formation Brine			Softened Brine		
Salt	**PPM**	**Wt.%**	**Salt**	**PPM**	**Wt.%**
NaCl	8600	0.86	NaHCO3	840	0.084
CaCl2 2H2O	870	0.087	NaCl	7944	0.79
MgCl26H2O	200	0.02			
Total	9670	0.96	Total	8784	0.874

Table 3-4: Synthetic Brine Composition of Formation and Softened Brine

By matching the 0.8 wt.% polymer viscosity at low shear rate, the viscosity dependence on shear rate is then modeled using Meter and Bird's (1964) **Eqn.2.2.3.**

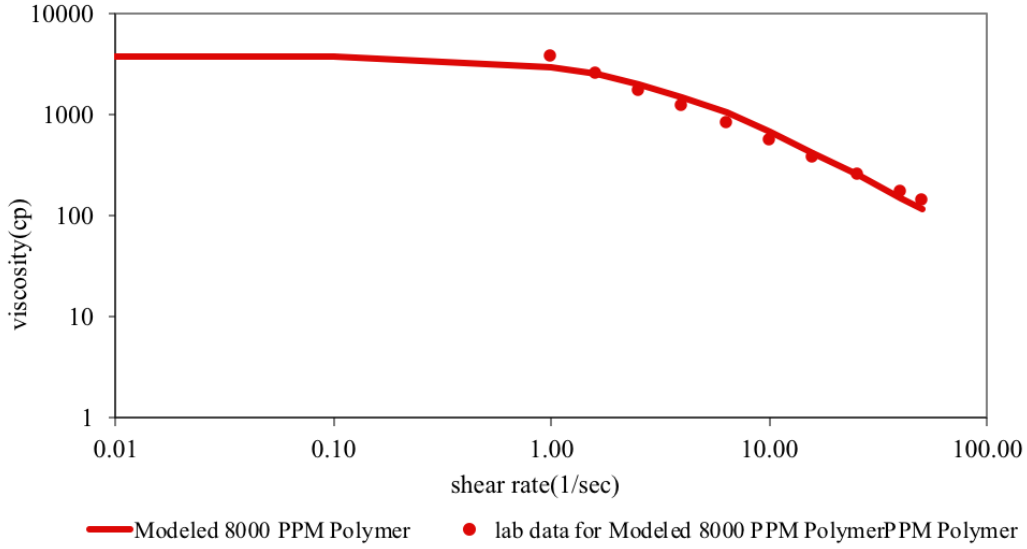

Figure 3-3: Viscosity vs. Shear rate model vs. Lab data at 0.8 wt.% Polymer Concentration

For CMG-STARS, the same polymer (HPAM 3630) was used in all the corefloods; the same input parameters for the polymer were used in all models. The models define the polymer viscosity as a function of shear rate by utilizing tabulated lab data of polymer shear rate vs. viscosity (lab data shown in **Figure 3-3**). The lab measurement of polymer viscosity at 70 °C was added to the input file directly as a table of viscosity vs. shear rate (1/day). The data from the table provides the component (polymer) viscosity; using the

components viscosities, the final phase viscosity is calculated using the non-linear mixing function from **Eqn. 2.3.16** and **Eqn. 2.3.17**.

$$\ln(\mu) = \sum_{i=S} f_i(X_i).\ln(\mu_i) + N.\sum_{i\neq S} X_i \ln(\mu_i)$$

$$\mathrm{N} = \frac{1 - \sum_{i=S} f_i(X_i)}{\sum_{i\neq S} X_i}$$

The polymer viscosity defined using the nonlinear logarithmic function is shown in **Figure 3-4**. The model is set to yield an exponential increase in solution viscosity with increase in polymer concentration.

The salinity effect for a polymer solution can be incorporated given the slope of the log-log plot of polymer viscosity vs. salinity (**Eqn. 2.3.1**). The salinity impact on the polymer adsorption is shown section 3.2.3. A table of viscosity versus temperature for each component is added to the model. Since the models were at a fixed temperature, no interpolation of viscosity at different temperatures was needed.

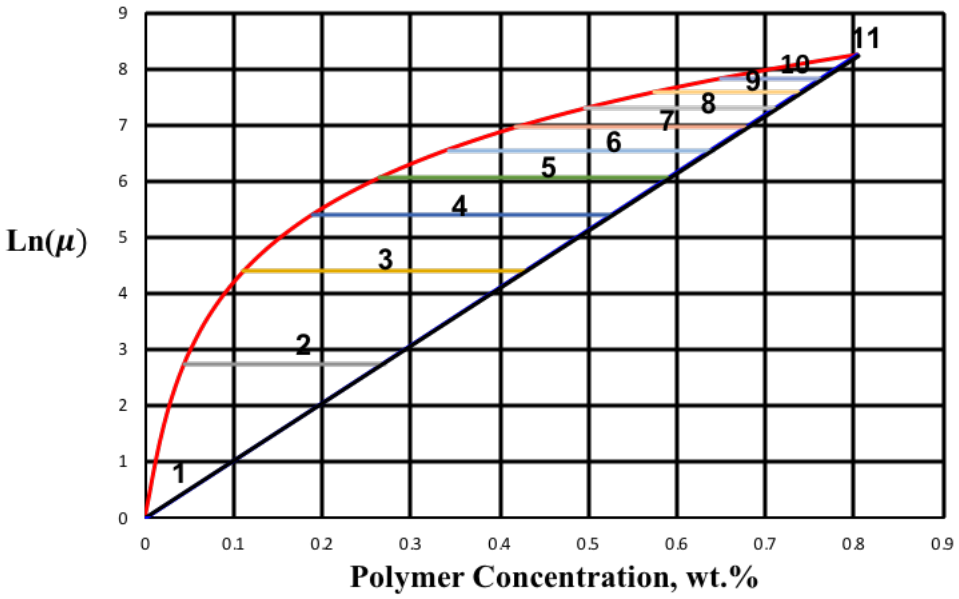

Figure 3-4: Viscosity as A Function of Polymer Concentration Using Non-Linear Mixing Function With 11 Entries

3.2.2 Surfactant Model

The phase behavior measurements showed similar behavior for both Phenol-7PO-15EO and C9-11-8EO surfactants; therefore, the same surfactant model has been used to match all the corefloods. The only varying input is the molecular weight of the surfactants. Phenol-7PO-15EO with MW of 1.159 kg/gmole and C9-11-8EO with MW of 0.493 kg/gmole. The surfactant has only a Winsor type I phase behavior with oil and brine. The measured oil solubilization ratio is approximately 3.

To model the surfactant behavior using UTCHEM, the lab measured solubilization ratio vs. salinity is needed to determine the parameters of the binodal curves (solutions of Hand's model shown in **Eqn. 2.2.20**. Because the subject surfactants are of non-ionic nature, the solubilization ratio is independent of salinity. Hence the nonionic behavior is modeled by assuming the height of binodal curves is the same regardless of the salinity and also assumes the same value of salinity for the lower and upper salinity inputs. Calculated values of solubilization ratio vs. salinity of interest is then generated and shown in **Figure 3-5**.

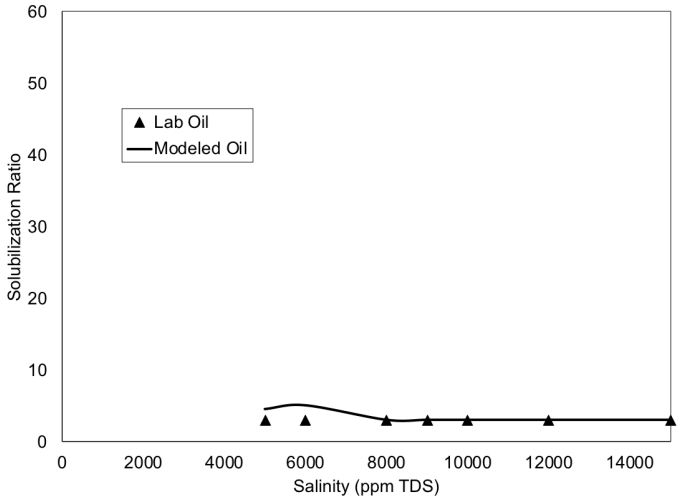

Figure 3-5: Solubilization Ratio Vs. Salinity Comparison Between Model and Lab Data (not all lab points are actual measurement, but assumed based on the nonionic behavior)

In CMG-STARS, on the other hand, the surfactant is modeled by providing a table of concentration vs. IFT (surfactant or oil concentration) and also by providing liquid-liquid partition coefficient *K*-values. The phase behavior data of the surfactant in this experiment is limited, therefore the parameters of binodal height curve that were used to match the experiment in UTCHEM, and Chun Huh correlation (**Eqn. 2.2.34**) were utilized to generate surfactant concentration vs. IFT table. The table was added to the CMG model as shown in **Figure 3-6.** The generated IFT values match the data point of measured IFT value at 1% surfactant concentration (approximately 0.03 mN/m).

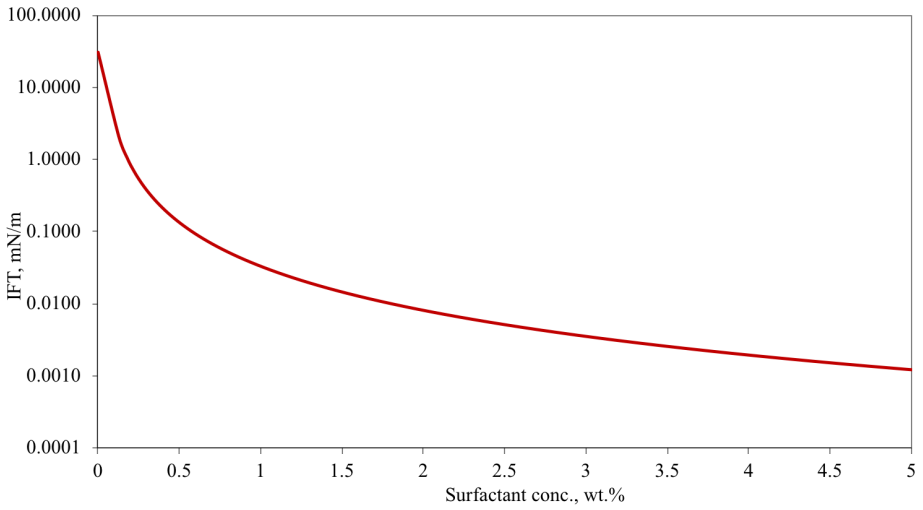

Figure 3-6: IFT vs. Surfactant Concentration Calculated by UTCHEM Surfactant Matching Parameters

The liquid partition coefficient *K*-values are a function of pressure, temperature and concentration as was shown in section 2.3.2.1. In our study, this parameter *K* is used as a matching parameter.

3.2.3 Adsorption Model

UTCHEM models the adsorption of both surfactant and polymer using Langmuir-type equations **Eqn. 2.2.13-14** and **Eqn. 2.2.37-38**:

$$\widehat{C_{3,4}} = \min\left(\widetilde{C_{3,4}}, \frac{a_{3,4}\left(\widetilde{C_{3,4}} - \widehat{C_{3,4}},\right)}{1 + b_{3,4}\left(\widetilde{C_{3,4}} - \widehat{C_{3,4}}\right)}\right)$$

$$a_{3,4} = \left(a_{(3,4)1} + a_{(3,4)2} C_{SEP}\right)\left(\frac{k_{ref}}{k}\right)^{0.5}$$

The parameters $a_{3,4}$, $b_{3,4}$ are parameters determined by matching the lab measured adsorption to the modeled data. No data was available for polymer adsorption; so, it is assumed to be a typical value of 42 ug/g. The adsorption measured for surfactant is 112 ug/g at 1% surfactant concentration. The adsorption curve generated by the model for the surfactant is shown in **Figure 3-7**. The adsorption in the model is irreversible with concentration, but reversible with salinity.

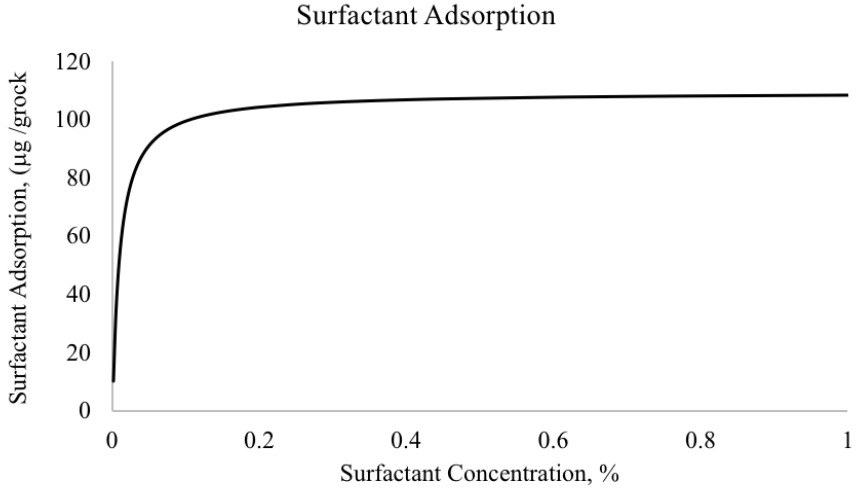

Figure 3-7: Adsorption Curve of Surfactant Generated Using the Model

CMG-STARS models the surfactant adsorption either by providing tabulated data of adsorption vs. adsorbing component concentration, or by using **Eqn. 2.3.18** shown below**.** In our work both methods are used.

$$ads = \frac{(tad_1 + tad_2 * Xnacl) * ca}{(1 + tad_3 * ca)}$$

where tad_1, tad_2 and tad_3 are parameters determined by matching the equation with the lab measured data. The adsorption value of surfactant measured in the lab was converted

to mole fractions using the following conversion in **Eqn. 3.2.1**. The tad values are adjusted so that the resulting value at 1% surfactant concentration is matched with the lab value.

$$ads\left(\frac{mol}{cm3}\right) = \frac{ads\left(\frac{mg}{g}\right) * 0.001 * (1 - \emptyset) * \rho rock\left(\frac{g}{cm3}\right)}{\emptyset * MW\left(\frac{g}{mole}\right)} \quad (3.2.1)$$

3.2.4 Relative Permeability Model

For each coreflood, the relative permeability model parameters (end points relative permeability, exponents, residual saturation to waterflood) for the waterflood part (low capillary number-no surfactant) were estimated using the fractional flow theory. The parameters were determined by matching the calculation of oil recovery to the experimental oil recovery during the water flood part. The known parameters for the fractional theory calculation are the initial saturations and fluids viscosities. Since 100% of the oil was recovered in most of the coreflood experiments, the residual saturations for the high capillary number part (surfactant is present) are assumed to reduce to zero, the relative permeability curves are therefore assumed to be straight lines as shown in **Figure 3-8.**

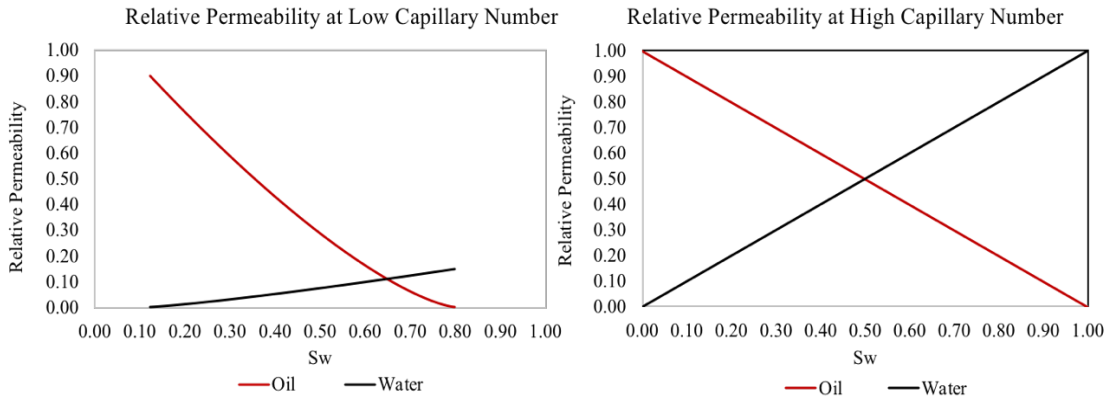

Figure 3-8: Generated Relative Permeability Curves for Coreflood 1 at low (Left) and High Capillary Numbers (Right)

Between the low and high capillary number relative permeability inputs, the residual saturations are computed as a function of trapping number (**Eqn. 2.1.3)**; end points and relative permeability exponents are interpolated linearly in between. In UTCHEM the calculation of the residual saturation as a function of trapping number is based on correlation developed by Delshad (1990) as follows in **Eqn.3.2.2**.

$$S_{\ell r} = \min\left(S_{\ell}, S_{\ell r}^{high} + \frac{S_{\ell r}^{Low} + S_{\ell r}^{high}}{1 + T_{\ell} N_{T\ell}}\right) \tag{3.2.2}$$

where $N_{T\ell}$ is the trapping number in phase ℓ, T_{ℓ} is a positive input parameter, $S_{\ell r}^{Low}$ and $S_{\ell r}^{high}$ are the provided residual saturations at low and high capillary or trapping number, respectively. The endpoint relative permeabilities and exponents are linearly interpolated as below **Eqn. 3.2.3**-**4**.

$$k_{\ell r}^{\circ} = k_{\ell r}^{\circ low} + \frac{S_{\ell' r}^{Low} + S_{\ell' r}}{S_{\ell' r}^{Low} + S_{\ell' r}^{high}} (k_{\ell r}^{\circ high} - k_{\ell r}^{\circ low}) \tag{3.2.3}$$

$$n_{\ell} = n_{\ell}^{low} + \frac{S_{\ell' r}^{Low} + S_{\ell' r}}{S_{\ell' r}^{Low} + S_{\ell' r}^{high}} (n_{\ell}^{high} - n_{\ell}^{low}) \tag{3.2.4}$$

The relative permeability is then calculated using Corey Type equation:

$$k_{rl} = k_{\ell r}^{\circ} \bar{S}_{\ell}^{n_{\ell}} \tag{3.2.5}$$

where $\bar{S}_{\ell}^{n_{\ell}}$ is the normalized saturation defined as:

$$\bar{S}_{\ell}^{n_{\ell}} = \frac{S_{\ell} - S_{\ell r}}{1 - \sum_{\ell=1}^{np} S_{r\ell}}. \tag{3.2.6}$$

In CMG, the interpolation between two sets can be based on an interpolation variable defined by the user. The interpolation variable can be a component concentration or capillary number. The latter is used for this work. This is done be first calculating and interpolation factor:

$$\omega_{\ell}^{i} = \left(\frac{x^{i} - x_{\ell}^{A}}{x_{\ell}^{B} - x_{\ell}^{A}}\right)^{n_{\ell}} \tag{3.2.7}$$

where i represents the block number, ℓ represents the phase, an x represents the interpolation variable. A and B refer to the relative permeability sets at low and high capillary numbers that were pre-defined. n_ℓ is the curvature exponent of the relative permeability curve. The saturation end point is then calculated as:

$$S_{\ell r}^{i} = \left(1 - \omega_{\ell}^{i}\right) S_{\ell r}^{A} + \omega_{\ell}^{i} S_{\ell r}^{B} \tag{3.2.8}$$

The relative permeability of the block:

$$k_{r\ell} = \left(1 - \omega_{\ell}^{i}\right) k_{r\ell}^{A} + \omega_{\ell}^{i}\, k_{r\ell}^{B} \tag{3.2.9}$$

In the interpolation above, the interpolation variable x is a reflection of a capillary number; The relative permeability set at low N_c corresponds to input parameters DTRAPW and DTRAPN, which are equal to log(N_c) at which the water and oil start to detrap , respectively (residual saturation start to reduce). Similarity, the relative permeability set at high N_c corresponds to input parameters DTRAPW and DTRAPN at which the complete detrapping occurs. These inputs define the capillary desaturation curve, described in next section.

3.2.5 Capillary Desaturation Curve CDC Parameters

Another input parameter with almost similar values for all the models is the trapping parameters. The trapping number is used to interpolate between the relative permeability curves as described in previous **section 3.2.4**. This parameter is used with keyword *DTRAPW and it is simply the logarithmic value of the capillary number where capillary number N_c is defined as in **Eqn. 2.1.2:**

$$N_c = \frac{k\Delta P}{\sigma L}$$

A typical CDC for wetting and non-wetting phase saturations is shown in **Figure 3-9**. The residual saturations during water floods remain in the flat region of the curve because of the low capillary number. Due to the high permeabilities of some of the cores,

the DTRAPW/N values for detrapping was set at low capillary numbers of around -4 to -6. This number corresponds to the onset of detrapping, or the knee of the curve where a critical capillary number is achieved (Lake *et al.*,2014). The high capillary number limiting value was set around -1.2 to -1.3, which corresponds to complete detrapping point.

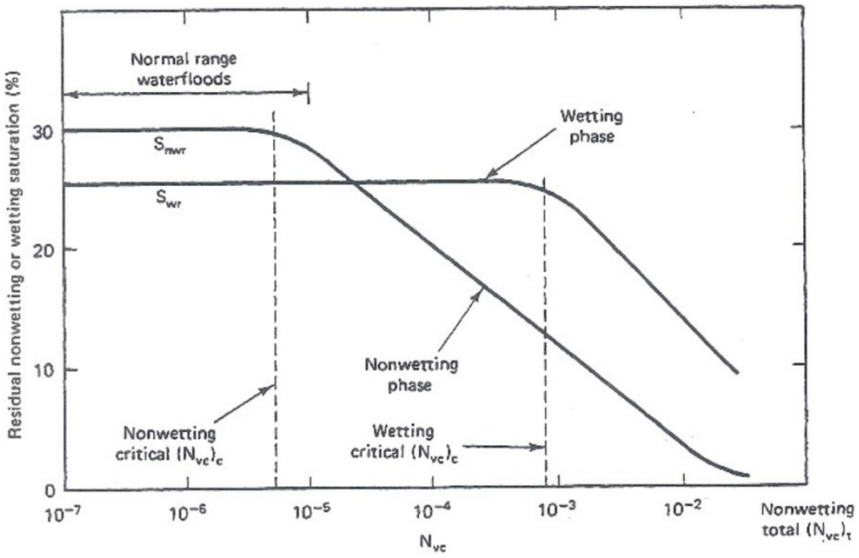

Figure 3-9: Typical Wetting and Non-Wetting Phases Residual Saturation CDC (Lake *et al.*, 2014)

3.3 MODEL UNCERTAINTIES

Relative Permeability: The relative permeability has a crucial effect on recovery and pressure drop. The relative permeabilities were estimated with the aid of fractional flow theory in 1D corefloods, once the analytical match of the oil recovery with lab data was achieved, the relative permeability curves were then used to define the relative permeability at low capillary numbers. The analytical match of oil recovery follows the assumptions of the fractional flow theory; (i) one dimensional flow, (ii) homogeneous, (iii) isotropic, (iv) isothermal, (v) incompressible flow, (vi) negligible gravity and capillary pressure, (vii) Darcy's law apply and (viii) no fingering (Pope, 1980). Due to the viscosity

contrast between the oil and water in the core, it is however expected to have fingering, inclusion of viscous fingering model could capture the fluid behavior more accurately although capturing viscous fingering is not the goal of this work.

Permeability reductions during polymer transport: no evidence of permeability reduction is seen on the core scale; no reduction was needed to match any of the corefloods. If permeability reduction is suspected, further measurements will be needed to quantify the reduction. Incorporating permeability reduction can improve the recovery results by the mechanism described in **section 2.2.1.3**: reduction in aqueous phase permeability due to polymer adsorption. The impact of this factor is studied in later chapter 5 under the sensitivity analysis of SP pilot.

Polymer degradation: No polymer protection packages were used in any of the core experiments. Some of the viscosity effluent data and pressure drops behavior could be interpreted as degradation (presented in next section, coreflood HM simulation results). However, this was not modeled; ignoring the degradation did not have any effect on the oil recovery, but some differences in pressure drops were observed. In the field, the polymer protection package will be used to prevent polymer degradation.

The phase behavior data of the surfactant is limited, however a model that mimics the behavior of the nonionic surfactants was constructed using the available lab data; interfacial tension at 1% surfactant, solubilization ratio vs. salinity (which is assumed constant because of the nonionic type of the surfactant.

3.4 COREFLOOD DATA DESCRIPTION

Details on core properties, flood type, chemical injection rate and volume, and oil recovery data are shown in **Table 3-5**. Most of the floods are of tertiary nature with SP slug sizes ranging 0.2-0.4 PV followed by 1.5-1.6 polymer drive PD.

	Coreflood 1	Coreflood 2*	Coreflood 4	Coreflood 5	Coreflood 6	Coreflood 7	Coreflood 9	2D Cell
Nature of Flood Process Type	Tertiary SP + P	Tertiary SP + P	Tertiary SP + P	Tertiary SP + P	Secondary SP + P	Tertiary SP + P	Tertiary SP + P	Tertiary SP + P
Injection Brine Used	Softened Formation Brine	Formation Brine	Formation Brine	Formation Brine	Formation Brine	Formation Brine	Formation Brine	Formation Brine
Salt Concentration	NaCl (0.6%)	NaCl (0.6)	NaCl (1.0%)	NaCl (1.0%)	NaCl (1.0%)	NaCl (1.0%)	NaCl (1.0%)	NaCl (1.0%)
Surfactant Used	Phenol-7PO-15EO	Phenol-7PO-15EO	C9-11-8EO	C9-11-8EO	C9-11-8EO	C9-11-8EO	C9-11-8EO	C9-11-8EO
Polymer Used	Flopam 3630	Flopam 3630	Flopam 3630	Flopam 3630	Flopam 3630	Flopam 3630	Flopam 3630	Flopam 3630
Viscosity of Oil at 70°C, cP.	330	330	330	370	370	370	370	370
Sand/ Core type	Sand Pack (Synthetic)	Sand Pack (Synthetic)	Sand Pack (Synthetic)	Core (Bentheimer)	Sand Pack (Synthetic)	Sand Pack (Synthetic)	Sand Pack (Synthetic)	Sand Pack (Synthetic)
Orientation	Vertical	Vertical	Vertical	Vertical	Vertical	Vertical	Vertical	2D Horizontal
Permeability, D	28.45	12.5	8.23	1.58	19	7.7	5.6	9.47
Porosity, %	34.6	38.2	36.8	23.3	38.7	36.7	35	
Initial oil saturation, %	89	89.3	89	88.7	90	90	67.6	82.5
SP and Polymer Injection								
Flow Rate Water flood	0.1 ml/min	0.112 ml/min	0.027 ml/min	0.084 ml/min	NA	0.106 ml/min	0.077 ml/min	0.157 ml/min
Flow Rate Chemical Flood	0.025 ml/min	0.028 ml/min	0.027 ml/min	0.056 ml/min	0.028 ml/min	0.027 ml/min	0.028 ml/min	0.157 ml/min
PV injected (SP/Polymer)	0.4/1.5	0.4/1.5	0.4/1.5	0.4/1.5	0.4/1.6	0.2/1.5	0.4/2	0.4/1.5
Polymer Concentration (SP/Polymer), PPM	8000/8000	8000/8000	8000/8000	8000/8000	9000/9000	9000/9000	5000/5000	9000/9000
Recovery Data								
Oil Recovery end of Water Flood, % OOIP	43%	49%	49%	48%	NA	48%	54%	50%
Total Recovery, % OOIP	99%	100%	100%	87%	100%	99%	89%	99%

Table 3-5: Description of Coreflood Properties, Chemical Injection and Oil Recovery Data*(Panthi *et al.* ,2019)

3.5 COREFLOODS HM RESULTS

The criteria for the models' success are their ability to match the oil recovery, oil cut, and pressure drop. The results of CMG-STARS and UTCHEM for coreflood 1 are compared in

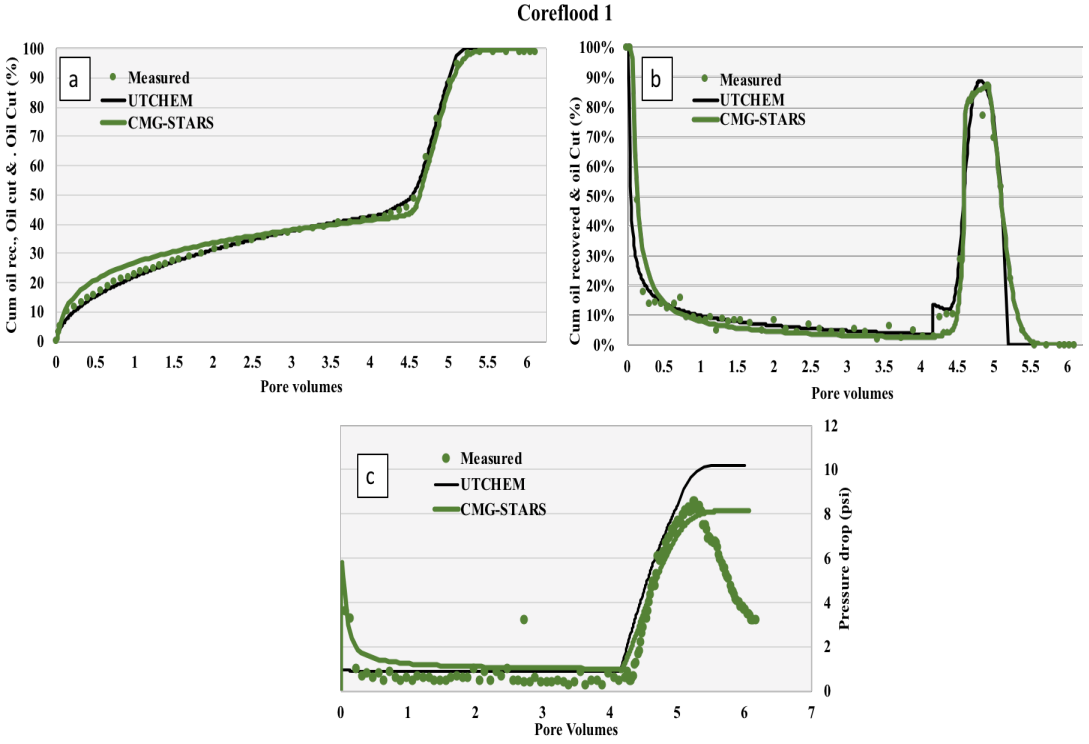

Figure 3-10. Both simulators show good agreement with the laboratory data especially with oil recovery and cut. As for the pressure drop, both simulators yield the same trend after 5 PV injected (all the oil has been produced) while the measured data is indicating decreasing pressure drop. It is believed this is due to polymer degradation, as will be discussed shortly. Overall, the results from UTCHEM and CMG-STARS are close despite the big differences in the polymer viscosity and surfactant models used.

Comparison between coreflood effluent measurements and CMG-STARS results of oil recovery and cut as a function of pore volumes injected for the eight corefloods are shown in **Figure 3-11** through **Figure 3-18.** The plots show good agreements between

modeled and measured data as the models were able to capture the trend of oil cut and overall recoveries. In most of the simulation runs, the models slightly overestimate the oil recovery during the waterflood part; since relative permeability curves are the only tuning parameters needed to match the waterflood, this behavior could be due to the uncertainty associated with the relative permeability curves generated using the fractional flow theory in 1D, which ignores the effects of viscous fingering. However, overall successful agreement with recovery of waterflood and total recovery within +-3% difference.

Matching pressure drop could be more challenging than matching the recovery. **Figure 3-19** through **Figure 3-26** show the comparison between simulated and measured pressure drops for each coreflood experiment. There is a difference between lab and modeled data in which the latter is generally predicting constant pressure drop during polymer drive, whereas lab measurement is showing decreasing pressure drop. The reason is that the model does not incorporate polymer degradation. Some of the viscosity effluent data support this explanation; **Figure 3-27** shows a significant decrease in a polymer viscosity of a sample collected after 1 PV of polymer drive injection in coreflood 5. The impact of incorporating degradation is presented in **Figure 3-28,** which shows the pressure drop for coreflood 5 assuming lower polymer concentrations during polymer drive process. After SP slug injection with 8000 ppm polymer, three different polymer concentrations were assumed: 7000 ppm, 6000 ppm and 5000 ppm for similar periods of time. The result did not alter the recovery or oil cut because all oil was produced by approximately 5 PVs injected, but the pressure drop decrease mimicked the lab trend. The polymer concentration used in coreflood 9 is significantly less than other experiments (5000 ppm); it is believed that this lower concentration, coupled with viscosity degradation have resulted in an even lower effective polymer viscosity. In simulating this coreflood, the match was achieved by applying polymer degradation (injecting at decreasing polymer concentrations) during the

polymer drive. Better match to the oil recovery and pressure drops was achieved when polymer degradation was applied. Overall, taking into account the various uncertainties, there is a satisfactory agreement between CMG-STARS results and lab measurements for all the corefloods.

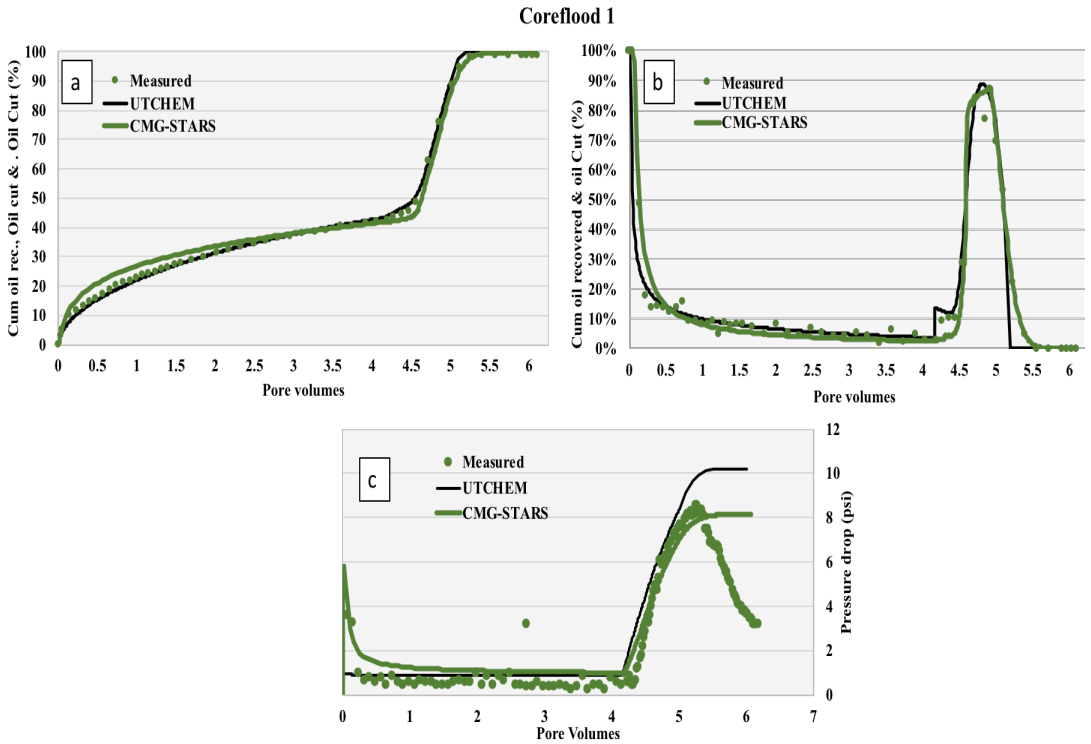

Figure 3-10: Coreflood 1 Simulation Comparison Between UTCHEM and CMG-STARS showing a) Oil Recovery b) Oil Cut and c) Pressure Drop

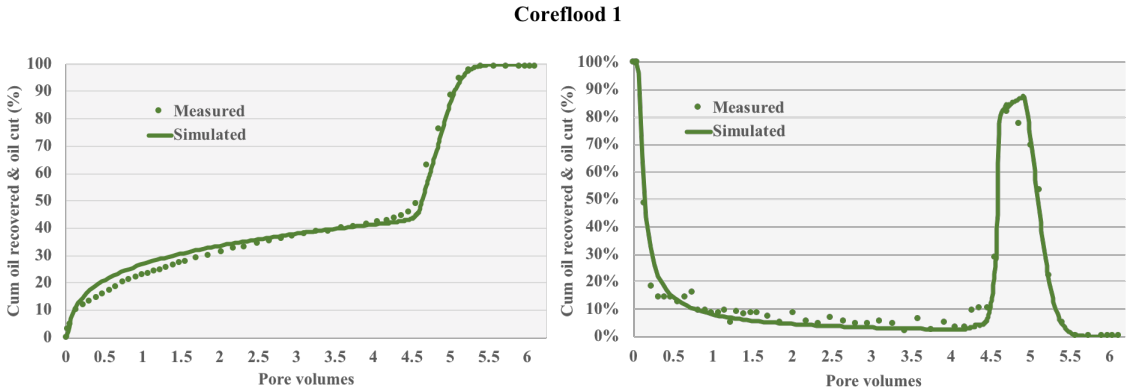

Figure 3-11: Coreflood 1 Oil Recovery (Left) and Oil Cut (Right) with Injected Pore Volumes

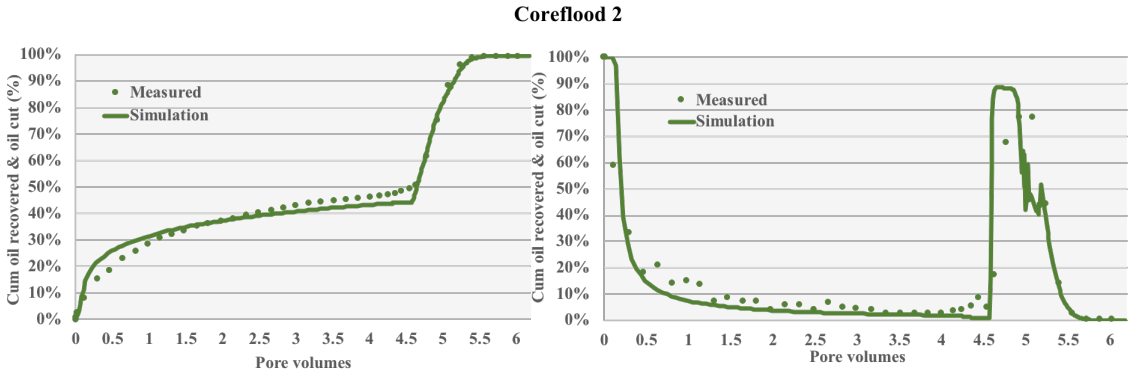

Figure 3-12: Coreflood 2 Oil Recovery (Left) and Oil Cut (Right) with Injected Pore Volumes

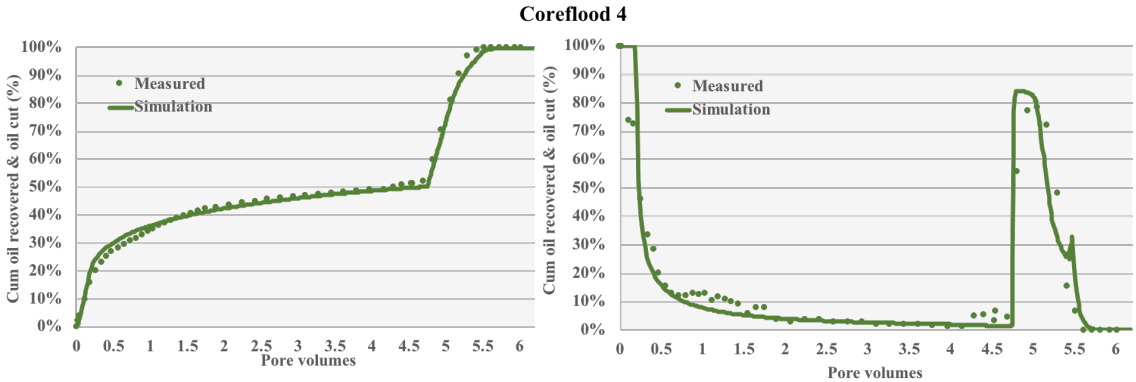

Figure 3-13: Coreflood 4 Oil Recovery (Left) and Oil Cut (Right) with Injected Pore Volumes

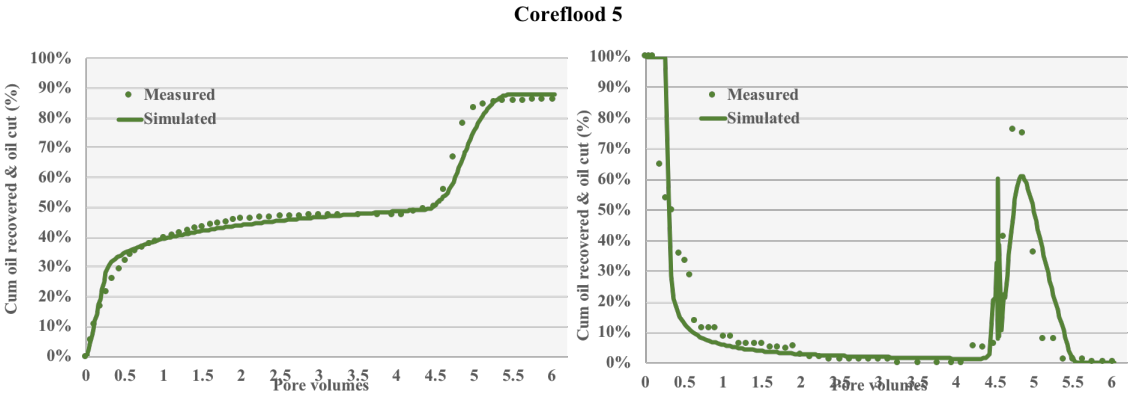

Figure 3-14: Coreflood 5 Oil Recovery (Left) and Oil Cut (Right) with Injected Pore Volumes

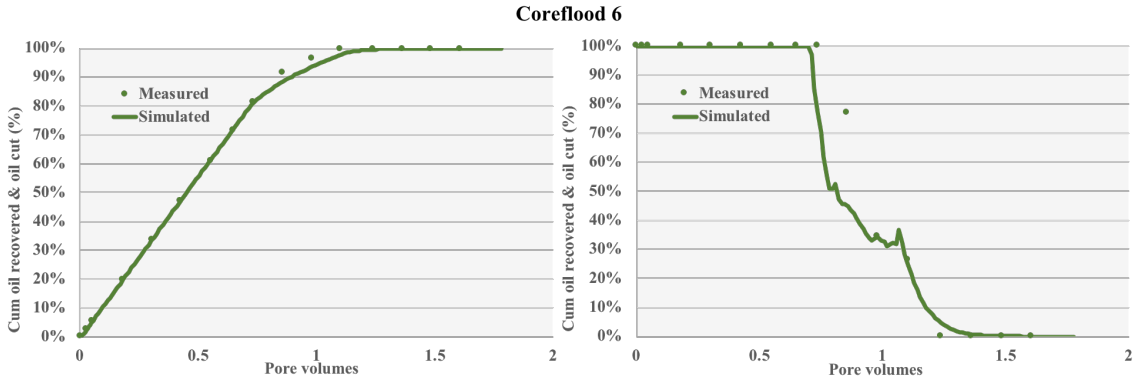

Figure 3-15: Coreflood 6 Oil Recovery (Left) and Oil Cut (Right) with Injected Pore Volumes

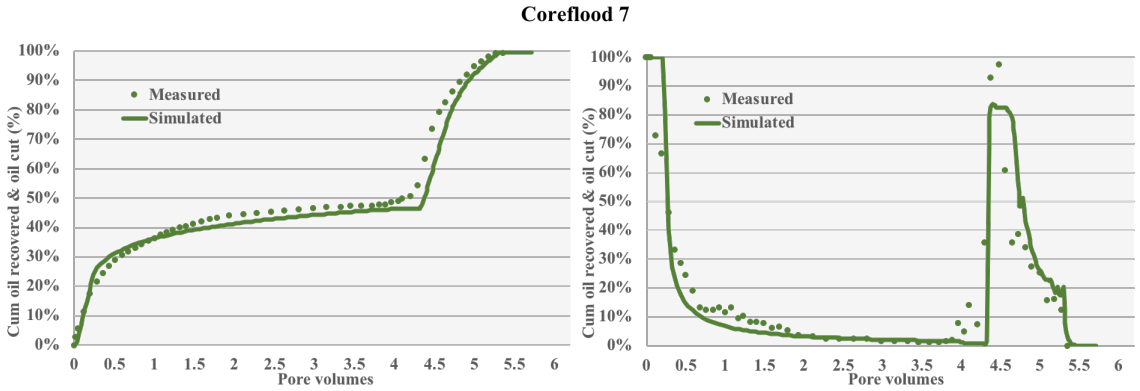

Figure 3-16: Coreflood 7 Oil Recovery (Left) and Oil Cut (Right) with Injected Pore Volumes

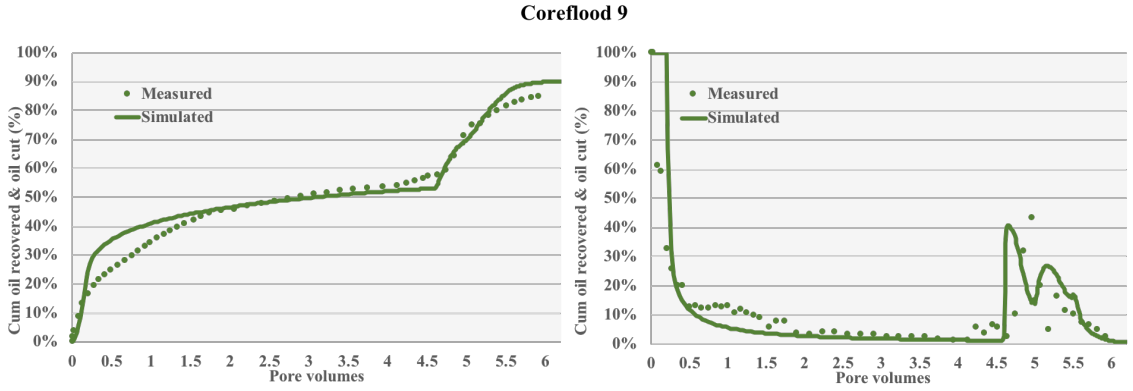

Figure 3-17: Coreflood 9 Oil Recovery (Left) and Oil Cut (Right) with Injected Pore Volumes

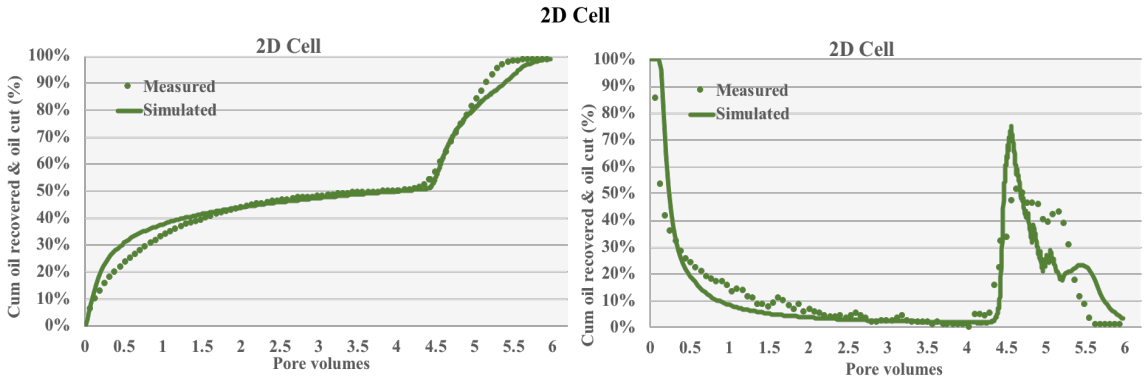

Figure 3-18: 2D Cell Oil Recovery (Left) and Oil Cut (Right) with Injected Pore Volumes

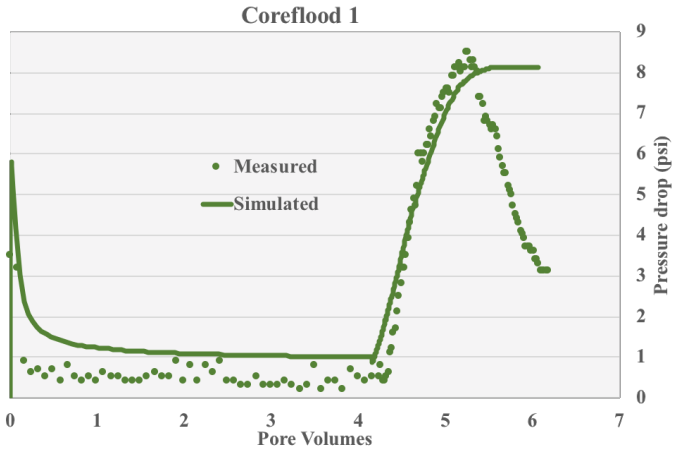

Figure 3-19: Measured and Simulated Pressure Drop for Coreflood 1

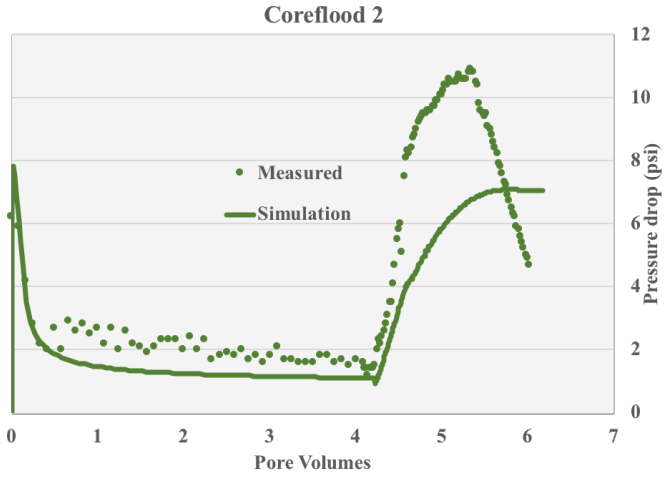

Figure 3-20: Measured and Simulated Pressure Drop for Coreflood 2

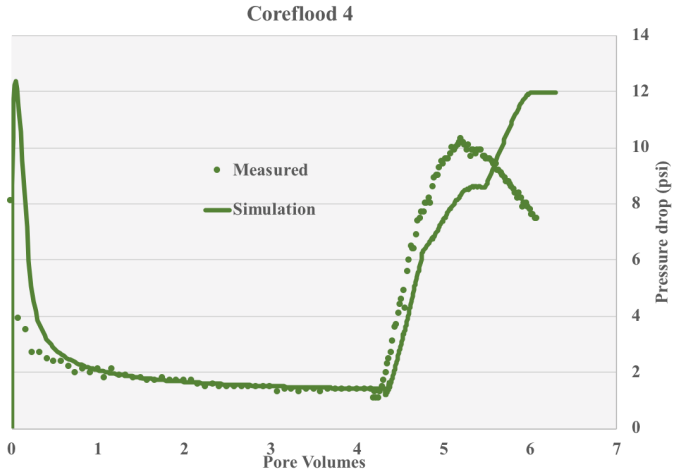

Figure 3-21: Measured and Simulated Pressure Drop for Coreflood 4

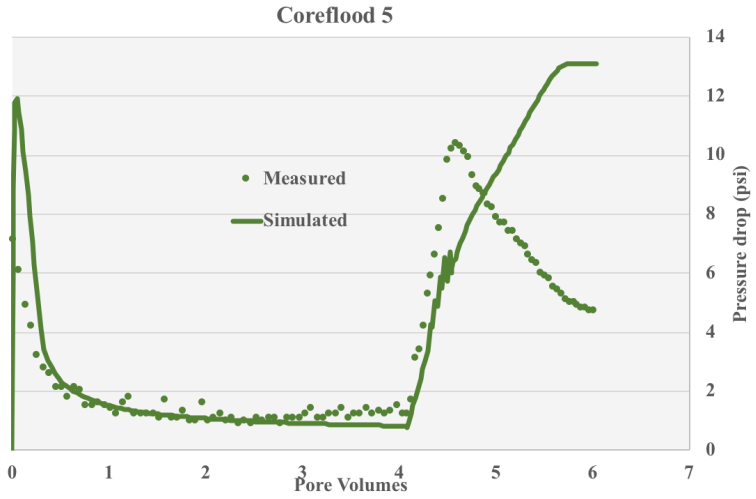

Figure 3-22: Measured and Simulated Pressure Drop for Coreflood 5

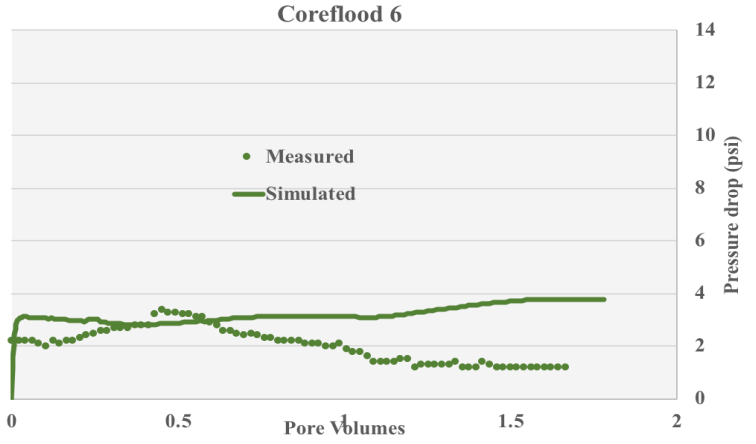

Figure 3-23: Measured and Simulated Pressure Drop for Coreflood 6

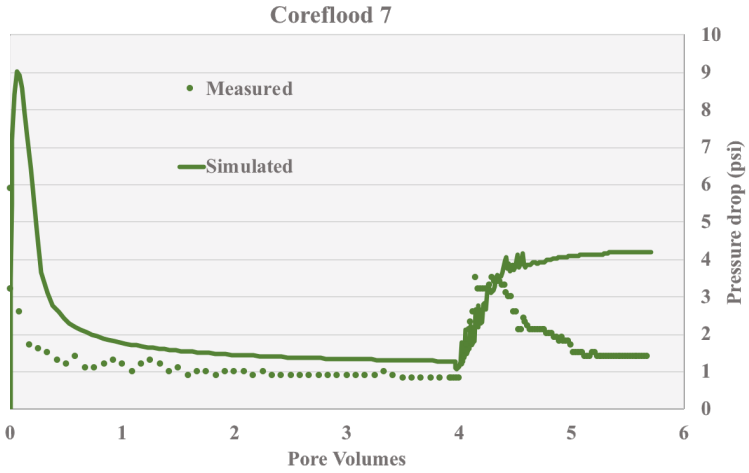

Figure 3-24: Measured and Simulated Pressure Drop for Coreflood 7

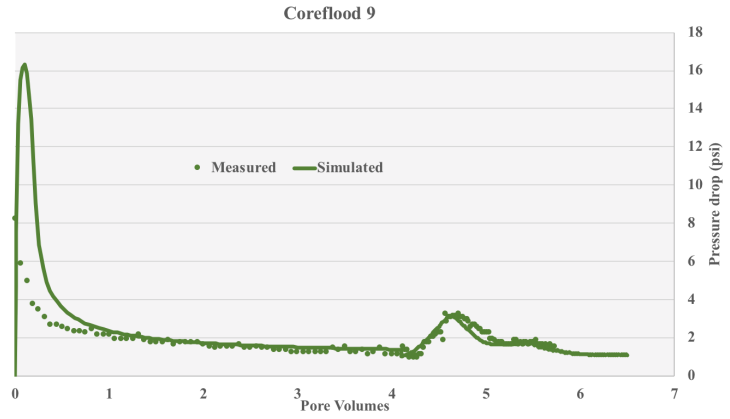

Figure 3-25: Measured and Simulated Pressure Drop for Coreflood 9

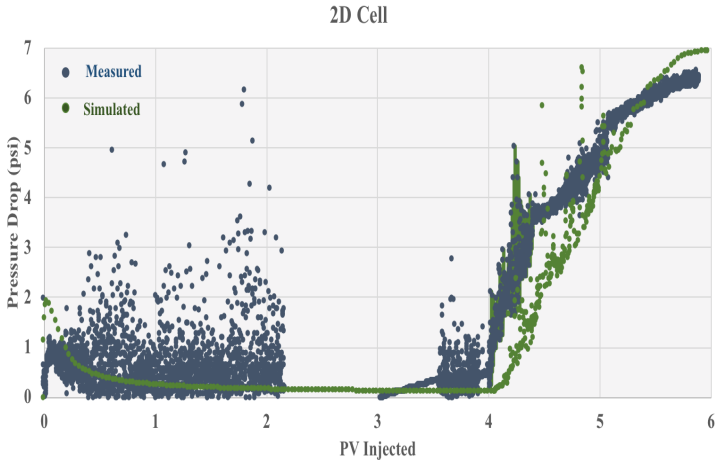

Figure 3-26: Measured and Simulated Pressure Drop for 2D Cell

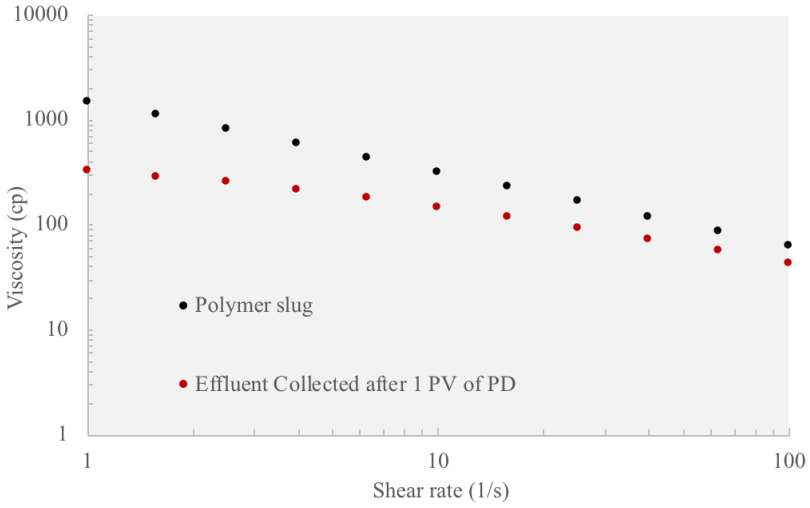

Figure 3-27: Polymer Viscosity Measurement Vs. Shear Rate of a Sample Collected after 1 PV of Polymer Drive Injection in Coreflood 5

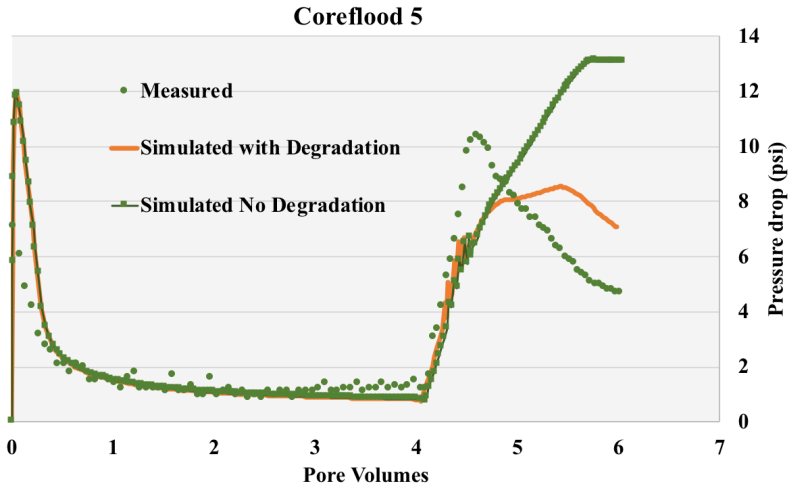

Figure 3-28: Measured and Simulated Pressure Drop for Coreflood 5 with Incorporating Polymer Degradation

3.6 COREFLOODS HM CONCLUSIONS

Based on the simulation results, some key parameters were derived by the history match and they are crucial to the designs of single well and multi well chemical tests discussed in the following two chapters 4 and 5. **Table 3-6** summarizes the history match inferred key parameters. Based on the history matching, the following is concluded:

- Numerical simulation models are developed in CMG-STARS to model 8 core floods. The models resulted in an excellent match with experimental oil recovery and oil cut.
- Pressure drop match indicated polymer degradation in some corefloods. Polymer protection package was not used in corefloods and are recommended for field pilots.
- Similar simulations results are observed between UTCHEM and CMG-STARS despite the big differences in the models.
- The importance of modeling corefloods is to establish basis for the polymer and surfactant models to apply these models (inputs) to the pilot design model

HM Key Parameters	Value
Capillary desaturation Curve parameters	**Low capillary number:** $DTRAPW$ -4 to -5 $DTRAPN$ -4 to -5 **High capillary number (surfactant present):** $DTRAPW$ -1.2 to -1.3 $DTRAPN$ -2 to -2.3
Rel. Perm at high capillary number	k_{rw}^{o}=1, k_{ro}^{o}=1 m=1, n=1 S_{or}=0
Surf. Conc. Vs. IFT	***Figure 3-6***
Polymer Shear rate vs. Viscosity	Lab measurements for 5000-9000 PPM

Table 3-6:Key Parameters Used in Corefloods And Design Models

Chapter 4: Single Well Chemical Test SWCT Design

This chapter presents an introduction to single well chemical tests, main features and theory behind it, followed by a discussion about the SWCT model construction and validation, design process and sensitivities. The chapter concludes with SWCT design remarks and recommendations.

4.1 INTRODUCTION AND OBJECTIVE

A robust characterization of reservoir properties is essential to the success of the enhanced oil recovery techniques. Tracer testing is a well-established technique and its success is demonstrated by various field applications for its capability in estimating reservoir heterogeneity and fluid saturations. Tracer testing can be either conducted as interwell tracer test (IWTT) or single well tracer test (SWTT). In the interwell tests, one or more injectors are tagged with unique tracers and production data is collected from one or more producers. Whereas in single well tests, only one borehole is needed for injection and extraction. The advantage of interwell tests over single well tests is their accessibility to larger areas of investigation which allows them to provide valuable data regarding reservoir heterogeneity. On the other hand, the area of investigation of the single well test is limited to near wells. However, the small area allows for relatively less testing time and less uncertainty with the test interpretation. The single well chemical tests have been accepted as a reliable technique of calculating the residual oil saturation. Although other S_{or} estimation methods are available including core analysis and well logging, these methods have their limitations and they generally represent measurement that is averaged over small volume of within only the vicinity of the well. The SWCT have the advantage of directly measuring in situ and to deeper extent compared to the conventional S_{or} determination methods. Due to its reliability and practicality, SWCT is predominantly used to measure

the oil saturation and assess performance of the EOR technique before commencing the field scale implementation. It could also be used with the purpose of accurately estimating the original oil in place.

The adopted design philosophy is that SWCT is needed to confirm the efficacy of the chemicals in field conditions prior to larger scale applications, and also to determine the residual oil saturation to chemicals. The objective of the work presented in this chapter is to design a single well chemical test incorporating the polymer and surfactant models described in the previous chapter. The design is constructed by determining the (i) surfactant-polymer SP slug sizes and concentrations for desired residual saturation, and (ii) optimum parameters for time saving and appropriate test interpretations.

4.2 SWCT Literature Review

4.2.1 Development of SWCT

The single well test method was first patented by Deans (1971) and has been applied in numerous fields to determine the residual oil saturation to waterflood. The method includes injecting a reactant tracer in water into a well where the oil saturation is at the residual to waterflood. The oil phase is essentially immobile. The reactant tracer, miscible in the mobile water phase, reacts with the water to produce two tracers with different partition coefficients, of which one tracer has negligible solubility in the immobile oil phase. Measurable quantities of both tracers should be produced by the reactant. the flow direction is then reversed by allowing the tracers to be produced from the same injection location. By measuring the produced volumes that correspond to the maximum concentrations of each detected tracer, the fluid saturations can be determined by applying the principles of chromatography.

Cooke (1971) proposed a method that entails injecting two tracers with different partition coefficients in a well and producing the tracers from another location (well). The tracers are assumed to be substantially soluble in one mobile phase with little solubility in the remaining immobile phases. Each of these tracers is retarded in their transport through the reservoir based on their partition coefficient. The separation in the production of the tracers is related to the quantity of mobile and immobile fluids. Monitoring and detecting both tracers in different location is important for the chromatographic analytical technique, where relative differences in the quantity of fluids between the two locations are proportional to the fluids' saturation. This technique can also be applied in a single well with two different vertically spaced perforated zones. However, when the flow direction in this single well method is reversed, the tracer curves separation can dissipate, which makes the measurement of S_{or} not possible. Tomich *et al.* (1973) resolves the issue of the reversibility as the method involves the irreversible chemical reaction (hydrolysis) of producing in situ a second tracer that has negligible to no solubility in the immobile phase.

Deans and Shallenberger (1974) expanded on the Tomich *et al.* (1973) method and suggested a SWCT to estimate the connate water saturation. Using the same principle in estimating the S_{or}, the method employs injecting crude oil that contains tracer in a formation where water is the immobile fluid. Bragg *et al.* (1976) used the SWCT to estimate the residual gas saturation in a water invaded locations in gas reservoirs. Tomich and Dean (1975) patented another method of single well tracer test that estimates the residual oil saturation; however instead of relying on the tracers' chemical reactions, the separation of the tracer profiles is due to the fluid drift.

Descant (1989) used single well test to estimate the wettability by injecting tracer-containing reservoir brine and tracer-containing reservoir oil, separately in a sequential manner. The test is supported by monitoring the bottom hole pressure and water cuts.

Ferreira (1992a,1992b) expanded Descant's work by developing a single well wettability test that allows, in addition to wettability estimation, simultaneous determination of oil, water saturations and relative permeability parameters by applying history matching to the tracer data.

Tian *et al.* (2019) introduced a new procedure for the SWCT by excluding the assumption of immobile oil phase. The SWCT relies on the assumption that the oil phase is essentially immobile in the investigated area. Tian *et al.* (2019) omit this assumption to improve the accuracy of the SWCT calculation by considering two mobile phase flow. Their work modifies the calculation of the method of moments (MOM) and introduces a ratio parameter to the calculation of produced volumes. In addition, injection of a mixture of water and oil is required for this SWCT. This method has been tested against synthetic numerical simulations. It was concluded that the proposed simultaneous injection of oil and water in the field is prone to operational and stability issues.

Sheely and Baldwin (1982) were the first to use the SWCT to estimate the EOR process by utilizing multiple SWCTs and multiple reactant tracers with different partition coefficients. Three different tracers were injected after the surfactant slug to measure the average oil saturation at different distances away from the wellbore. Their work addresses the assumption of constant residual saturation; constant S_{or} is not valid with the presence of surfactant. Surfactant produces a distribution of residual saturation of approximately zero near the wellbore and a value of S_{or} close to the residual to waterflood at a distance away from the wellbore. However, the calculation is still valid if the volumetric average is considered in the calculations. Many SWCT applications have been conducted in the field to assess the efficacy of EOR methods: SWCT after miscible gas injection (Cockin *et al.,* 2000), after low salinity flood (McGuire *et al.,* 2005; Al-Shalabi *et al.,*2015), and after

surfactant polymer (Hernandez *et al.,* 2002; Jerauld *et al.,* 2010; Oyemade, 2010; Carlisle *et al.,* 2014; Fortenberry *et al.*, 2016).

4.2.2 Theoretical Basis for Calculating S_{or}

The assumptions of this tracer model include: (i) fluids are incompressible, (ii) oil phase is immobile (at residual), (iii) the chemical reaction occurs only in the aqueous phase, (iv) equilibrium mass transfer, (v) tracer mass flux is small compared to the water flow rate, and finally (vi) formation is homogenous and isotropic (Tomich *et al.*, 1973). The method depends on chromatographic retardation of the partitioning tracer which is described by Tomich *et al.* (1973) and Deans and Carlisle (2006). Assuming the water is moving with a velocity ν_w, and oil moving with a velocity ν_o, the velocity of the tracer is:

$$v_i = v_w f_{w_i} + v_o\left(1 - f_{w_i}\right) \tag{4.2.1}$$

where f_{w_i} represents the fraction of the tracer in the water phase. Because oil is at residual saturation, v_o equals to zero. When the water velocity is very small, the tracer molecule partitioning between the two phases (oil and water) is assumed to be near equilibrium, thus:

$$\frac{1 - f_{wi}}{f_{wi}} = \frac{K\, S_{or}}{1 - S_{or}} = \beta \tag{4.2.2}$$

where K is the partition coefficient of the tracer and it is the ratio of the tracer concentration in the oil phase to the concentration in the water phase. Replacing f_{wi} in **Eqn. 4.2.1** by the expression in **Eqn. 4.2.2** yields:

$$v_i = \frac{v_w}{1 + \beta} \tag{4.2.3}$$

Rearranging the equation above:

$$\beta = \frac{v_w}{v_i} - 1 \tag{4.2.4}$$

where β is referred to as the retardation factor. The number of tracer molecules in water and oil respectively, in a control volume is given as below:

$$n_{i_w} = C_{i_w} S_w V_c \tag{4.2.5}$$

$$n_{i_o} = C_{i_o} S_{or} V_c \tag{4.2.6}$$

where C_{i_w} and C_{i_o} refer to the equilibrium molecules per unit volume concentration of tracer in water and oil, respectively. S_w is the saturation of water. And V_c is the control volume in which the partition of tracer between the phases is assumed to be at equilibrium.

The retardation factor is determined by

$$\beta = \frac{n_{i_o}}{n_{i_w}} \tag{4.2.7}$$

Adding the above expression in **Eqns. 4.2.5** and **4.2.6** yields

$$\beta = \frac{C_{io} S_{or}}{C_{iw} S_w} \tag{4.2.8}$$

The partition coefficient of tracer is given by

$$K = \frac{C_{io}}{C_{iw}} \tag{4.2.9}$$

Substituting the above expression in **Eqn. 4.2.8** gives

$$\beta = \frac{K\, S_{or}}{1 - S_{or}} \tag{4.2.10}$$

Rearranging the above expression, we can calculate for the residual saturation:

$$S_{or} = \frac{\beta}{\beta + K} \tag{4.2.11}$$

The fluid volume produced at the time the reactive tracer concentration is peaked Q_A is related to the quantity of fluid produced at the time the second (product non-

partitioning) tracer concentration is peaked Q_B by the following, (by using **Eqn. 4.2.3** and **4.2.4**):

$$Q_A = Q_B(1+\beta) \tag{4.2.12}$$

Eqn. 4.1.11 can be written as:

$$S_{or} = \frac{\beta}{\beta + K} = \frac{\frac{Q_A}{Q_B} - 1}{\frac{Q_A}{Q_B} - 1 + K} \tag{4.2.13}$$

This expression is used in estimating the residual oil saturation, S_{or}.

4.2.3 Features of SWCT

As described by many authors (Deans, 1971; Deans and Carlisle, 2006), the procedure for conducting the SWCT is generally outlined as follows:

1. Laboratory measurement of partition coefficient of desired tracer should be conducted prior to the test using reservoir conditions. A desired partitioning tracer (or ester) is recommended to have a retardation factor β within the range of 0.5-1.5, which means the partition coefficient of the tracer should be in the range shown below (Deans and Majoros, 1980):

$$\frac{0.5\ (1 - S_{or})}{S_{or}} < K < \frac{1{,}5\ (1 - S_{or})}{S_{or}}$$

2. The investigated zone should be watered out. The candidate well for the test should produce only water. Oil is essentially immobile around the wellbore as in **Figure 4-1a**. If well produces some oil, water is injected for some amount of time (preflush) to displace the oil and reach the S_{or}.
3. The tracer (usually an ester) is injected in the wellbore. As the ester is in injected it starts partitioning to the oil based on its partition coefficient.

Thus, the ester moves at a velocity lower than the flowing water because oil is stationary.

4. A push fluid, or water is injected to push the ester containing water further away from the wellbore to cover a larger volume and produce clear tracer profiles. **Figure 4-1b**.
5. The well is shut-in for "soaking" period to allow the ester's reaction with water to form the product tracer (alcohol). The shut-in period depends on the reaction rate of the reactant tracer. Measurable amounts of product tracer should be produced. **Figure 4-1c.** The reactant tracer reaction with water produces alcohol and acid; Ester + H_2O = alcohol + acid.
6. The well is opened for production and both tracers, remaining ester and product alcohol, are flowed back to the wellbore. Because the alcohol has essentially negligible solubility in the oil, it flows at velocity faster than the ester and is approximately equal to the velocity of water. The ester is retarded and thus flows back at a lower velocity, **Figure 4-1d**. The chromatographic separation in the produced tracer profiles then allows for the estimation of the residual oil saturation.

This is generally the procedure of the SWCT. When using the test to evaluate the EOR technique (ASP/ SP... etc.), this test might be repeated; conducting test prior to chemical injection to establish S_{or} to waterflood. After the EOR is applied, the test can be repeated to assess the S_{or} to the injected chemicals.

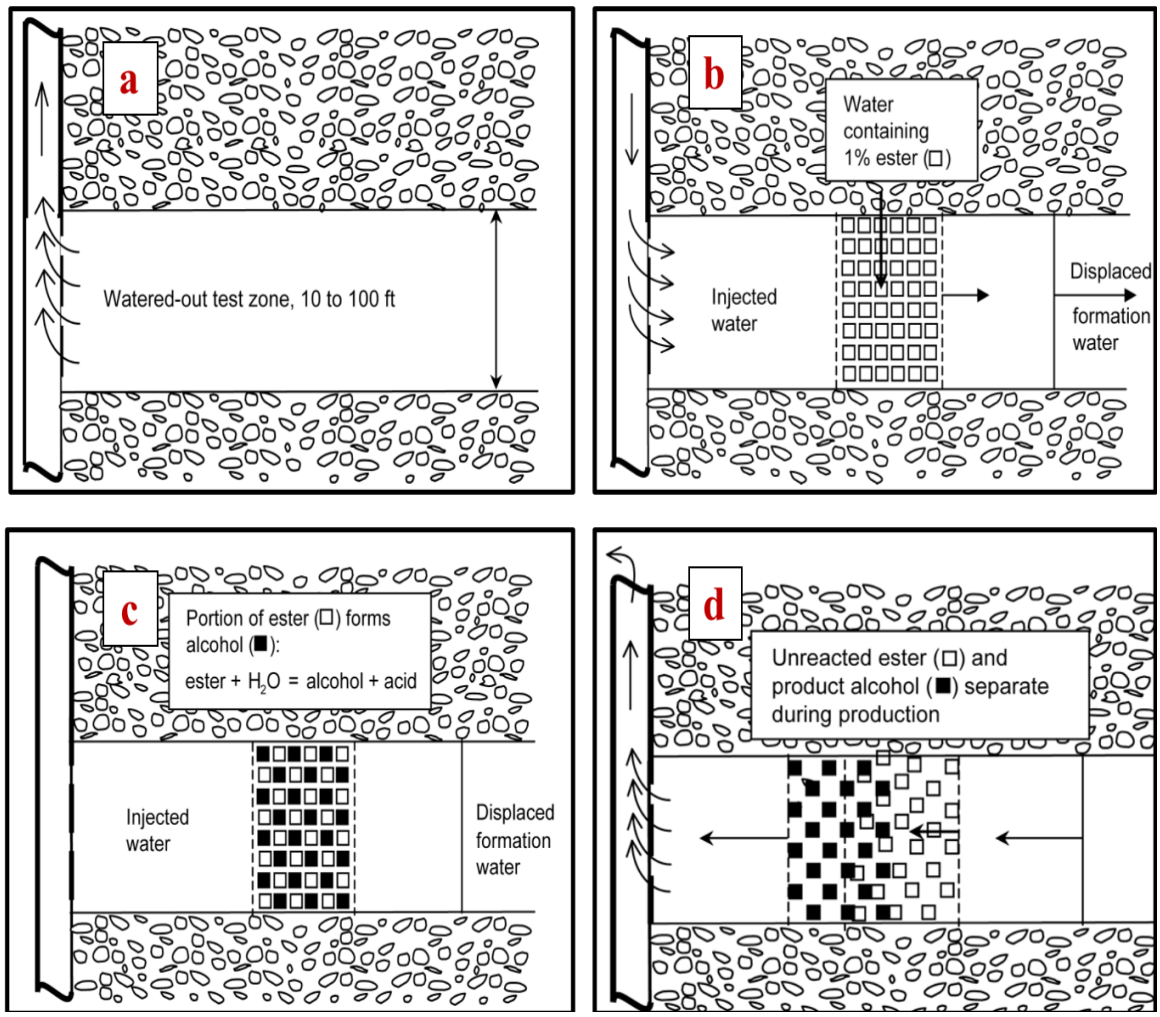

Figure 4-1: Schematics of SWCT Procedure a) Zone Is At Residual Oil Saturation, Water Is The Only Mobile Phase b) Ester Is Injected Followed By Chase Fluid c) Shut In "Soak" Period To Allow Ester Reaction To Form Alcohol d) Both Ester And Alcohol Flow Back To The Well At Different Velocities (Deans and Carlisle, 2006).

4.3 Model Construction and Validation

4.3.1 Field Pilot Area

The field pilot area has been proposed on the basis of well and reservoir properties; the existing 5-spot area has 4 injectors and 1 central producer; the wells are in a close proximity to each other which allows for faster interpretations of the test. The 5-spot area

is 150 m x 150 m, the producer is 70 m away from each injector. The area has good quality of reservoir in terms of porosity and permeability; with permeability ranging 1000-10000 mD and porosity ranging 15%-26%. **Figure 4-2** shows a top and a 3D view of the 5-spot area. As depicted in the figure, the area contains multiple layers.

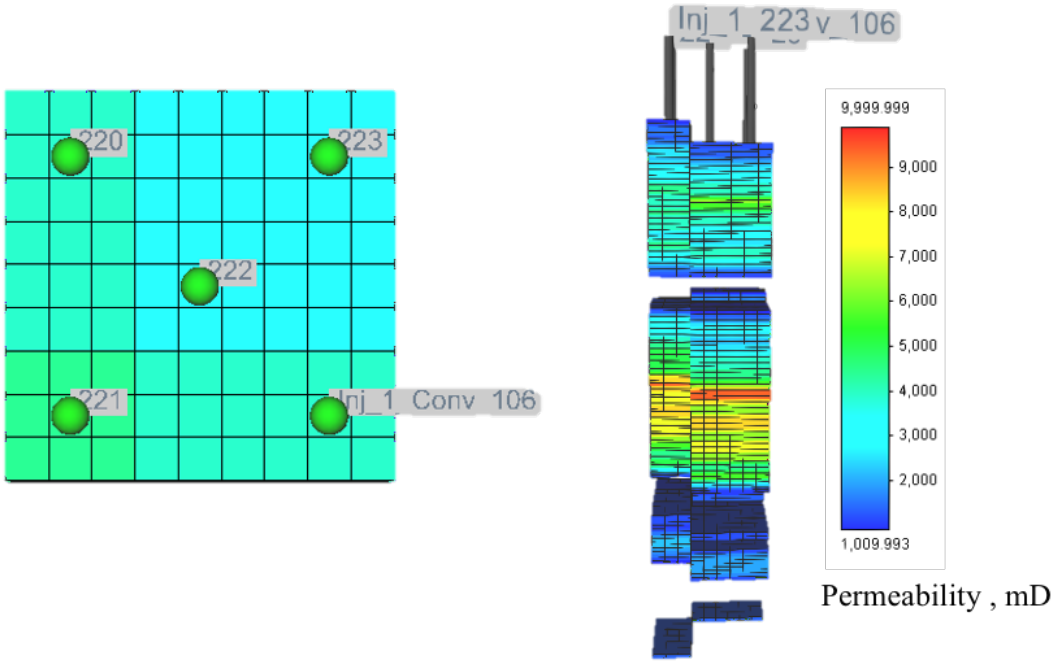

Figure 4-2: Field 5-Spot Area Areal View (Left) 3D View Of The Permeability Distribution In The Area (Right)

4.3.2 Grids Setup

To reduce simulation time, a single well radial model has been constructed by mimicking the properties of the one well from the 5-spot pilot area of the field model. The model assumes a constant initial oil saturation that is equal to the residual saturation of 33% to waterflood. There are 4 wells in the model: two at the center and two boundary wells. The two wells at each point mimic injection and production at the point, respectively. The wells at the boundary act as the opposite of the center wells; they are included to avoid

pressure buildup. Well locations are shown in **Figure 4-3** The figure also shows the model is constructed radially with small grid sizes near with wellbore and gradually increasing further away from the well. The model captures the vertical permeability variation presented in the field's original model as shown in **Figure 4-4 ,**which represents the permeability distribution of the case, the ratio of the vertical to horizontal permeability is 1**.** Similar to the original field model, the single well model contains three main sand layers, of which is the top layer, where the well is currently perforated, is the interest in our work, as shown in **Figure 4-5.** The pore volume of interest is the pore volume of 8 m radius and 6 m thickness (thickness of the layer where the well is perforated as depicted in **Figure 4-5. Table 4-1** summarizes the model parameters for the SWCT.

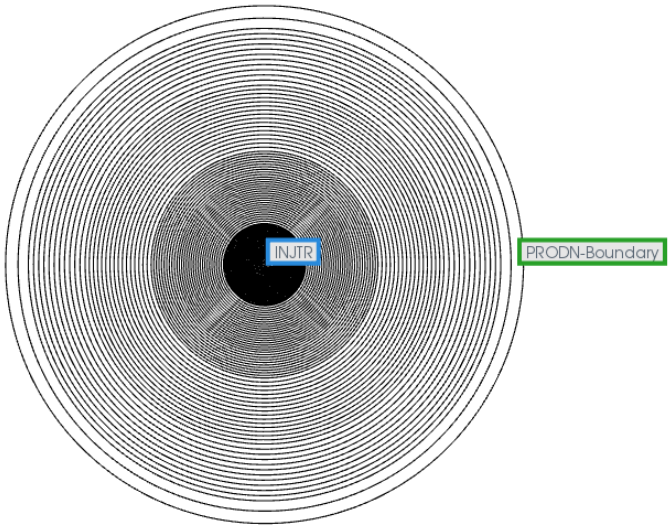

Figure 4-3: Areal Top View of the Grids Setup and Wells Locations

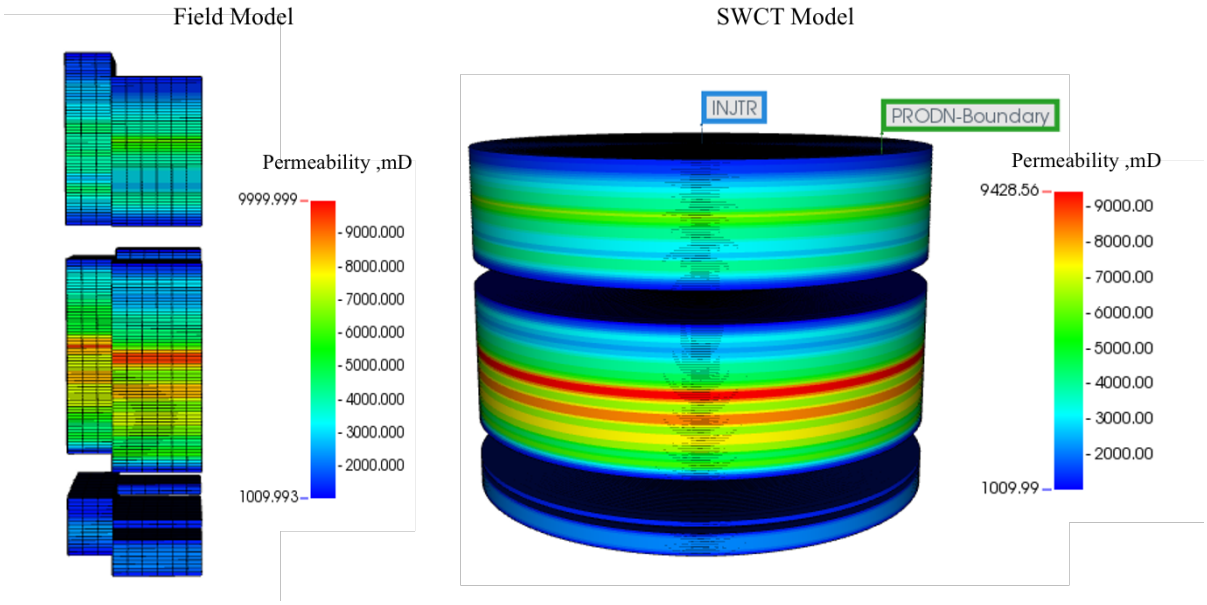

Figure 4-4: Permeability Distribution of The Radial SWCT Model. Permeability in the 5-Spot Are from The Field Model (Left), SWCT (Right)

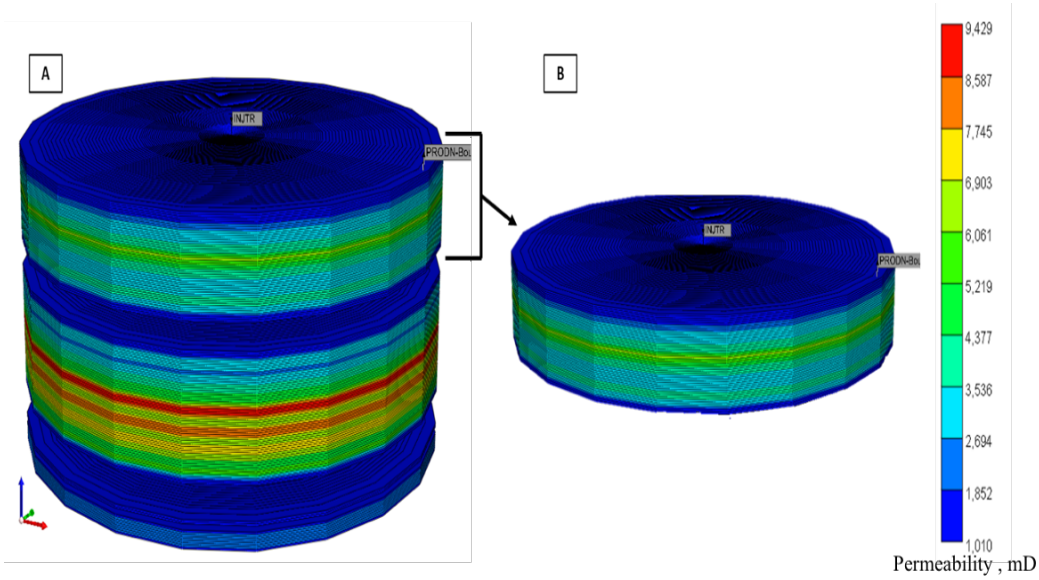

Figure 4-5: Permeability Distribution of The Radial SWCT Model A) Showing All Layers of The Model B) The Top Layer of Interest

Model Parameter	Value
Number of grids	100*1*153
Grid size	r= variable, =360, z= variable
Grid Type	Radial
Outer Radius, m	25
Thickness, m	24
Pore Volume, m^3	8608
Pore Volume of Interest, m^3	302
Oil Saturation	0.33
Permeability	Variable
Porosity	Variable

Table 4-1: Summary of Model Grid Setup Parameters

4.3.3 Tracers and Chemical Reaction

The partitioning tracer used is Ethyl acetate (Etac): the reactive tracer that partitions to oil, and it is a commonly used tracer in similar applications. N-Propyl alcohol (NPA): used as a cover tracer to confirm the shape of the reactive tracer in cases of extreme hydrolysis and drift. Iso-Propyl alcohol (IPA): usually injected during tracer injection and push volume injection, it is a non-reactive material balance tracer. Ideally before test implementation, laboratory measurement of the tracer properties should be conducted for compatibility and to determine partitioning and reaction rate data. The partition coefficient varies depending on the reservoir fluid properties and temperature. For the purposes of our work, the partition coefficient of the ethyl acetate is assumed to equal to 2 at reservoir conditions, which is within the range of 2-6.5 reported by other authors (Tomich *et al.,* 1973; Deans and Carlisle, 2006 ; Carlisle *et al.,* 2014; Al-Shalabi *et al.*, 2015; Fortenberry *et al.,* 2016). The injected and product chemical tracers are summarized in **Table 4-2**.

The chemical reaction of the tracers is crucial to the test performance. The hydrolysis of the ester is shown in **Eqn. 4.3.1** below, where *x* is the stoichiometric coefficient required to balance the equation.

$$x\ CH_3CO_2[C_nH_{2n+1}] + x\ H_2O \rightarrow x\ C_nH_{2n+1}OH + x\ CH_3COOH \quad (4.3.1)$$

The reaction is modeled in CMG by the following equation:

$$rf = rrf\ e^{-\frac{E_a}{T_{abs}R}} \Pi c_i \quad (4.3.2)$$

where rrf is reaction coefficient, E_a is the activation energy, T_{abs_a} is the absolute temperature, R is the universal gas constant, Πc_i is product of concentrations of the reacting components. The input of this reaction is the stoichiometric coefficients of the reactants and products, and the reaction parameters. The stoichiometric coefficients for the reaction of the ethyl acetate are equal to 1. As for the reaction coefficient, it is expected the higher value will yield in the reaction occurring more frequently, thus more ethanol would be produced and less ethyl acetate would be recovered. The values chosen in these runs were based on the magnitude seen in similar numbers from the literature (Deans and Ghosh, 1994). The value of this is commonly determined through history matching, in our case the value is assumed to be 2.40E^{-05} (input of rrf.) The unit of this varies in CMG based on the type of the reaction. In this case, the units are gmol m^{-3} day^{-1}.

Tracer	Tracer Objective	Concentration, ppm	Partition Coefficient
Ethyl-Acetate (Etac)	Reactive tracer	10000	2
Ethanol	Product tracer	-	-
Normal Propyl Alcohol (NPA)	Cover tracer	2000	-
Isopropyl Alcohol (IPA)	Material balance tracer	5000	-

Table 4-2: Summary of The Types and Concentrations of Injected and Produced Tracers

4.3.4 Homogenous SWCT Model

Numerical methods have been used by Tomich *et al.* (1973) and Deans and Carlisle (2006) to determine the residual oil saturation in which the S_{or} is determined by achieving the best fit with the produced tracer data. The analytical method yields accurate calculations in homogenous systems; therefore, a homogeneous radial model SWTT case was constructed to confirm the validity of the model. The S_{or} of the model is given and assumed constant to be compared against the analytically calculated residual oil saturation. Based on the assumptions mentioned in section 4.2.2, there should be a very close agreement between the calculated and simulated S_{or}. The homogenous case grid and permeability distribution is shown in **Figure 4-6**. The case has porosity of 25% and permeability of 3500 mD.

The homogeneous case procedure details are presented in **Table 4-3.** The injection and production rates of the well are 150 m^3/d. The simulated stages of the test included 0.1 days of tracers injection (0.05 of PV of interest), 0.4 days of push water to push the tracers away from the wellbore (0.2 PV), soak in period of 4 days to allow the hydrolysis of Etac, and finally the well is flowed back for 5.5 days. The tracer curves as a function of produced volume are shown in **Figure 4-7**. The residual calculation is calculated using the produced reservoir fluid volumes at each tracer peak as was shown in **Eqn. 4.2.13**. Comparison between the model input S_{or} (0.33) and analytical calculation is shown in **Table 4-4.** The analytical calculation result in S_{or} = 0.328, thus the error is approximately -0.479%. This shows that there is a good agreement between the simulation model and the analytically calculated S_{or}.

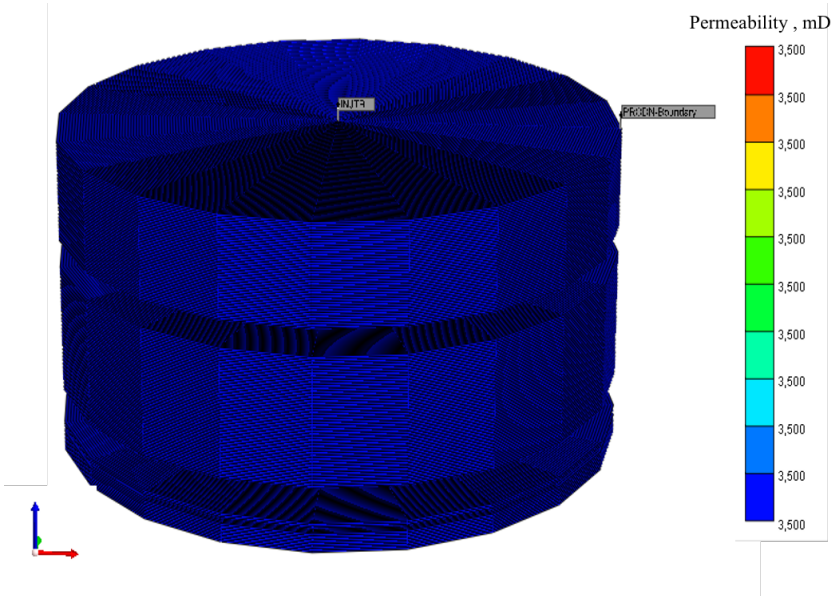

Figure 4-6: Homogenous Permeability Field for The Validation Model

Homogeneous Case Details	
Injection Rate, m^3/day	150
Production Rate, m^3/day	150
Etac Concentration, ppm	10000
Etac injected, m^3	0.166
Etac Recovered, m^3	0.138
Etac recovery, %	83%
Stage	**Duration, days**
Tracers injection	0.1
Push Water	0.4
Shut in	4
Production	5.5

Table 4-3:Details of Homogenous Case Injection and Sequence

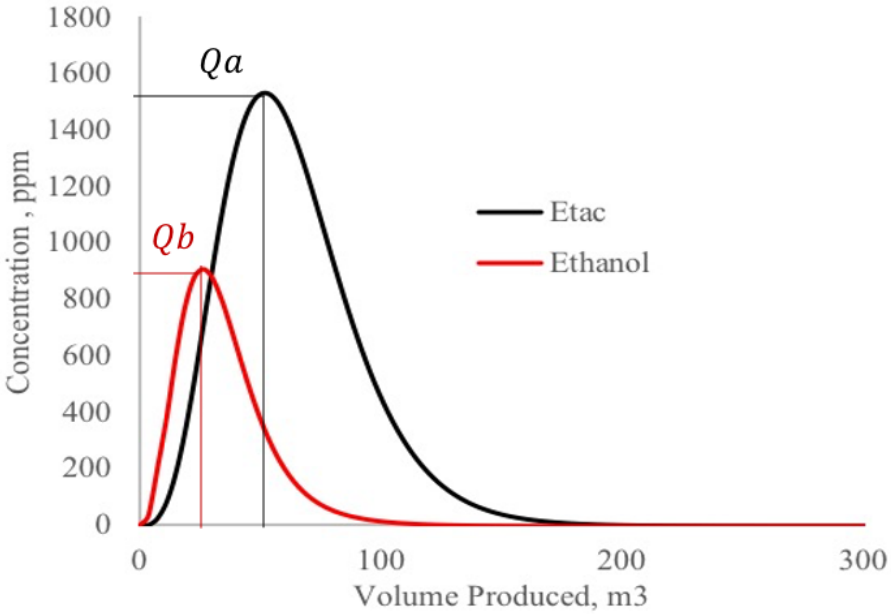

Figure 4-7: Reactant Tracer (Etac) And Product Tracer (Ethanol) Produced Concentrations for The Homogenous Case

Case	Etac Peak Volume, m^3	Alcohol Peak Volume, m^3	Analytical S_{or}	Simulation S_{or}	Error, %
homogeneous	26.84	53.09	0.328	0.33	-0.479%

Table 4-4: Comparison Between Simulation Input S_{or} And Analytical S_{or}

4.3.5 Model Uncertainties:

- Dispersion, drift, dilution: No dispersion is accounted for in the models. The values could be assumed during the history match process.
- Tracers reaction rates: Reaction rate is assumed in the model but is within a reasonable range. The exact value requires lab testing the tracer; however, the assumed value produces sufficient hydrolysis in a reasonable amount of time.

4.4 SWCT Design Workflow

Figure 4-8 shows the key parameters that were evaluated for the design of the SWCT. The process entailed analyzing the effect of SP slug size, polymer concentration,

tracer and push volumes, and well rates with two polymers, i.e., FP3630 (used in corefloods) and polymer defined in the original field CMG file provided by the operator of the field, referred to herein as polymer 1. All the sensitivities are conducted using CMG-STARS. Based on the sensitivity results, optimum design parameters are hence recommended.

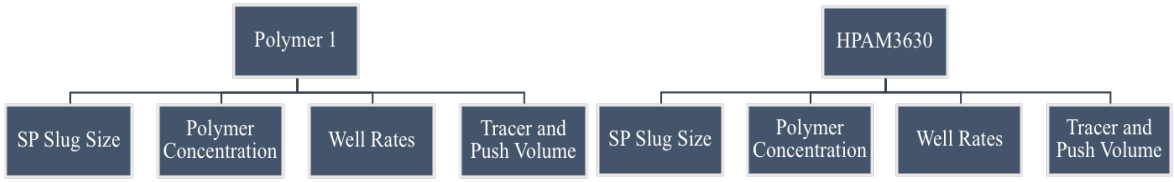

Figure 4-8: SWCT Sensitivity Key Parameters

4.4.1 Summary of SWCT Sensitivity Cases

A total number of 78 sensitivity cases were run to evaluate the impact of different factors and determine optimum design parameters; **Table 4-5** lists the simulation cases. The PV in the table corresponds to 302 m^3, which is the pore volume of interest for a layer thickness of 6 m and radius of 8 m. Every parameter was evaluated for two polymer descriptions while keeping all other parameters fixed.

Sensitivity Parameters			
Polymer	**Tracer size, days**	**Push size, days**	**No. of Cases**
Polymer 1	0.05,0.1,0.15,0.20,0.25,0.30	0.4, 0.6, 0.7 ,0.9 ,1	30
FP3630	0.05,0.1,0.15,0.20,0.25,0.30	0.4,0.7,1	18
Polymer	**Concentrations, ppm**		**No. of Cases**
Polymer 1/ FP3630	1500, 2500, 5000, 8000		8
Polymer	**Rate, m^3/day**		**No. of Cases**
Polymer 1/ FP3630	10,15,20,30,40,50		12
Polymer	**SP size, PV**		**No. of Cases**
Polymer 1/ FP3630	0.01,0.05,0.1,0.20,0.30		10

Table 4-5:SWCT Sensitivity Cases Setup Summary

Table 4-6 summarizes the two step SWCT adopted in this work. The table shows the injection sequence and duration in SWCT:

- Step 1: Usually this step includes a preflush, which is a waterflood to displace the oil around the wellbore and reduce it to residual saturation. Since the pilot area has undergone polymer flood in the field, the oil saturation in our model initial conditions is at residual, so the preflush was not necessary. Instead, the tracer slug is injected, and different sizes are evaluated during the sensitivity.
- Step 2: Injection of water with IPA tracer. This step pushes the injected tracers away from the wellbore to increase the investigated radius and allows for clear tracer production profiles. The IPA is injected as it could help in identifying dilution issues. Different sizes of push volumes are evaluated during the sensitivity.
- Step 3: The well is shut in to allow the hydrolysis of the Etac to produce measurable amounts of Ethanol. Depending on the reactivity of the reactant tracer and the reservoir conditions, the soak in period is usually between 1-10 days (Deans and Carlisle ,2006). The shut-in period in our design is 4 days.
- Step 4: The well is open for production. Tracer profiles are analyzed and S_{or} to waterflood is determined.
- Step 5: SP is injected to further reduce the S_{or} below the residual to waterflood. Different sizes of SP are evaluated during the sensitivity.

Steps 1 through 4 are then repeated to measure the S_{or} after the SP injection. All the tracer tests are conducted with polymers during tracer injection to minimize the impact of fingering which might occur during displacements of viscous oils.

Stage	Operation	Duration, days
1	Tracers injection (Etac, IPA, NPA)	Varies
2	Push Water (IPA)	Varies
3	Shut in	4
4	Production	5
5	SP injection	Varies
6	2nd Tracers injection (Etac, IPA, NPA)	Varies
7	2nd Push Water (IPA)	Varies
8	2nd Shut in	4
9	Production	5

Table 4-6: Two Step SWCT Injection Sequence Used in the Sensitivity Runs

4.5 SWCT SENSITIVITY RESULTS

4.5.1 Polymer Concentration Sensitivity

Each polymer was simulated at 4 concentrations: 1500,2500,5000 and 8000 ppm, with the same SP slug size of 0.2 PV. For polymer#1 (defined in the field case) the fixed push and tracer sizes at different concentrations were 0.7 days and 0.15 days, respectively. For FP3630 cases, the fixed push and tracer sizes were 1 day and 0.15 days, respectively. The produced tracer curves were analyzed to calculate the S_{or} before and after SP slug, as shown in **Figure 4-9** and **Figure 4-10**, respectively. For both polymers, the calculated residual oil saturation shows a decrease with increasing polymer concentrations although no surfactant was injected yet. At relatively low concentrations (1500-2500 ppm), the calculated S_{or} is in the margin of up to 20% error with model input S_{or} of 0.33. At higher concentrations, further noticeable decrease of S_{or} is observed. This is due to high concentrations exerting high pressure gradients resulting in high capillary numbers, as evident from the model, an increase of capillary number from $3.33*10^{-12}$ to 0.002 was observed, consequently reducing the saturation few meters away from the wellbore. **Figure 4-11** shows r-z 2D view of oil saturation before SP injection at different FP3630

concentrations. The figure shows the reduction in oil saturation below residual occurred for up to 3 meters away from wellbore when concentration was high (8000 ppm) as compared to low concentration (1500 ppm). The calculated S_{or} after SP injection shows a significant decrease in saturation to below 10%, and it could be inferred from the results that the high polymer concentrations also contributed to lower oil saturation in addition to the impact of surfactant. **Table 4-7** summarizes the S_{or} calculations of both polymers, and shows approximate distance traveled by Etac.

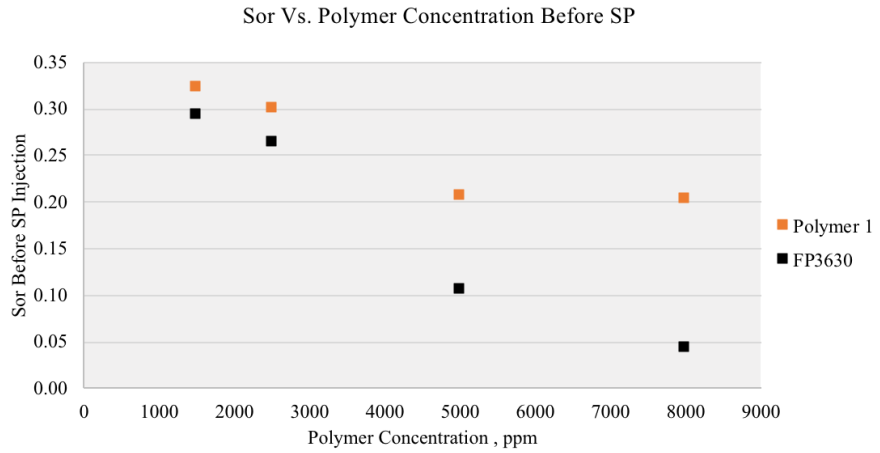

Figure 4-9: Calculated S_{or} Before SP Injection for Both Polymers

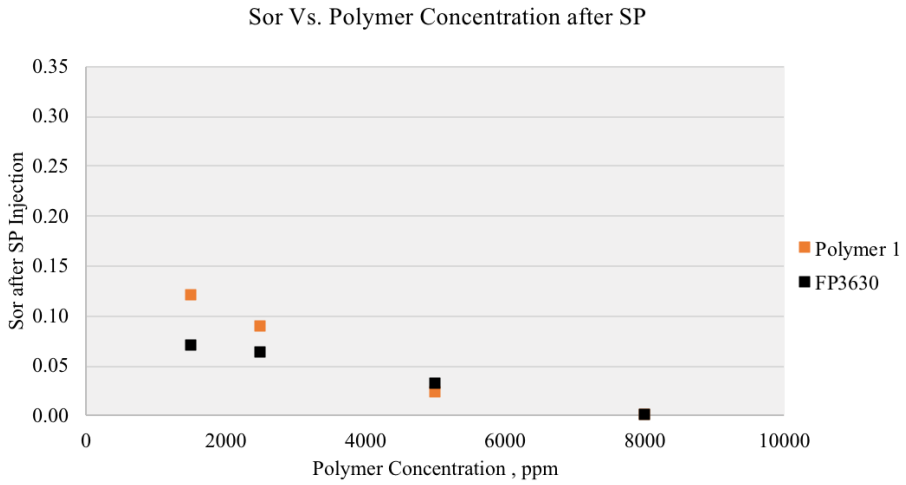

Figure 4-10: Calculated S_{or} after SP Injection for Both Polymers

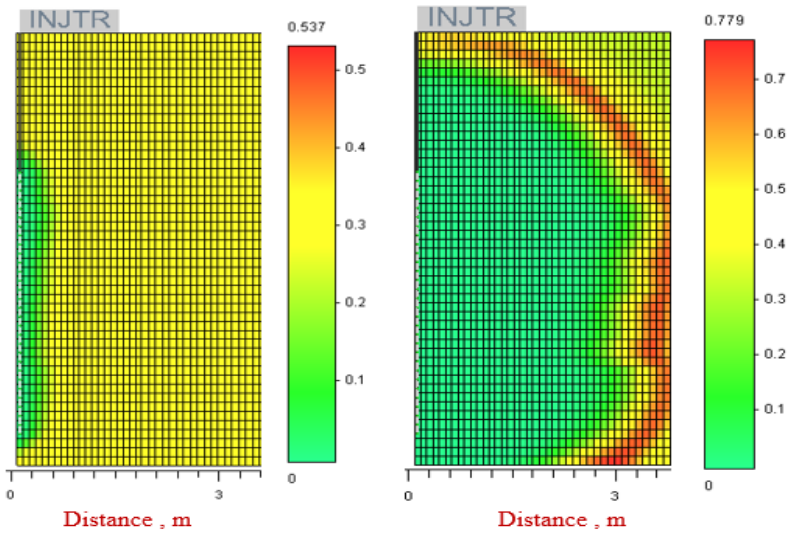

Figure 4-11: Oil Saturation Before SP Injection (After 4 Days) For 1500 PPM Case (Left) And 8000 PPM Case (Right) Of FP3630 Polymer

	Polymer Concentration. PPM	Tracer Distance Traveled, m	Volume Produced at Alcohol Peak, m^3	Volume Produced at Etac Peak, m^3	β	S_{or}
S_{or} Calculation after SP Injection						
Polymer 1	1500	4.50	18.28	35.78	0.96	0.32
	2500	4.50	18.93	35.18	0.86	0.30
	5000	4.50	19.12	29.11	0.52	0.21
	8000	4.50	17.91	27.10	0.51	0.20
FP3630	1500	4.50	27.12	49.61	0.83	0.29
	2500	4.50	30.45	52.95	0.74	0.27
	5000	4.50	30.82	39.56	0.28	0.12
	8000	4.50	30.30	33.44	0.10	0.05
S_{or} Calculation after SP Injection						
Polymer 1	1500	4.50	33.41	42.59	0.27	0.12
	2500	4.50	35.60	42.60	0.20	0.09
	5000	4.50	37.71	39.49	0.05	0.02
	8000	4.50	37.49	37.49	0.00	0.00
FP3630	1500	4.50	50.00	57.50	0.15	0.07
	2500	4.50	50.67	57.48	0.13	0.06
	5000	4.50	53.01	56.48	0.07	0.03
	8000	4.50	53.98	53.98	0.00	0.00

Table 4-7: Summary of Analytical S_{or} Calculation Results for Polymer 1 And FP3630 At Different Polymer Concentrations

4.5.2 SP Slug Size Sensitivity

Each polymer was simulated at 5 different SP slug sizes (in PV of interest):0.01,0.05,0.1,0.2 and 0.3. All cases were run at the same rate (50 m^3/d), same polymer concentration (2500 ppm) and same push and tracer sizes. The results in **Table 4-8** showed no significant decrease of S_{or} when small SP sizes of 0.01 and 0.05 were injected, and at least 0.20 PV of SP is required to reduce the residual to below 10%. It is worth noting that polymer#1 results show lower S_{or} values because in these cases no adsorption is assumed, and the values are considered optimistic. When surfactant adsorption is included, the values are similar to FP3630. This also to show the significance of adsorption in these tests. **Figure 4-12** shows cross-sectional oil saturation profiles with increasing SP sizes from **Figure 4-12a** to **Figure 4-12e**, in which all cross sections are at the same scale from the center to the boundary. It could be observed how increasing the SP slug size resulted in lower residual saturating even further away from the wellbore.

S_{or} Calculation after SP Injection					
FP3630					
SP size	Slug Volume, m3	Volume Produced at Alcohol Peak, m^3	Volume Produced at Etac Peak, m^3	B	S_{or}
0.01	3.02	31.02	53.51	0.73	0.27
0.05	15.08	33.72	51.22	0.52	0.21
0.1	30.16	38.57	47.32	0.23	0.1
0.2	60.32	53.02	60.52	0.14	0.07
0.3	90.48	55.73	59.47	0.07	0.03
Polymer 1					
0.01	3.02	19.46	31.96	0.64	0.24
0.05	15.08	28.26	34.50	0.22	0.22
0.1	30.16	33.27	39.52	0.19	0.19
0.2	60.32	35.77	35.77	0.00	0
0.3	90.48	35.76	35.76	0.00	0

Table 4-8: Summary of Analytical S_{or} Calculation Results at Different SP Sizes

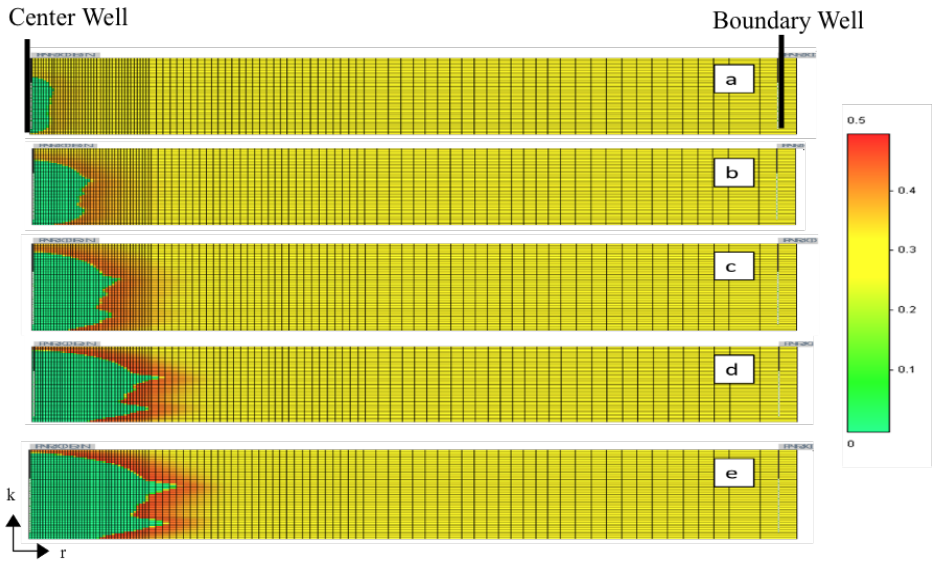

Figure 4-12:Cross Sectional View of Oil Saturation Profiles At a) 0.01 b)0.05 c) 0.1 d)0.2 And e) 0.3 PV SP Sizes.

4.5.3 Push and Tracer Size Sensitivity

Push and tracer sizes sensitivity were conducted to evaluate its impact on the analytical residual saturation calculation and tracer distance traveled. **Figure 4-13** and **Figure 4-14** show the result of the first (before SP) and second (SP) calculated S_{or} values for polymer#1 and FP3630 at different push and tracer injection durations, respectively. The results don't show a noticeable impact of tracer size; however, the push volume slightly affected the S_{or} calculation after SP injection as higher S_{or} is observed at higher push volumes **(Figure 4-13(right)** and **Figure 4-14(right)).** The higher the push volumes could mean larger distance is evaluated, so it is possible the higher calculated residual is due to larger distance is accounted for in the calculation. **Figure 4-15** shows the approximate Etac travel distance for different push and tracer durations. Both higher push and tracer durations resulted in higher travel distance of Etac. It is possible higher tracer durations reduced the dilution of tracer therefore higher concentrations of Etac were observed with larger distances.

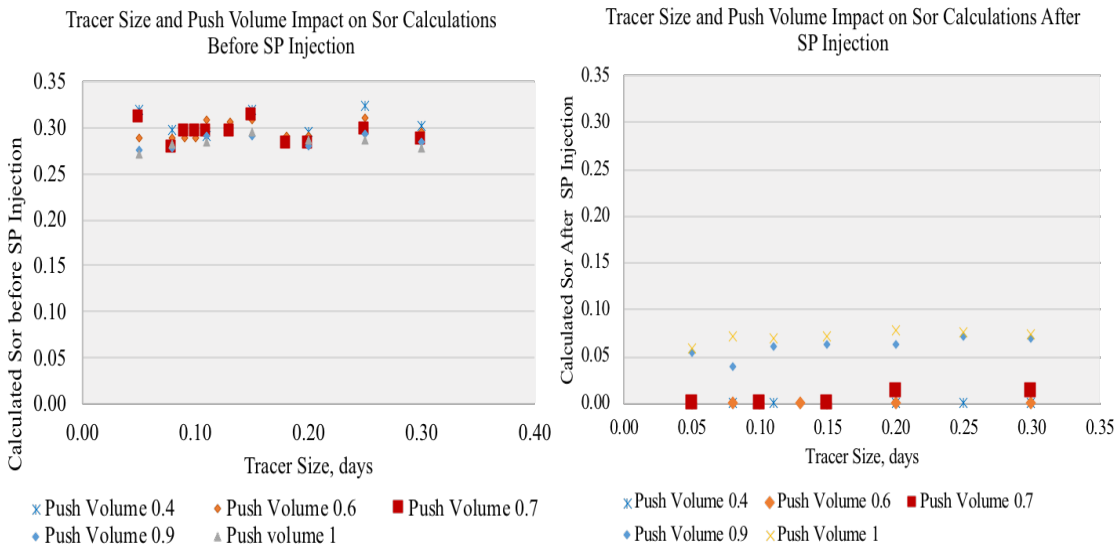

Figure 4-13:Polymer 1 Calculated S_{or} Prior to SP Injection(Left) and after SP Injection(Right) at Different Tracer Sizes and Push Volumes

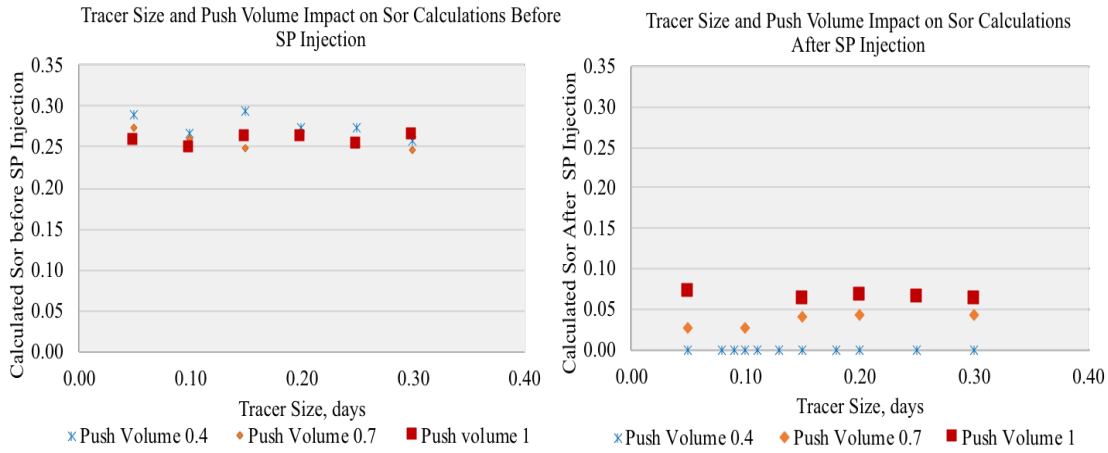

Figure 4-14:FP3630 Calculated S_{or} Prior to SP Injection(Left) and after SP Injection(Right) at Different Tracer Sizes and Push Volumes

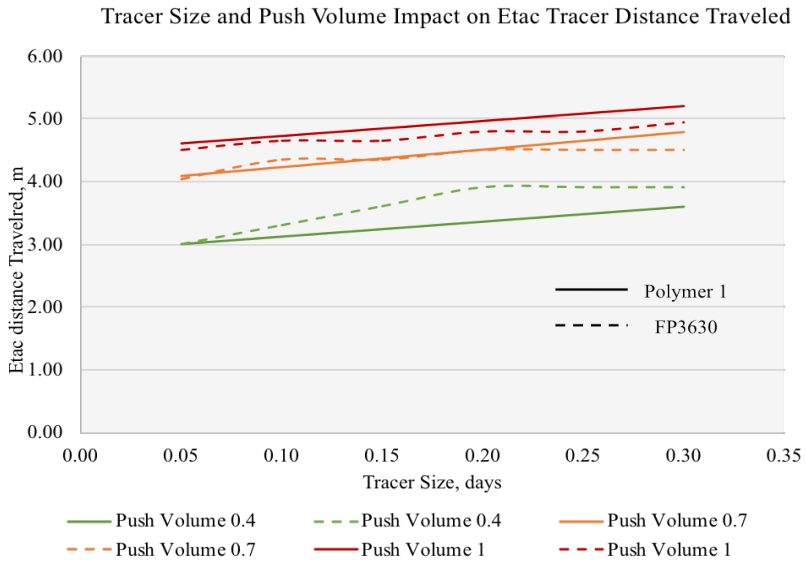

Figure 4-15:The Impact of Tracer Size and Push Volumes on the Etac Distance Traveled for Cases Including FP3630 and Polymer 1

4.5.4 Well Rates Sensitivity

Rates sensitivity covers the range 10-50 m^3/day per 6 m pay thickness, with the maximum at 50 m^3/day as it is a typical rate from the field model and to avoid injecting at high pressures. The rates were varied but the tracer, SP and push sizes were unchanged. Summary of total test duration at different rates is shown in **Table 4-9** The impact of rates on the calculation of S_{or} is summarized in **Table 4-10 .**

Rate, m^3/day	Test Duration
10	55.5
15	42.7
20	34.8
30	23.8
40	22.38
50	21.2

Table 4-9: Test Duration Required at Different Well Rates

	FP3630					
	Before SP			After SP		
Rate, m^3/day	Volume Produced at Alcohol Peak, m^3	Volume Produced at Etac Peak, m^3	S_{or}	Volume Produced at Alcohol Peak, m^3	Volume Produced at Etac Peak, m^3	S_{or}
10	31.44	46.19	0.19	52.46	55.21	0.03
15	29.87	46.72	0.22	52.55	56.3	0.03
20	29.17	47.17	0.24	52.67	57.17	0.04
30	29.26	48.76	0.25	52.86	58.86	0.05
40	29.44	50.44	0.26	52.02	58.17	0.06
50	30.45	52.95	0.27	53.02	60.48	0.07
			Polymer 1			
10	28.72	41.47	0.18	50	54	0.04
15	27.75	42.75	0.21	51.75	56	0.04
20	27.24	43.24	0.23	51.8	57	0.05
30	26.45	44.45	0.25	51.6	58.35	0.06
40	26.36	45.64	0.27	52.17	59	0.06
50	17.79	32.78	0.3	37.6	37.5	0

Table 4-10: Summary of Calculated S_{or} at Different Rates

The calculated S_{or} deviates significantly from the model input value with decreasing rates, although the same amounts of tracers and push volumes are injected in all cases. However, this does not mean the residual saturation changed, but rather the interpretations of produced tracer curves. **Figure 4-16** shows the tracer curve of reactive tracer (Etac) – solid line- and product tracer (ethanol) –dashed lines- as a function of produced water volume. At lower rates, less Etac was recovered whereas more ethanol was produced, which means the longer testing period allowed the Etac to react before the soak in time, as a result more hydrolysis occurred. It is possible the severity of hydrolysis affected the curve shape slightly (especially the tail end) and consequently the peak, which is the point used in the calculation, making the interpretation of S_{or} different. Evidence that no actual reduction in S_{or} occurred is shown in **Figure 4-17** , which shows the oil saturation profile during the first production period for the case of 10 m^3/d rate.

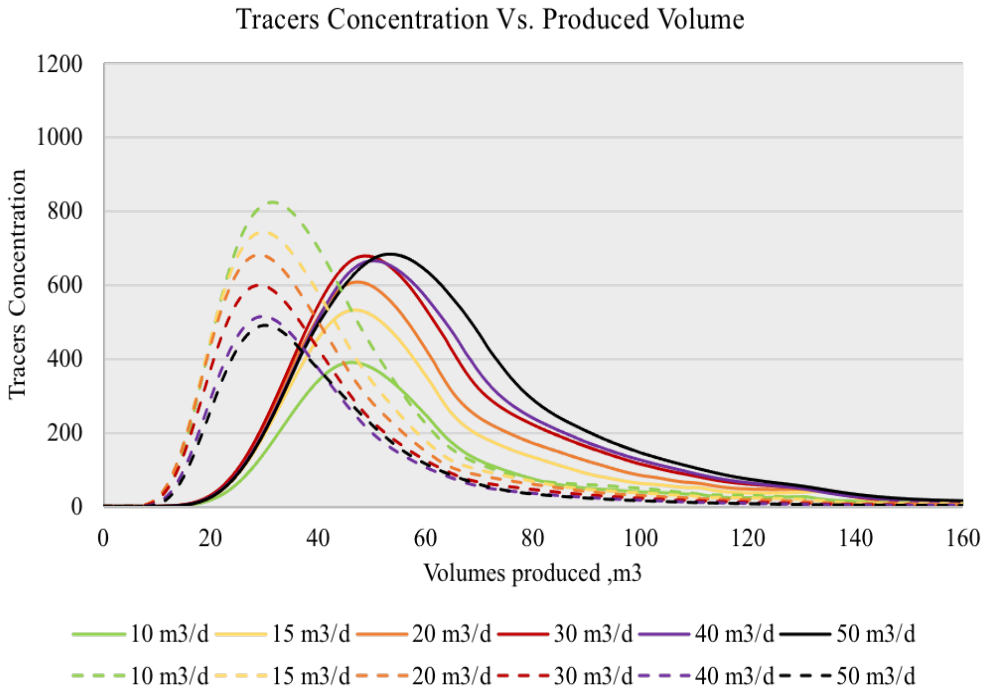

Figure 4-16:Etac and Ethanol Tracer Curves at Different Well Rates

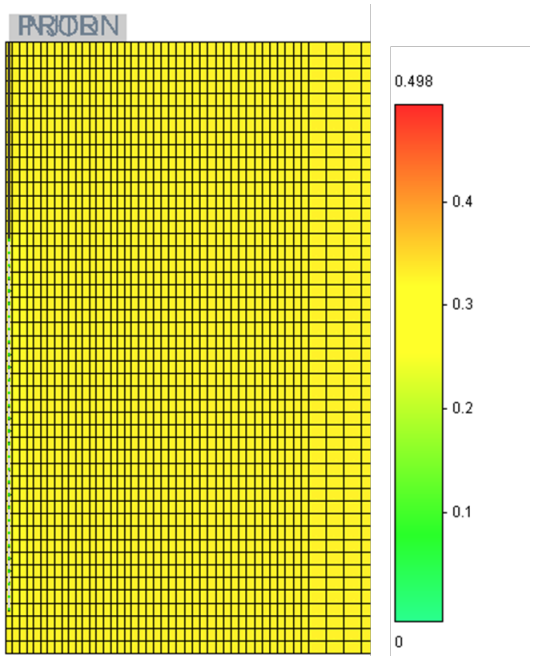

Figure 4-17:Oil Saturation Distribution close to the Wellbore Showing Constant S_{or} at Initial Value 0.33

4.6 SWCT DESIGN CONCLUSIONS

The residual oil saturations calculated during the first step (prior to SP injection) by the analytical equation was accurate within 20% error. No dispersion was accounted for in the models. Reaction rate was assumed in the model within a reasonable range; the assumed value produced sufficient hydrolysis in a reasonable amount of time. The assumed parameters used in the models: Etac reaction rate, shut in time (related to reaction rate), partition coefficient would require further lab testing to determine exact values. They were assumed in the model. The pore volume of interest mentioned herein (302 m^3) corresponds to 8-meter radius. The 8 m /26 ft. radius is within a range of typical radius of investigation for SWCT from 10 to 50 ft (Deans and Carlisle, 2007). The effect of each sensitivity parameter is summarized below:

Polymer Concentration: High concentrations (> 5000 ppm) altered the oil saturation within a few meters around the wellbore and resulted in lower residual saturation prior to SP injection. The reduction in S_{or} was confirmed by the oil saturation profile before SP injection. Although 1500 ppm showed good results, higher concentrations are preferred to account for possible dilution and degradation during field applications. Both FP3630 and polymer 1 showed similar results.

Surfactant Polymer (SP) Size: A slug size of 0.2 PV (60 m^3) showed zero S_{or} in the case where no adsorption was included, and around S_{or}=0.06 in both polymers when adsorption of 8.1 gmol/m^3 was included.

Well Rates: Low well rates (< 50 m^3/day) allowed the reactive tracer to react with water and resulted in more hydrolysis before tracer production and lower Etac recovery. The tracer curves were almost independent of well rates at lower rates. Tracer-polymer injection prior to SP injection did not reduce S_{or} at low rates.

Tracer Push Volume: Push volumes of 1 day (50 m^3 = 0.17 PV) showed reactive tracer travel distance of 5 m. The calculated S_{or} showed a systematic increase of calculated S_{or} with increasing push volume possibly due to a larger inspection volume.

4.7 SWCT DESIGN RECOMMENDATIONS

For a radius of investigation of 8 m, pay thickness of 6 m and PV of 302 m^3, the following recommendations are provided:

- SP slug size of at least 60 m^3 (0.2 PV) is required to reduce S_{or} to less than 10%.
- Push volume of 50 m^3 (1 day at 50 m^3/day per 6 m pay thickness) is recommended to investigate approximately 5 meters radius.
- Tracer solution sizes in the range of 8-15 m^3 (0.15 to 0.30 days duration at 50 m^3/d rate) were sufficient S_{or} determination.
- A polymer of 2500 ppm with the tracer injection showed good result with analytically calculated S_{or} during the test prior to SP injection.
- A rate of 50 m^3/d per 6 m pay thickness is recommended for fast testing period and easy interpretation of produced tracer curves.

Chapter 5: Multi-Well Chemical Test Design

This chapter presents the design process of the interwell tracer test and the surfactant polymer SP field pilot. It starts with an introduction and review of the IWTT and its interpretation methods. Followed by a discussion about the IWTT design process, sensitivity results and design recommendations. Lastly, the chapter discusses the SP pilot design workflow, sensitivity and recommendations.

5.1 INTRODUCTION AND OBJECTIVE

Inter-well tracer test IWTT is a tool that has been used in the oil industry both qualitatively and quantitatively to evaluate various reservoir and well characteristics. The test entails injecting one or more tracers into one or more injection wells and monitoring tracer response from producers (Cooke, 1971). The utilization of inter well tests by the petroleum industry started during the 1950s, where the tests focused on qualitative understanding of the reservoir such as determining high permeability channels (Watkins and Mardock, 1954). The test enhances the understanding of the reservoir heterogeneity by tracking the movement and flow paths of the tracer-tagged solvents in the reservoir, assuming that the tracers in fact echo the movement of the solvent (or the injected water) (Zemel, 1995). It can provide crucial information pretraining to; well-to-well connectivity, confinement, high permeability channels (thief-zones), fractures, reservoir heterogeneity, sweep efficiency, residual oil saturation (with partitioning tracers) (Watkins and Mardock, 1954; Maroongroge, 1994; Asakawa, 2005; Shook *et al.,* 2009, Sharma *et al.,*2014). Appropriate and timely implemented tracer testing has been demonstrated to be useful for design optimization or risk mitigation prior to EOR field pilot implementation (Cheng *et al*., 2012). In designing chemical EOR tests using numerical simulations, the understanding of the reservoir's heterogeneity is as good as the geological characterization in the model.

The IWTT test can provide direct information from tracer production data about well-to-well connectivity and reservoir transmissibility within a reasonable interwell scale with no need of arithmetic averaging in the area of interest, which might be typical in a numerical simulation. Therefore, the test could sometimes be used to improve static and dynamic field models.

The significance of the work presented in this chapter stems from the notion that IWTT is needed to enhance the reservoir characterization of the pilot area, and multi-well test is needed to evaluate the sweep efficiency in reservoir conditions. The objective of the work presented in this chapter is first to design an interwell tracer test IWTT to assess the heterogeneity in the pattern chosen for pilot. This is done by determining required tracers' amount, concentration and well rates for sufficient and timely test interpretations. Second, design a multi-well SP test by identifying suitable choices for key design parameters: SP composition, SP slug size, polymer drive concentration and well rates. Based on the simulation study results, design recommendations are provided.

5.2 Literature Review of Interwell Tracer Tests (IWTTs) Quantitative Interpretation Methods

The first implementation of interwell tracer testing dates back to the 1950s; Watkins and Mardock (1954) used radioactive iodine tracer to determine transit time between wells and identify high permeability zones in waterflooded reservoir with qualitatively focused analysis. Brigham and Smith (1965) were the first to quantitively analyze the tracer data and develop an analytical solution to predict the shape of tracer curves, peak concentrations and breakthrough times of a homogenous five-spot. Their method is limited to reservoirs with mobility ratios near unity, in addition, their calculation requires prior understanding of dispersion and areal sweep. Wagner *et al.* (1974) modified Brigham's model by

including the effects of dilution of tracers due to the production of associated gas and gas expansion at surface conditions. Abbaszadeh and Brigham (1984) further extended Brigham and Smith's model to include more flood patterns at mobility ratio of one. Tang and Harker (1991) reported first field application and interpretation of inter well tracer test to determine residual gas saturation. Allison *et al.* (1991) used simulation methods to analyze tracer data in a multi-phase large scale reservoir, their analysis was compared with the analytical model of Abbaszadeh and Brigham (1984).

The method of Moments MOM is a well-established method for the calculation of residual saturation. MOM and Residence time analysis RTD was first introduced by Danckwerts (1953) to determine the volume swept in chemical reactors. His method was later adapted in the oil industry by Deans (1978), and Cooke (1971) who patented a method to estimate residual saturation based on the difference of arrival times of partitioning tracers**.** Tester and Potter (1982), and Robinson and Tester (1984) used RTD to assess and diagnose the flow in fractured geothermal reservoir by determining the volume and the fluid distribution within the system. Maroongroge (1994) used first moment to analyze swept volume of a heterogeneous reservoir, also extended the first moment to non-partitioning tracers to calculate the residual oil saturation and developed vertical tracer profiling VTP to provide information about flow patterns in each layer. Jin *et al.* (1995) Used RTD to evaluate and approximate the volume of the contamination of non-aqueous phase liquids in the subsurface using the differences in mean residence times of the tracers. Shook *et al.* (2003) introduced a spreadsheet method to estimate flow geometry of single-phase geothermal reservoir using tracer effluent data. Using MOM, Asakawa and Sinha *et al.* derived equations to calculate saturation, and swept pore volumes for a general reservoir conditions (3D, heterogeneous, two phases, naturally fractured) (Sinha *et al.,* 2004; Asakawa, 2005). Shook and Forsmann (2005) extended the approach to estimate

heterogeneity and sweep efficiency. Shook *et al.* (2009) showed how to use residence time distribution analysis (RTDA) method to evaluate the time varying properties (sweep efficiency and saturation) from tracer data as a function of time. In this review section, the focus is on the theory presented by Shook (Shook *et al.,* 2009):

5.2.1 Swept Volume Calculation

The aforementioned methods rely on tracer mean residence time, or first temporal moment, which is the average tracer residence time between inlet and outlet (injector and producer). Sinha *et al.* define the residence time for a tracer slug in two phase flow as the following (Sinha *et al.*, 2004):

$$\bar{V} = \frac{\int_0^\infty q C_{total} t \, dt}{\int_0^\infty C_{total} dt} - \frac{V_{slug}}{2} \tag{5.2.1}$$

where total concentration of a tracer is defined:

$$C_{total} = f_w C_w + C_o f_o \tag{5.2.2}$$

A swept pore volume is the difference of the mean residence times between two tracers with different partitioning coefficient is given by:

$$V_{swept} = \frac{\bar{V}_1(K_1 - 1) - \bar{V}_2(K_2 - 1)}{K_1 - K_2} \tag{5.2.3}$$

In Shook *et al.* work, since the method is dependent on time or age distribution, RTD converts tracer concentrations to residence time distribution (and this is done for mathematical convenience). The conversion is as follows:

$$E(t) = \frac{C(t) * \rho * q}{M_{inj}} \tag{5.2.4}$$

The *E(t)* is the time distribution function, *C(t)* is the mass fraction of tracer in the produced fluid, q is the production flow rate, ρ is the density of produced fluid, and $M_{inj}$is the total mass of injected tracer. The unit of *E(t)* is the inverse of time.

The mean residence time is a time weighted average; therefore, it is affected by the tracer sampling and testing times. Since tracer sampling is usually terminated before tracer concentration falls to zero, exponential extrapolation of late time tracer tail is important to avoid underestimation of mean residence time (Shook and Forsmann, 2005). The mean residence time and the total swept pore volumes are as follows:

$$t^* = \frac{\int_0^\infty E(t)tdt}{\int_0^\infty E(t)dt} - \frac{t_s}{2} \tag{5.2.5}$$

$$V_p = \frac{m\, q_{inj} t^*}{M_{inj}} = V_{ij} = \frac{m}{M_{inj}}\left(q_i \frac{\int_0^\infty q_j C_{ij} t\, dt}{\int_0^\infty q_j C_{ij} dt} - \frac{V_{slug}}{2}\right) \tag{5.2.6}$$

where t_s represents the slug size (V_{slug}) , m is the amount of produced tracer, the pore volume above is the swept pore volume between a specific injector (i) and producer (j). Therefore, the total swept volume should be the summation of swept volume between each two well pairs. Shook and Foresman (2005), showed that tracer tails can be extrapolated using the function below, where tb represents the time in which after the plot of ln (*C*) vs. time becomes linear:

$$f(t) = b\, e^{-at} \quad for\ t > tb \tag{5.2.7}$$

Eqn. 5.2.6 becomes:

$$V_{ij} = \frac{m}{M_{inj}}\left(q_i \frac{\int_0^{tb} q_j C_{ij} t\, dt + \int_{tb}^\infty q_j C_{ij}\, t\, dt}{\int_0^{tb} q_j C_{ij} dt + \int_{tb}^\infty q_j C_{ij} dt} - \frac{V_{slug}}{2}\right) \tag{5.2.8}$$

Rewriting second integrals in numerator and denominator implies:

$$V_{ij} = \frac{m}{M_{inj}}\left(q_i \frac{\int_0^{tb} q_j C_{ij} t\, dt + q_j \frac{b}{a^2} e^{-at_b}(1 + at_b)}{\int_0^{tb} q_j C_{ij} dt + q_j \frac{b}{a} e^{-tb}} - \frac{V_{slug}}{2}\right) \tag{5.2.9}$$

Using RTDA, swept volume as a function of time for a conservative water tracer is as follows:

$$V_{wj}(t) = \frac{m}{M_{inj}} \int_0^t q_j \big(1 - Fw(\tau)\big) d\tau \tag{5.2.10}$$

$$Fw = \frac{\int_0^t q_j C_{ij} d\tau}{\int_0^\infty q_j C_{ij} dt} \tag{5.2.11}$$

With the presence of a partitioning tracer, the oil volume swept is:

$$V_{oj}(t) = \frac{1}{K} \int_0^t q_j \big(Fw(t) - Fo(\tau)\big) d\tau \tag{5.2.12}$$

where *K* is the partition coefficient of the partitioning tracer, Fw and Fo are the fraction recovery of the water and oil, respectively. Therefore, the total swept volumes will be the summation of both swept volumes of water and oil. Sweep efficiency is therefore the above equation divided by swept volume at infinite time. The advantage of RTDA over MOM is the that RTDA does not use the time averaged tracer data (integration of numerator of **Eqn. 5.2.6**), which eliminates the effects of the later time data, where tracer concentrations are at low detection limits, the weighting of these data can result in as considerable error in the calculations (Shook *et al.,* 2016).

5.2.2 Flow Geometry Estimation

The storage and flow capacity are dependent on zero and first moments of RTD; zero moment represents the amount of tracer recovered from production well, and first moment is the average residence time for the tracer between the injection and production wells. The storage capacity, therefore, is the mean residence time of flow paths moving faster than a flow path breaking through at time=*t* normalized by the total mean residence time (Shook *et al.* ,2009):

$$\Phi = \frac{\int_0^t E(\tau)\tau d\tau \Big/ \int_0^\infty E(\tau)d\tau}{\int_0^\infty E(t)tdt \Big/ \int_0^\infty E(t)dt} = \frac{\int_0^t E(\tau)\tau d\tau}{\int_0^\infty E(t)tdt} \quad (5.2.13)$$

The flow capacity is the cumulative produced tracer at time=*t* normalized by tracer recovery at infinite time, or the zero moment:

$$F(t) = \frac{\int_0^t E(\tau)d\tau}{\int_0^\infty E(t)dt} \quad (5.2.14)$$

Using the above equations an estimation of reservoir heterogeneity can be obtained by constructing F vs Φ diagram and evaluating Lorenz coefficient:

$$L_c = 2\,.\left\{\int_0^t F d\Phi - 0.5\right\} \quad (5.2.15)$$

5.2.3 Oil Saturation Calculation

Using MOM, Sinha *et al.* estimates the average oil saturation of the swept volume shown in **Eqn. 5.2.3** is (Sinha et *al.*, 2004):

$$\overline{So} = \frac{\bar{V}_1 - \bar{V}_2}{\bar{V}_2\,(K_1 - 1) - \bar{V}_1(K_2 - 1)} \quad (5.2.16)$$

Shook *et al.* defines the oil saturation as the swept oil volume over the total swept volume, hence, the oil saturation can be calculated as follows: (Shook *et al.,* 2009)

$$So(t) = \frac{V_o}{V_o + V_w} \quad (5.2.17)$$

5.2.4 Tracer Curves Later Times Extrapolation

When the test is terminated at early times, the estimation of the parameters of the exponential function in **Eqn. 5.2.7** could be challenging. Based on an analytical solution to the tracer transport in 1-D, Viig *et al.* describe the tracer decline curves using a fitting type curve, the extrapolation is applicable to a conservative tracer (Viig *et al.*, 2013):

$$c(t) = \frac{M_o}{\sqrt{D_o t}} \exp\left[-\frac{(t - t_o)^2}{D_o t}\right] \tag{5.2.18}$$

where M_o, D_o and t_o are fitting parameters. Sharma *et al.* (2014) proposed a log-normal model for faster estimations of tracer curves:

$$c(t) = \frac{C_o}{t^* \sigma_{lnt} \sqrt{2\,\pi}} \exp\left[-\frac{(\ln t - \mu_{lnt})^2}{2\,\sigma_{lnt}^2}\right] \tag{5.2.19}$$

where $t^* = (t - t^{BT})$, and t^{BT} is the tracer breakthrough time, σ_{lnt} is the standard deviation, μ_{lnt} the mean distribution, C_o is a scaling parameter to match tracer peak concentration. Dean *et al.* (2016). modified the log normal model to include partitioning tracers. They start by defining the mean residence time as the following:

$$\bar{t} = t_{conc \cdot mode_{NP}}\, e^{\frac{3}{2}\ln(1 - V_{DP})^2} \tag{5.2.20}$$

where $t_{conc \cdot mode_{NP}}$ is the concentration mode of the non-partitioning tracer, V_{DP} is the Dykstra-Parsons coefficient. The mode of the non-partition is related to the mode of the partition tracer as the following:

$$t_{conc \cdot mode} = \frac{F_o}{SW}\, t_{conc \cdot mode_{NP}} \tag{5.2.21}$$

F_o is different from the definition by the RTDA, F_o in this case is:

$$F_o = S_w + K\, S_o \tag{5.2.22}$$

The standard deviation and mean are obtained, respectively, using:

$$\sigma = -\ln(1 - V_{DP} F_o) \tag{5.2.23}$$

$$\mu = \frac{\ln(1 - V_{DP} F_o)^2}{-2} \tag{5.2.24}$$

A modification to **Eqn. 5.2.19** is hence proposed using a dimensionless concentration:

$$c_D = \frac{1}{2} erfc\left[-\frac{\ln\left(\frac{t}{\bar{t}}\right) - \mu}{\sigma\sqrt{2}}\right] - \frac{1}{2} erfc\left[-\frac{\ln\left(\frac{t - t_{slug}}{\bar{t}}\right) - \mu}{\sigma\sqrt{2}}\right] \tag{5.2.25}$$

5.3 SECTOR MODEL CONSTRUCTION

A sector model is cut with the dimensions of 2.2 × 2.04 km. Its pore volume represents 15% of the total field PV, and its hydrocarbon pore volume (HPV) represents 24% of the field HPV. The sector model has been cut on the basis of having boundaries sufficiently far from the pilot area so that at the boundary, minimum pressure effects are observed due to the injection in pilot area. The potential pilot area is the same SWCT pilot area described in **section 4.3.1**. The pilot is a 5-spot area with 4 injectors and 1 producer. the wells are in a close proximity to each other which allows for faster interpretations of the test. The 5-spot area is 150 m x 150 m, the producer is 70 m away from each injector. The area has good quality of reservoir in terms of porosity and permeability; with permeability ranging 1000-10000 mD and porosity ranging 15%-26%. The location of the pilot area inside the sector is shown in the yellow box in **Figure 5-1.** The plan is to inject a unique tracer into each of the injectors. The area contains multiple layers, as depicted in **Figure 5-2**. The current design of the IWTT targets layer 1, the same layer targeted in the SWCT for consistency. For the purpose of this design, the four tracers in the model are assumed to have similar properties, and their concentration in the produced water is solely based on the properties and flow paths of the reservoir they are injected in. **Figure 5-3** shows the injection location of each tracer (Tracer 1 in well 220, tracer 2 in 221, tracer 3 in 223 and tracer 4 in 106). Well 222 is the producer well. The test tracer injection start date for all the cases is 01/01/2018.

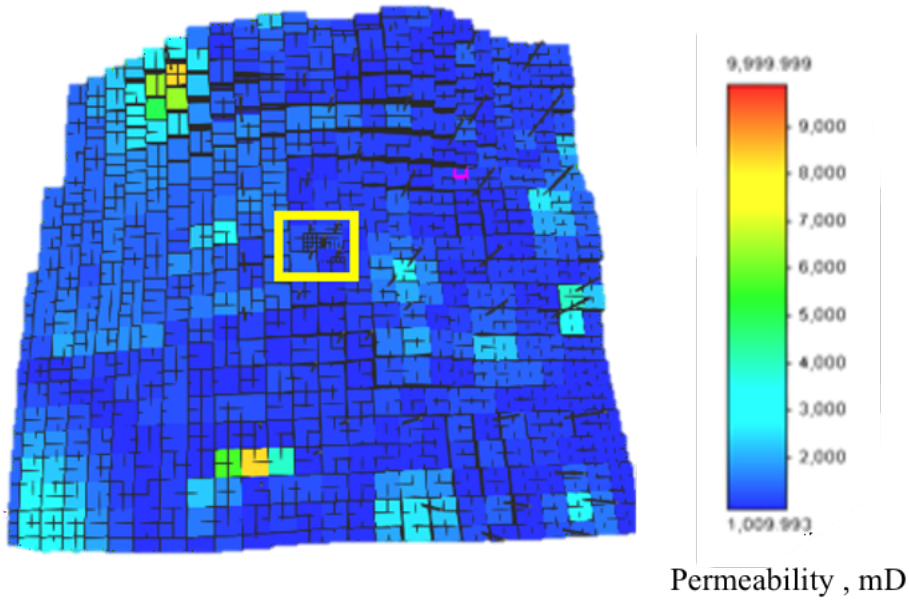

Figure 5-1: 3D View of Sector Model on a Permeability Distribution Map. 5-Spot Pilot Area Outlined by Yellow Box

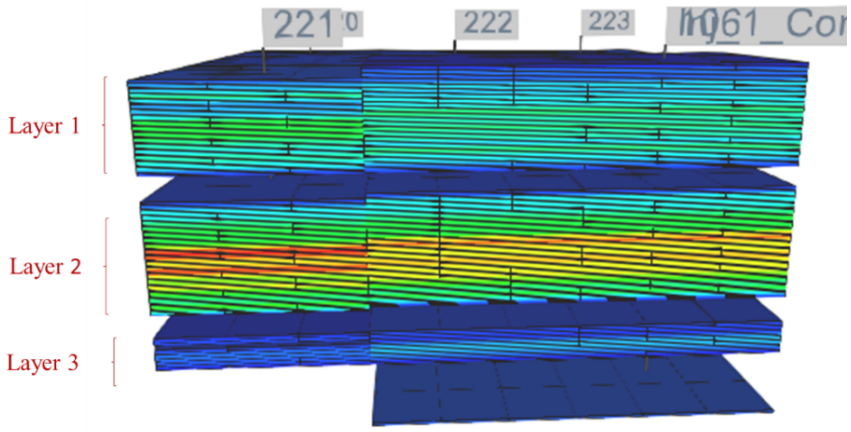

Figure 5-2: Layers of 5-Spot Area

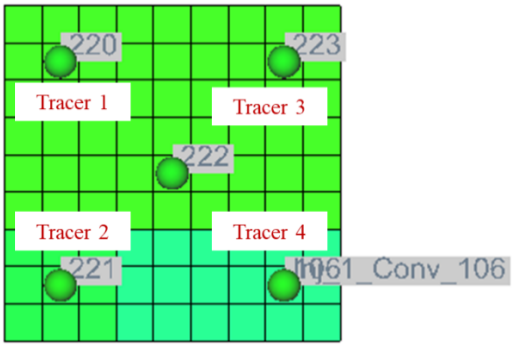

Figure 5-3: Tracer Injection Locations on An Aerial View of the 5-Spot Pattern

5.4 INTERWELL TRACER TEST IWTT DESIGN

5.4.1 IWTT Design Workflow and Sensitivity Cases

The general procedure for IWTT, as discussed in Cubillos *et al.* and Shook *et al.* can be summarized in **Figure 5-4** ,(Cubillos *et al.,* 2006; Shook *et al.,* 2009). The focus of the simulation work in this chapter is in the test design.

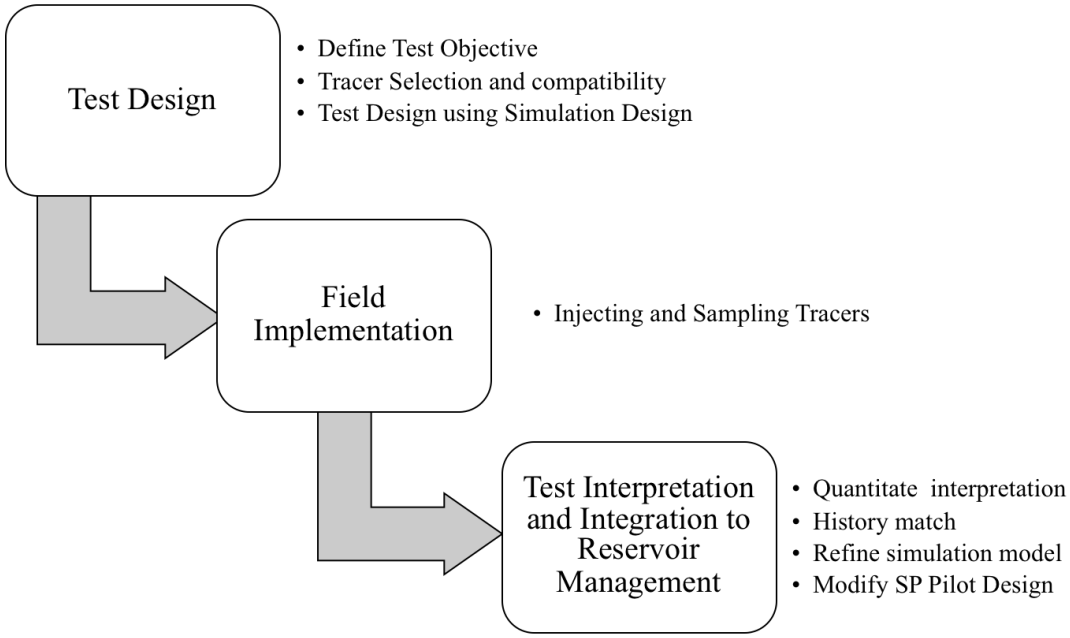

Figure 5-4: General Procedure for IWTT Design

- **The Objective of The Test:**

The design of the IWTT will be tailored to the objective of the test. Therefore, defining the objective is the first crucial element for designing the test. The objective of this test is to enhance our understanding of the quality and connectivity of the reservoir using merely produced tracer data, more specifically, qualitatively understand wells connectivity and thief zones, and estimate pilot area geometry, heterogeneity and swept pore volume (RTD method). This evaluation can provide valuable information for design optimization or risk mitigation prior to SP field or pilot applications. Therefore, the following test steps are proposed and simulated: Injection of passive tracers in 4 injection wells and production in the producer well. One unique passive tracer is to be used for each injection well.

- **Tracers Selection**

The tracers may react differently under different reservoir conditions; the passive tracers selected should be compatible with the reservoir. Ideally, tracer screening and compatibility testing should be conducted before test design, and they should meet the following criteria: high solubility in water, low detection limits, no degradation, stable under reservoir conditions, minimum adsorption, low cost, environmentally acceptable (Shook *et al.,* 2009). Of course, other factors such as availability and test easiness should be considered. For the purpose of our study, four conservative tracers have been chosen in order to start the design with the following assumptions in the model; no adsorption, and the tracers properties are assumed to be almost ideal and the same for the 4 tracers, meaning, their behavior is determined entirely by the reservoir properties and flow paths they encountered. although these assumptions may overestimate the tracer flow, it will be taken into account when choosing the tracer amount for the design to account for adsorption and dilution.

- **Simulation Study and Design**

The goal of the sensitivity analysis is to provide information about the following aspects of the design: amount of tracer to be injected, injection and production well rates, and estimating the time of breakthroughs, which impacts testing period and sampling program. Different scenarios have been tested, summary of the sensitivity cases is shown in **Table 5-1**.The assessment metric for each case was based on the following:

- Tracer peak concentrations: The produced tracers need to be at detectable limits.
- Tracer breakthrough times: They are important for test duration and sampling schedule.
- Tracer peak breakthrough times: they are important for test duration, at least part of the tracer curve tail need to be achieved for accurate calculations and interpretations.
- Tracer recovery

As shown in **Table 5-1**, six variables have been tested to evaluate the significance of each on the main aspects of the design. The variables include amount of tracer injected in kg per tracer, tracer concentration, well rates, total dispersion coefficient, injection of polymer solutions, and pore volumes injected. The subject pore volume is the pore volume of the top layer of the 5-spot area, PV=36011 m^3. In all the cases, the injectors are constrained to maximum bottom hole pressure of 20,000 kPa (2900 psi) and producer to minimum bottom hole pressure of 3,000 kPa (435 psi).

Sensitivity Variables					
Tracers Amount	**Tracers Concentration**	**Well Rates**	**Dispersion Coefficient**	**Polymer**	**Pore Volumes Injected**
Per tracer, kg	**PPM**	**m^3/d**	**m^2/d**	**PPM**	
4.5	1000	Shut-in surrounding wells	Zero	No Polymer	0.1
40	2000	20	E-5	2500	0.2
100	5000	30	E-4	5000	0.3
885	10000	40	E-3		0.5
2460		50	E-2		>1 PV
			E-1		
Total Cases	29				

Table 5-1: Summary of IWTT Sensitivity Cases

5.4.2 IWTT Sensitivity Results

- **Sensitivity to Tracer Concentration:**

All the cases for this sensitivity had fixed rates of 50 m^3/d and amount per tracer of 885 kg. The tracer concentration was varied from 1000 ppm to 10,000 ppm. **Figure 5-5** to **Figure 5-8** show the produced tracer profiles from well-222. The x-axis represents days since tracer injection begins. As seen from tracer curves, there is no significant differences between the cases. More details about the cases are presented in **Figure 5-9**. Tracers peak concentrations, breakthrough and recovery are generally the same for most of the tracers. Peak concentration breakthrough time, however, is significantly reduced for the tracers from case 1000 ppm to 10000 ppm with reduction range of 20-42% (15-42 days reduction). Although lower concentrations showed slightly better recoveries (for tracer 1; 14% recovery at 1000 ppm as opposed to 10% for 10000 ppm), the difference is not very big. On the other hand, injecting 885 kg of tracers at 1000 ppm and 50 m^3/d took approximately 18 days as opposed < 2 days for the 10000-ppm case. The tracer recovery is dependent on the heterogeneity of the reservoir around the injection well.

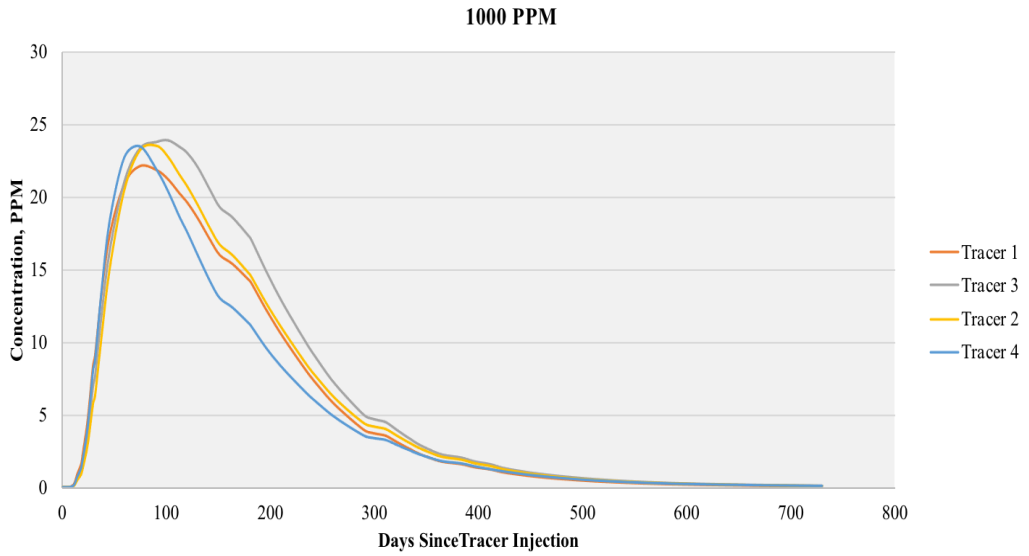

Figure 5-5: Producer Well-222 Produced Tracer Concentration with Time For 1000 PPM Tracer

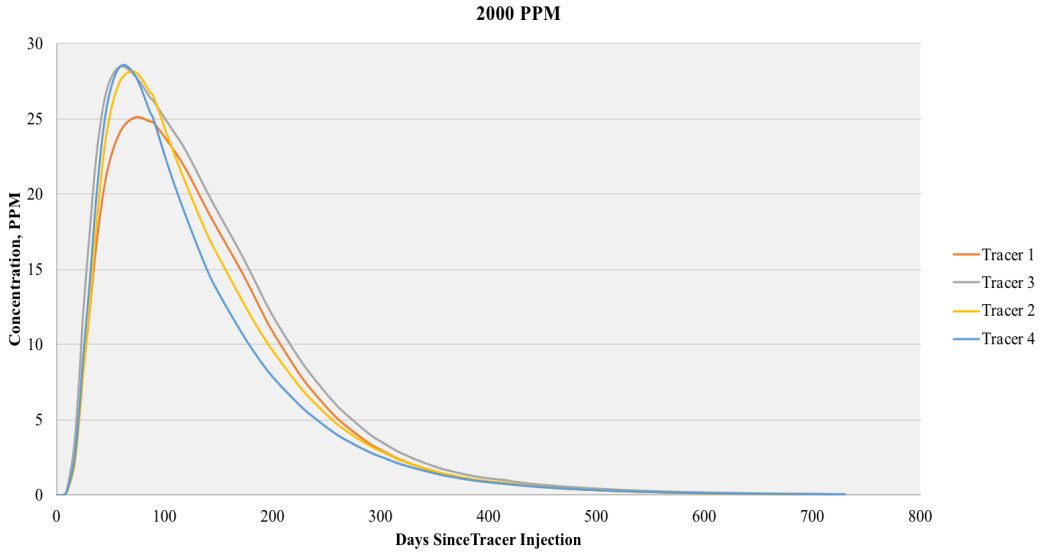

Figure 5-6: Producer Well-222 Produced Tracer Concentration with Time For 2000 PPM Tracer

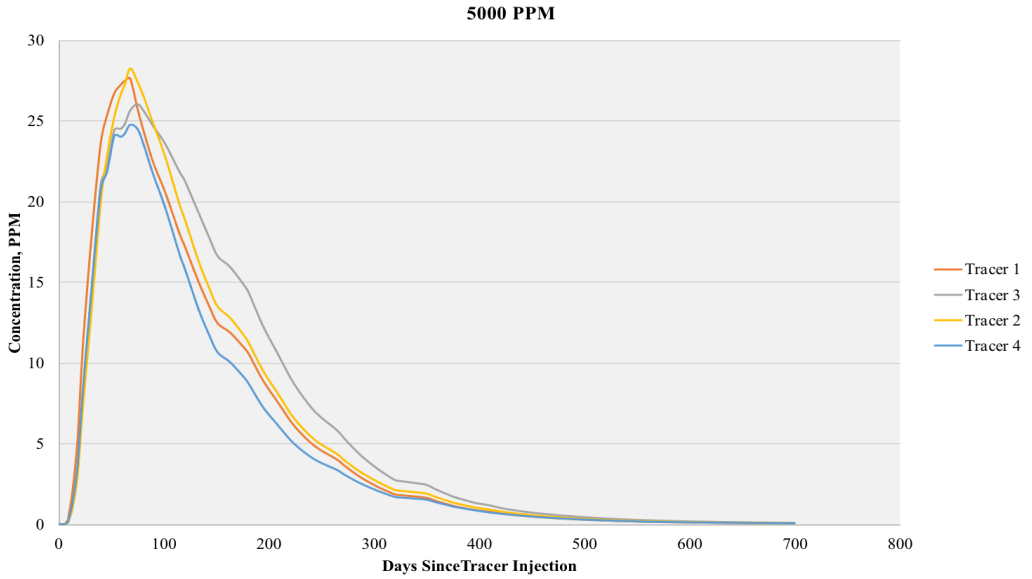

Figure 5-7: Producer Well-222 Produced Tracer Concentration with Time For 5000 PPM Tracer

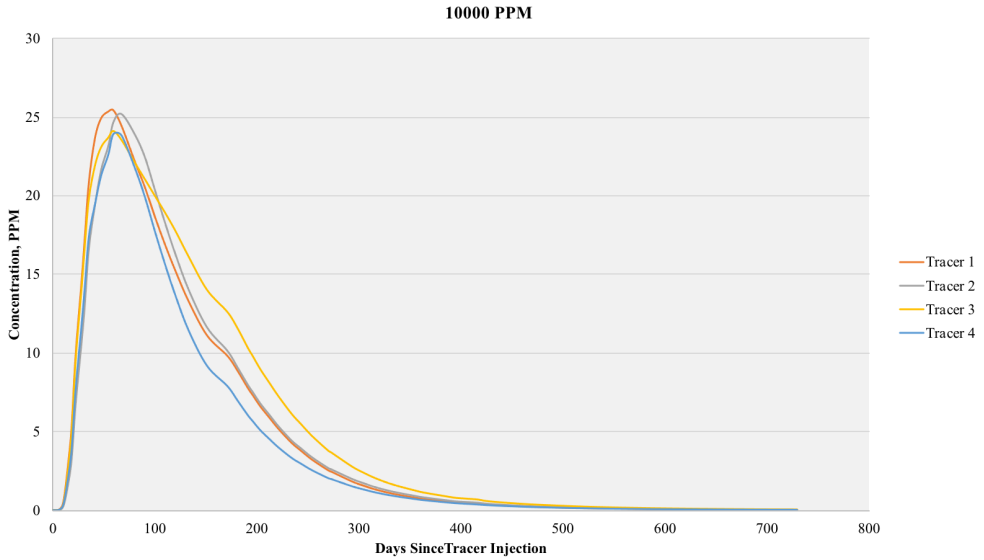

Figure 5-8: Producer Well-222 Produced Tracer Concentration with Time For 10000 PPM Tracer

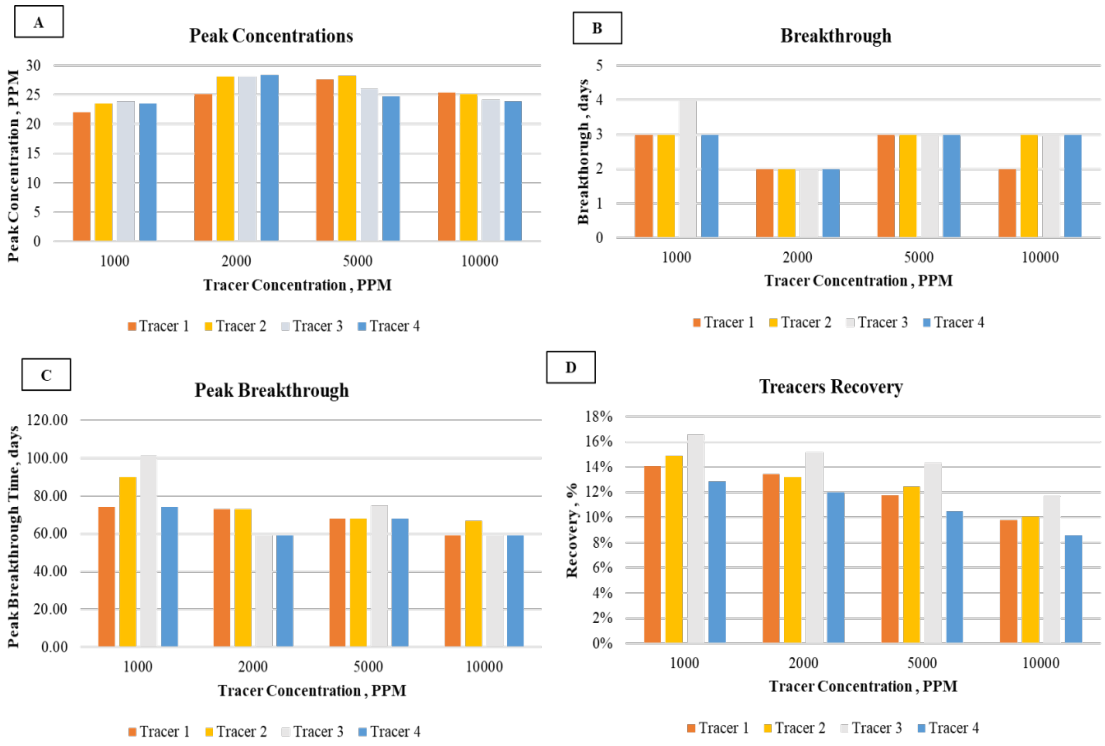

Figure 5-9: Producer Well-222 Produced Tracer Concentration with Time For 10000 PPM Tracer

- **Sensitivity to Tracer Amount:**

Five cases have been conducted for different amount per tracer in kg: 4.5, 40,100, 885 and 2460. The tracer curves are shown in **Figure 5-10** to **Figure 5-14**. This sensitivity shows a clear relationship between the amount injected and the tracer peak concentrations, which increases by orders of magnitude from the case of 4.5 kg per tracer to 2460 kg per tracer. Also, the larger the amount injected, the curve shifts more to the right therefore it is expected to observe tracer peak and tail at later times. In addition to the clear increase in peak concentrations in **Figure 5-15A**, an increase in recovery is also observed with more tracer injected. The spike in tracer breakthrough time in **Figure 5-15B** for the case of 40 kg per tracer could be just time step related and does not necessarily mean slower breakthrough. The drawback of larger amount is the more time needed to observe the peak

and the tail of the tracers; the peak concentration time for the 2460 kg per tracer case is almost 3 time the smallest case of 4.5 kg per tracer.

The choice of the required amount of injected tracer is influenced by the minimum tracer concentration (MTC) detectable in the field. Different detection limits have been reported in literature; Zemel reported around 20 ppb for salts (Zemel, 1995), Wagner *et al.* reported 20-25 PPM for salts, and 50 PPM for alcohols (Wagner *et al.,* 1977). Piole *et al.* reported 0.1 PPM detection limit for anion tracers and 0.0003 PPM for artificial tracer (Fluorescent dyes) (Piole *et al.,* 2012). It is recommended that the design of tracer amount should yield a peak concentration that exceeds at least 100 times that value in order to have meaningful results (Zemel, 1995). Since the detection limit is merely a gauging parameter, the minimum limit assumed to be within the range of the reported values, 10 ppb.

The design criteria for the amount of tracer is based on the highest tracer recovery and peak tracer values exceeding 10-100 times the minimum detectable limit. The recommended tracer mass is compared here with analytical estimate of required tracer mass. The analytical estimate is based on Zemel's method: tracer mass is 100 × MTC × PV (Zemel, 1995). Assuming MTC is 10 ppb, and targeted PV of 36011 m^3 (top layer 5-spot area), the calculation would yield 36 kg of total tracer required, 9 kg between each well pair (injection-production). However, this calculation is optimistic since the assumed MTC is very low, that is in addition to the implicit assumptions of the method (e.g. that tracer flows through the entire pore volume). Nevertheless, it is used as a baseline for minimum tracer amount. Comparing the recommended 9 kg per tracer of this method with the results of the sensitivity, it is clear that tracer mass of the magnitude of 10 kg produces very small concentrations at the peak, smaller than 100 times the assumed 10 ppb (0.01PPM). 885 kg per tracer produced peak concentrations that are sufficiently higher than 100× the MTC.

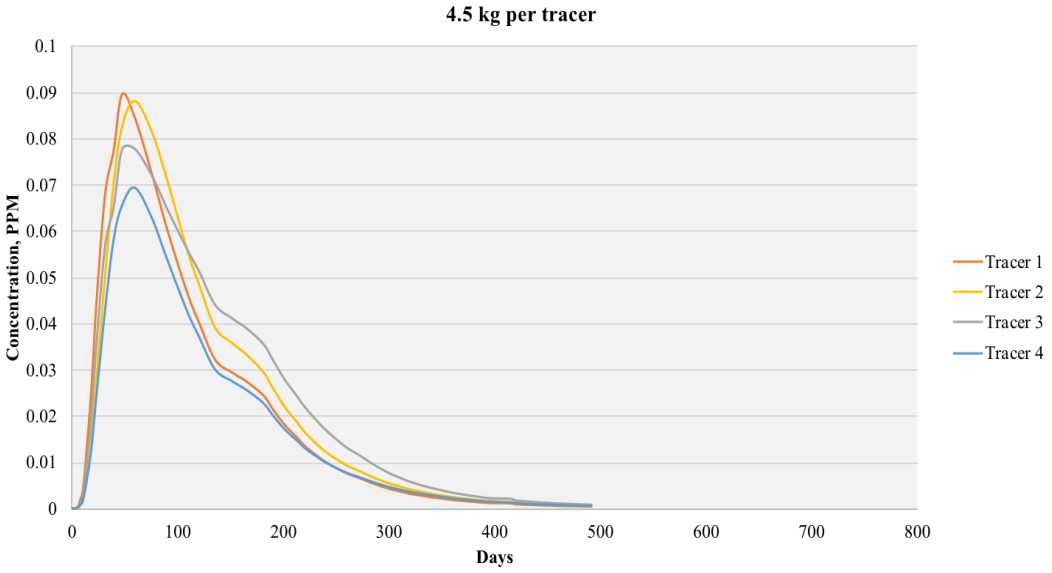

Figure 5-10: Producer Well-222 Produced Tracer Concentration with Time For 4.5 kg Per Tracer

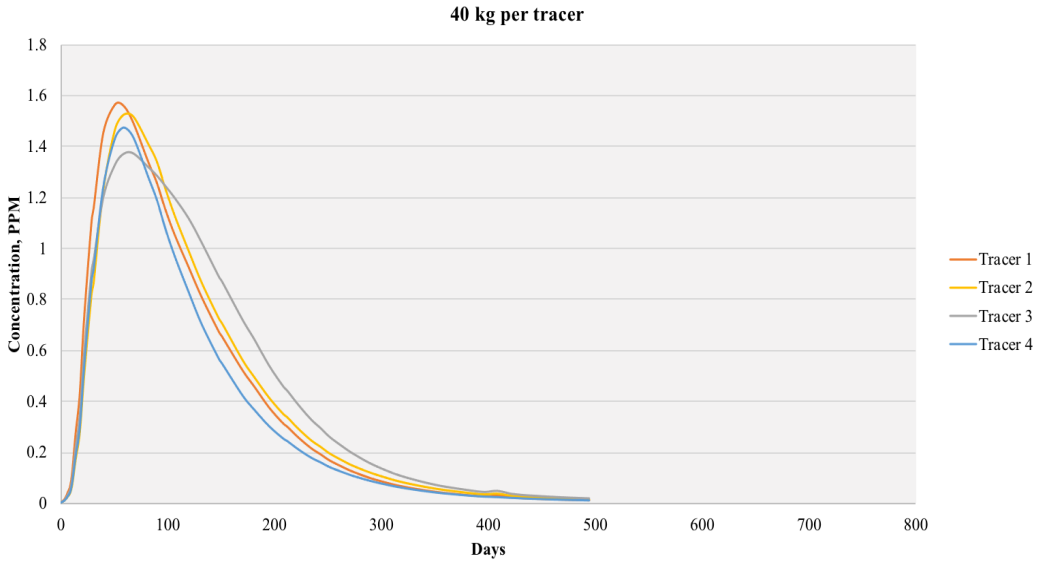

Figure 5-11: Producer Well-222 Produced Tracer Concentration with Time For 40 kg Per Tracer

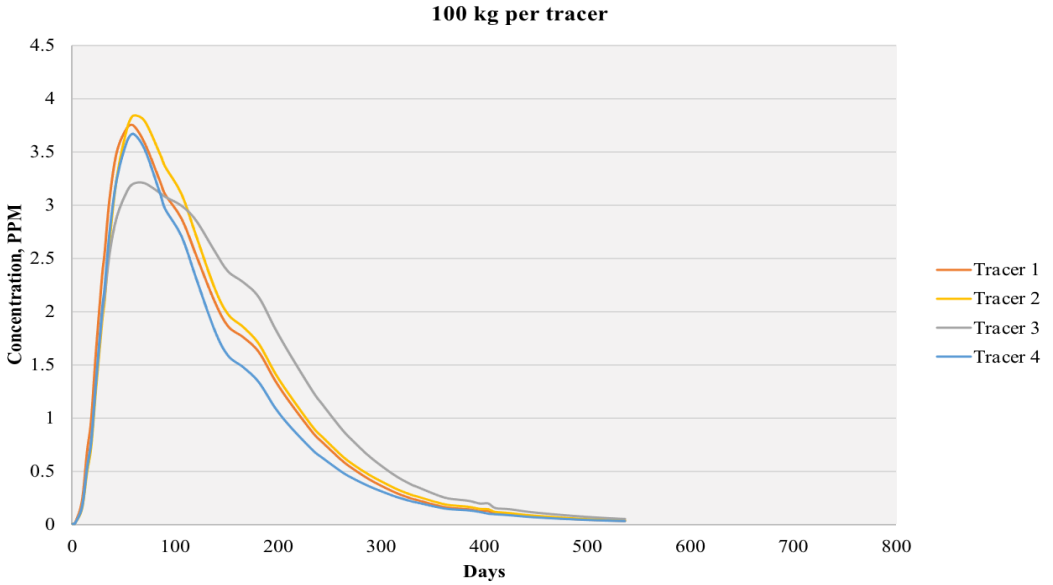

Figure 5-12: Producer Well-222 Produced Tracer Concentration with Time For 100 kg Per Tracer

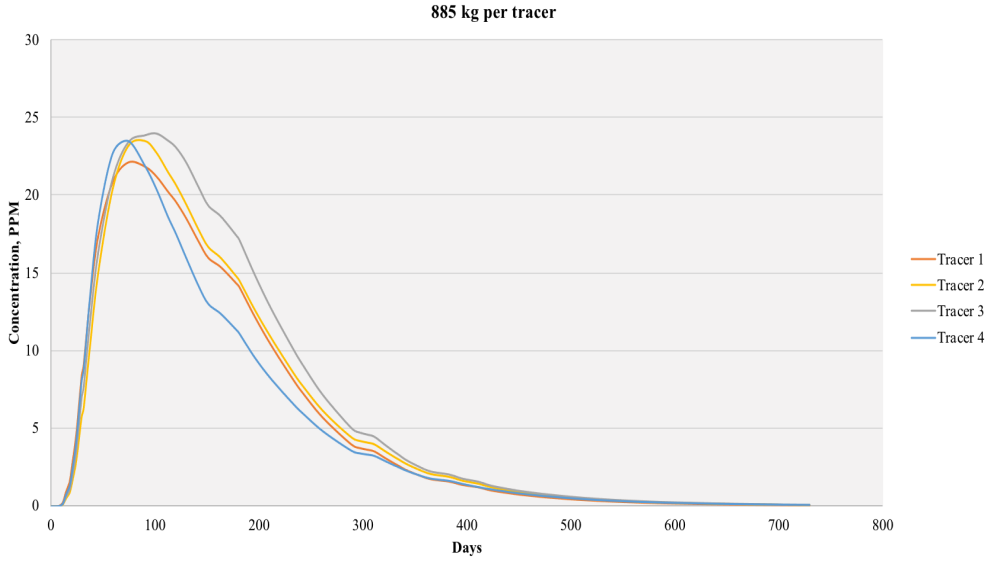

Figure 5-13: Producer Well-222 Produced Tracer Concentration with Time For 885 kg Per Tracer

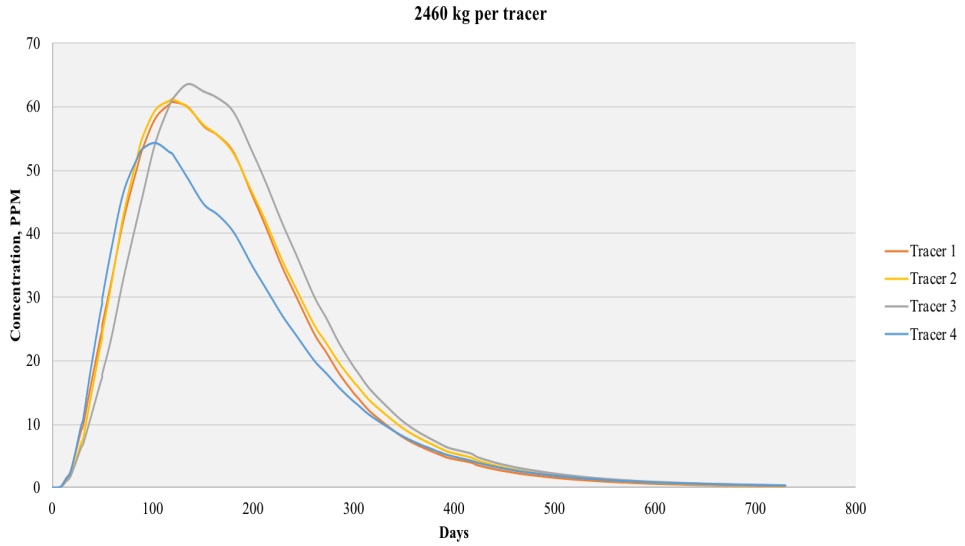

Figure 5-14: Producer Well-222 Produced Tracer Concentration with Time For 2460 kg Per Tracer

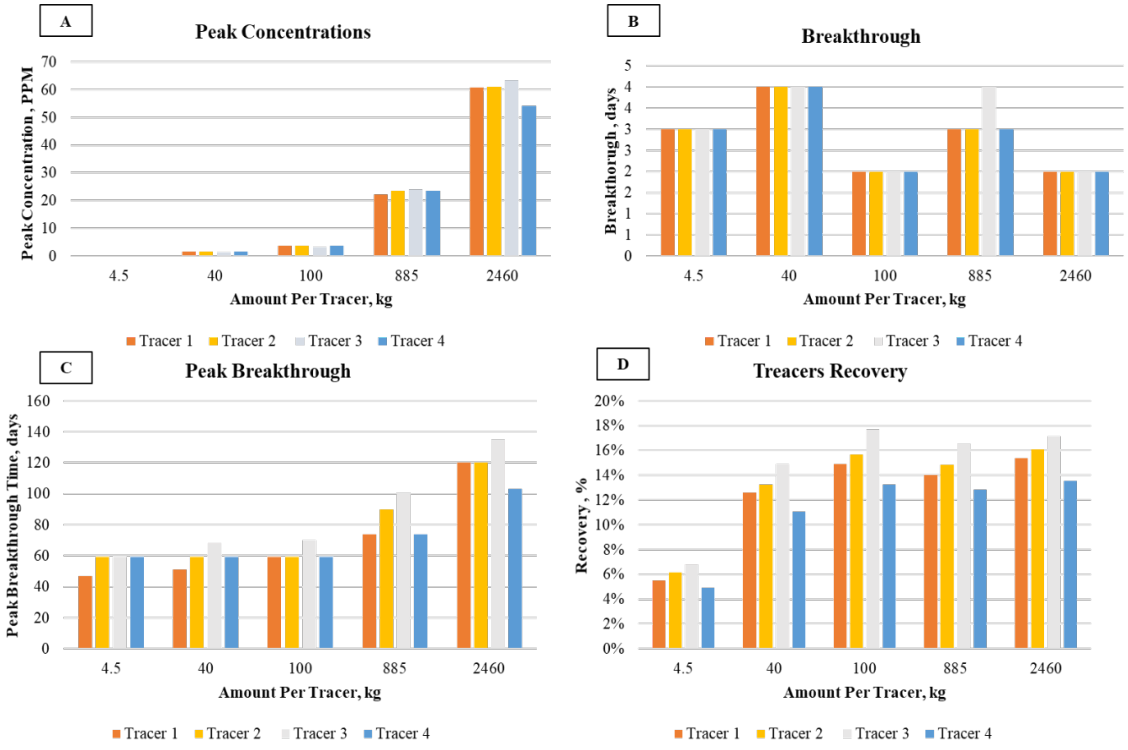

Figure 5-15: Peak Concentrations, Tracer Breakthrough, Peak Breakthrough and Recovery for Tracer Amounts Sensitivity

- **Sensitivity to Well Rates:**

The rates are typically designed so that the central producer of the five-spot pattern is a quarter of the total injection rates of the pattern wells. The rates are therefore set to be the same for all 5 wells in the 5-spot at different rates in m^3/d:50,40,30,20. All the cases have fixed values of the same amount injected per tracer (885 kg per tracer 3540 kg total) and tracer concentration (2000 PPM). The following **Figure 5-16** to **Figure 5-19** show the produced tracer curves from Well-222.It could be noticed the shape of the curves slightly shifts to the right and gets wider with decreased rates. More details are provided in **Figure 5-20.** As seen, peak concentrations and recoveries are slightly to moderately improved at lower rates for most of the tracers, this could be due to slightly lower pressurized pattern at lower rates, which reduces the amount of tracer traveling outside the pattern. However, lower rates are resulting in higher breakthrough times, especially when comparing peak breakthrough times, which increased almost two times from 50 m^3/d case to 20 m^3/d. This has significant impact on testing duration and termination times as longer times might not be practical or favorable.

Tracer recovery values and large times reflect the level of confinement. Another case was conducted to evaluate if results could be improved if pattern surrounding area builds up pressure to push tracers back inside the pattern. **Figure 5-21** shows tracer profile for this case. The case does not show much improvement, meaning more drastic actions (such as shutting the surrounding wells for a longer period before test) might be required that is hard to implement realistically.

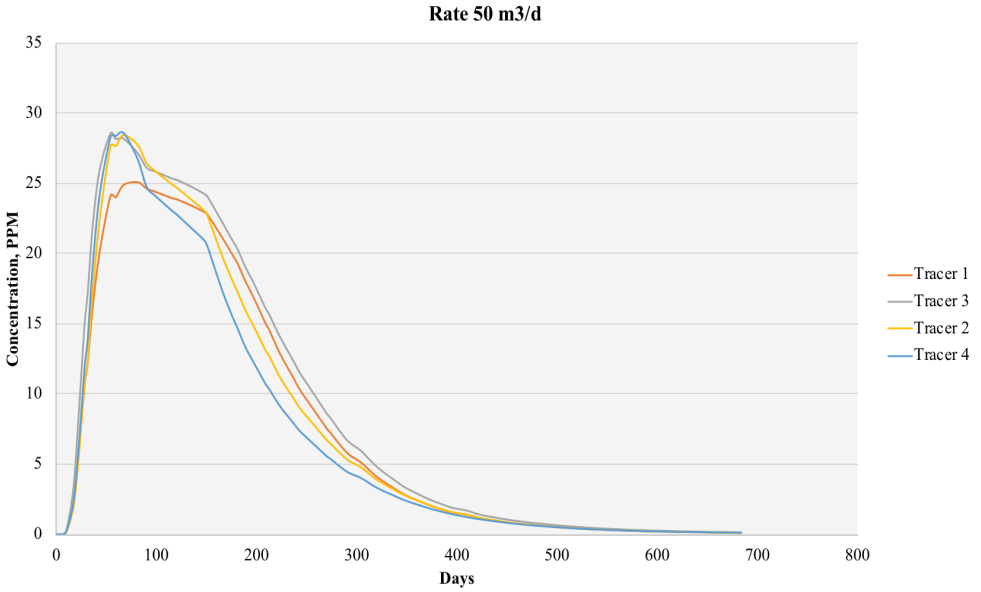

Figure 5-16: Producer Well-222 Produced Tracer Concentration with Time At 50 m^3/d

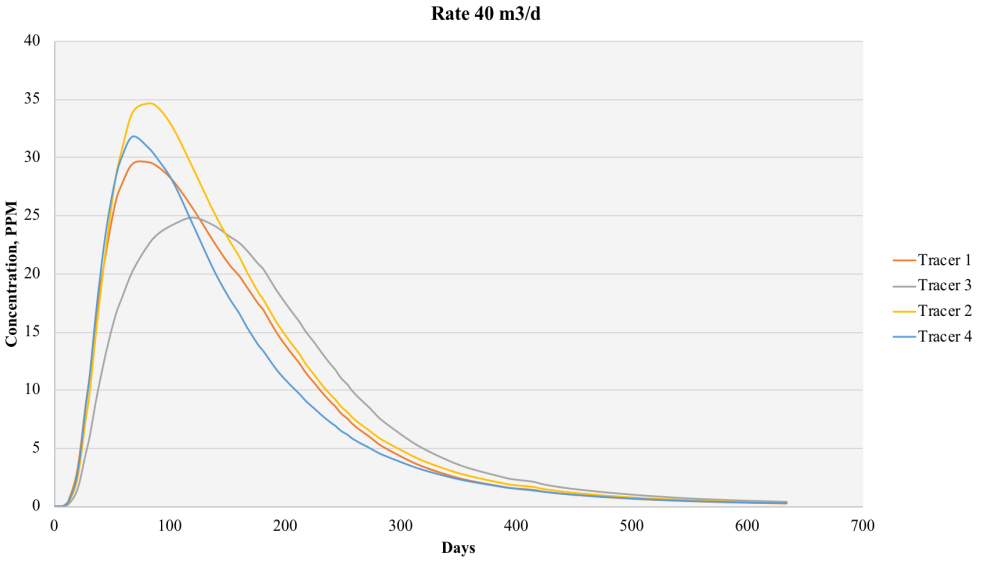

Figure 5-17: Producer Well-222 Produced Tracer Concentration with Time At 40 m^3/d

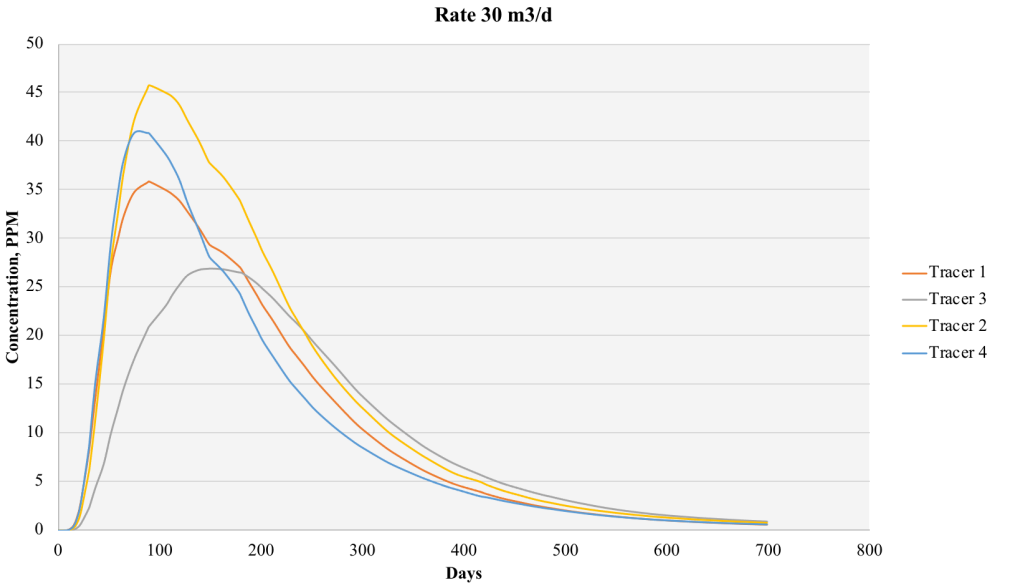

Figure 5-18: Producer Well-222 Produced Tracer Concentration with Time At 30 m^3/d

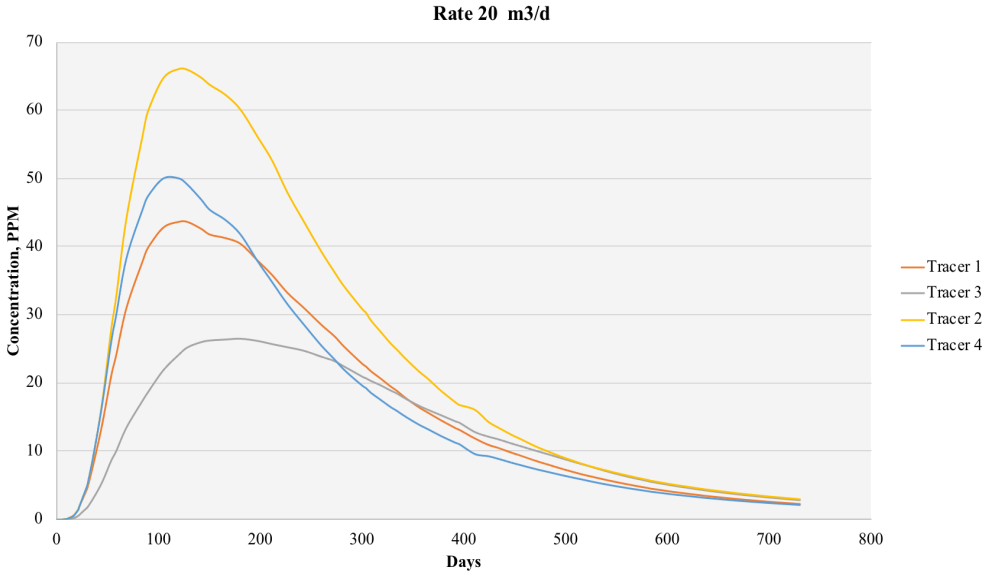

Figure 5-19: Producer Well-222 Produced Tracer Concentration with Time At 20 m^3/d

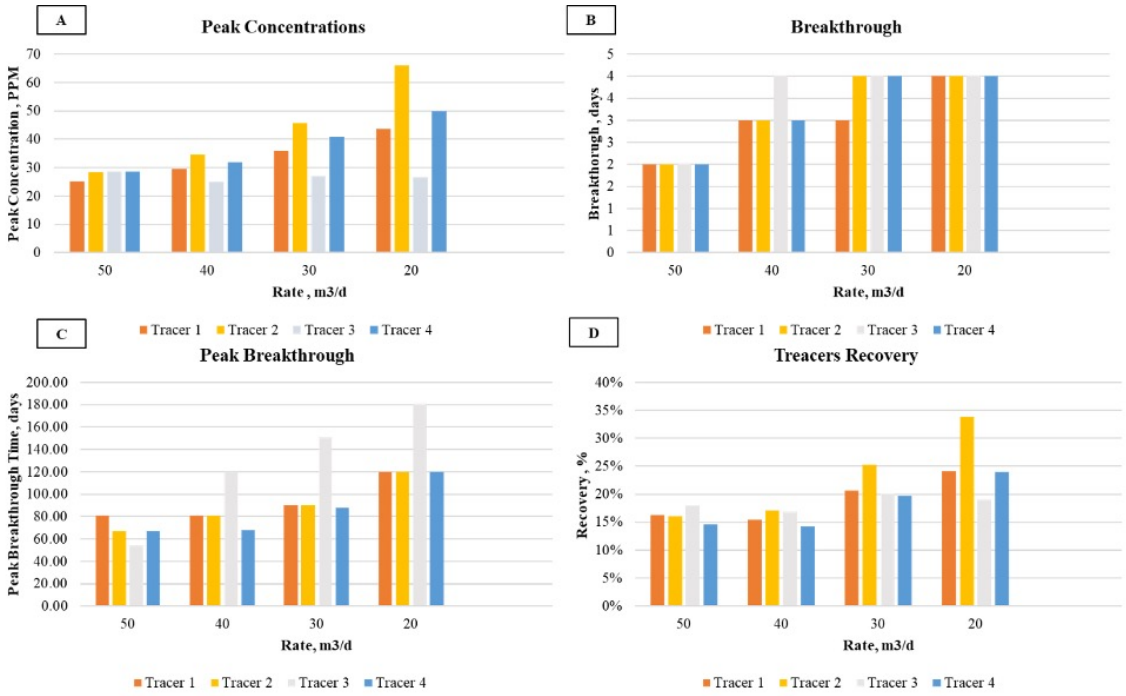

Figure 5-20: Peak Concentrations, Tracer Breakthrough, Peak Breakthrough and Recovery for Well Rates Sensitivity

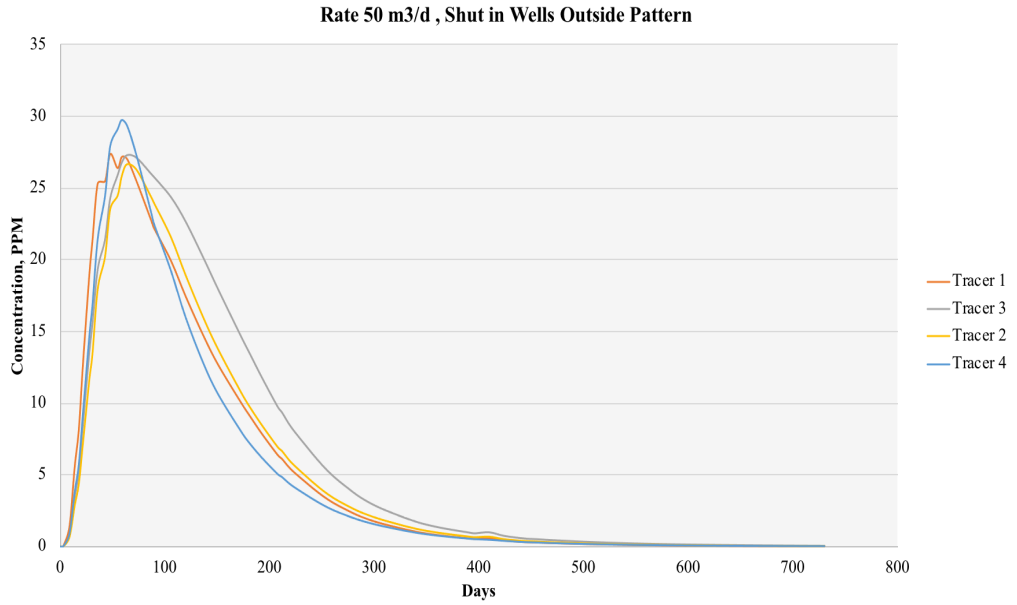

Figure 5-21: Well-222 Producer Tracer Curves for Case Of 50 m^3/d and Shut-in Wells Surrounding Pattern

- **Sensitivity to Total Dispersion Coefficient:**

This value is usually used as a history matching parameter for tracer profiles. To understand its impact and its magnitude on the tracer production; several cases were conducted with varying coefficients of different orders of magnitude (zero, 10^{-5}, 10^{-4}, 10^{-3}, 10^{-2}, 10^{-1} m^2/d). Results are shown in **Figure 5-22** to **Figure 5-27**. The results are as expected, the curves shift to the right with higher coefficient because more dispersion occurs, and peak times will be longer. Also, gradual reduction in peak concentrations. Details are shown in **Fig. 27**.

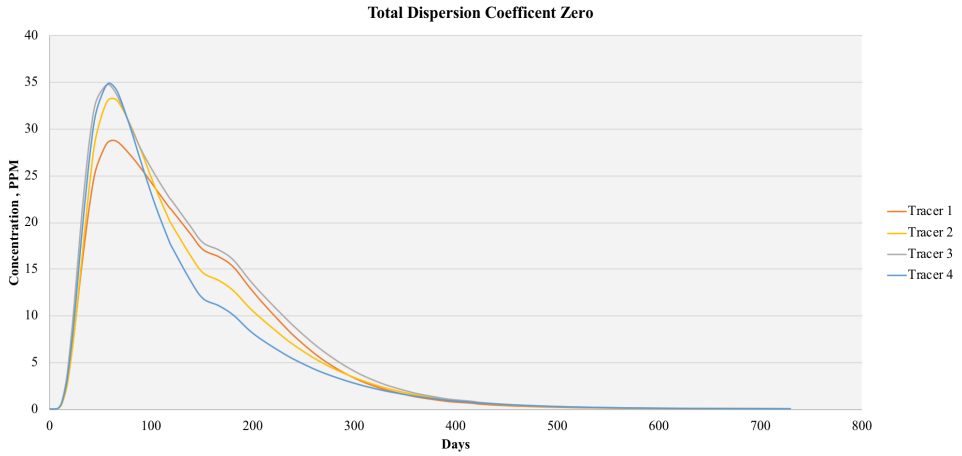

Figure 5-22: Well-222 Producer Tracer Curves for Case of Zero Dispersion Coefficient

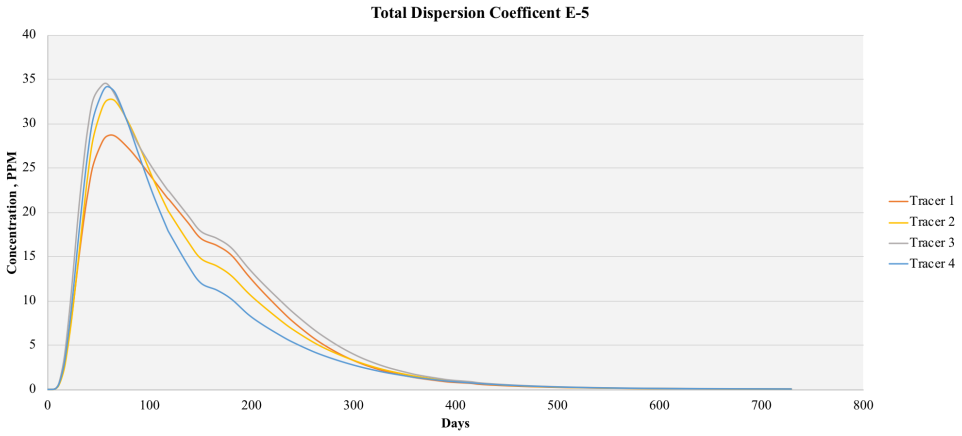

Figure 5-23: Well-222 Producer Tracer Curves for Case of E^{-5} Dispersion Coefficient

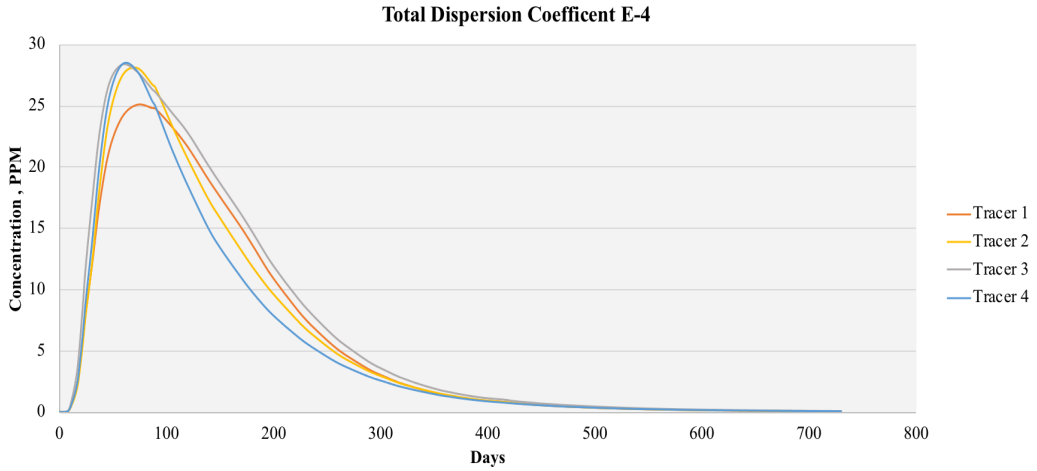

Figure 5-24: Well-222 Producer Tracer Curves for Case of E^{-4} Dispersion Coefficient

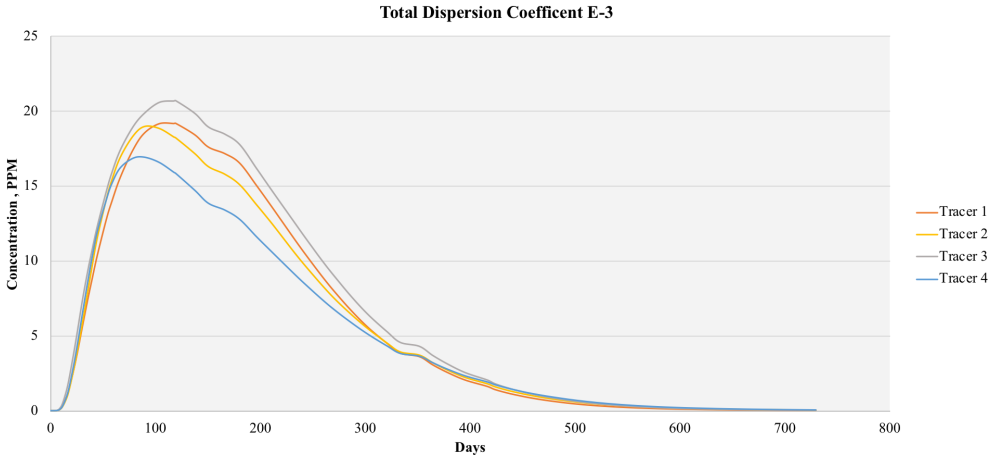

Figure 5-25: Well-222 Producer Tracer Curves for Case of E^{-3} Dispersion Coefficient

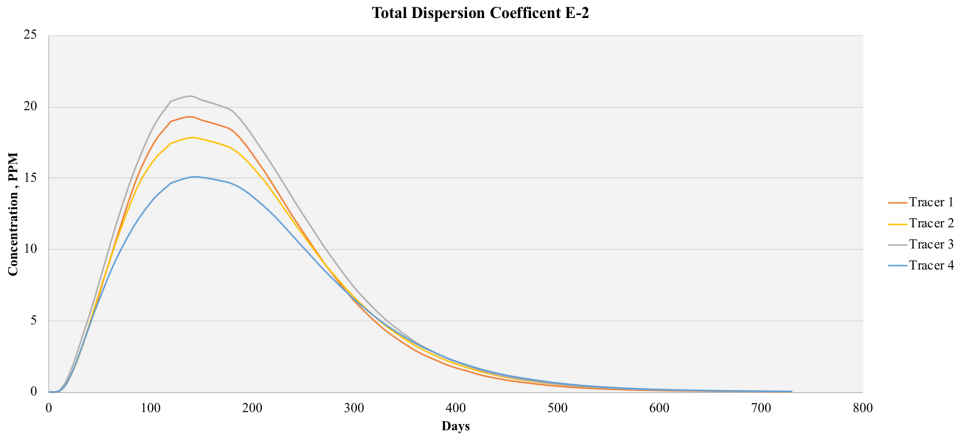

Figure 5-26: Well-222 Producer Tracer Curves for Case of E^{-2} Dispersion Coefficient

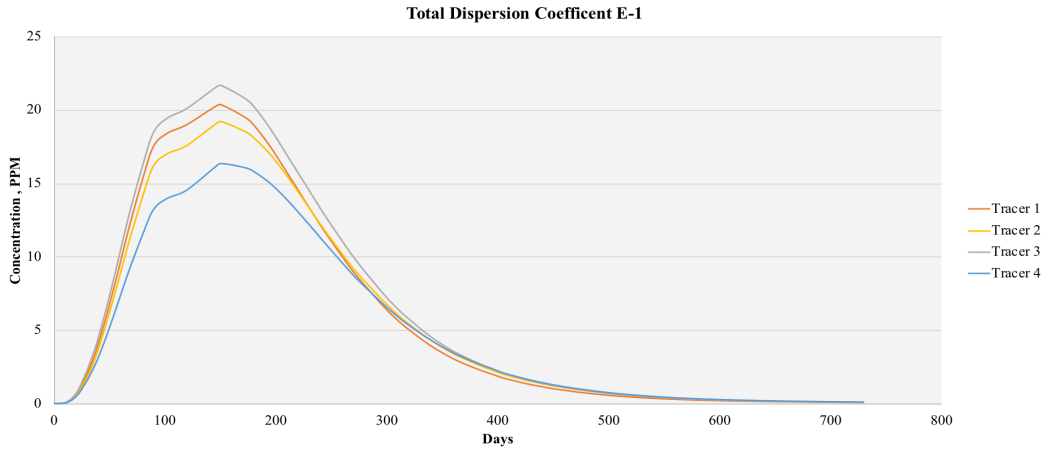

Figure 5-27: Well-222 Producer Tracer Curves for Case of E^{-1} Dispersion Coefficient

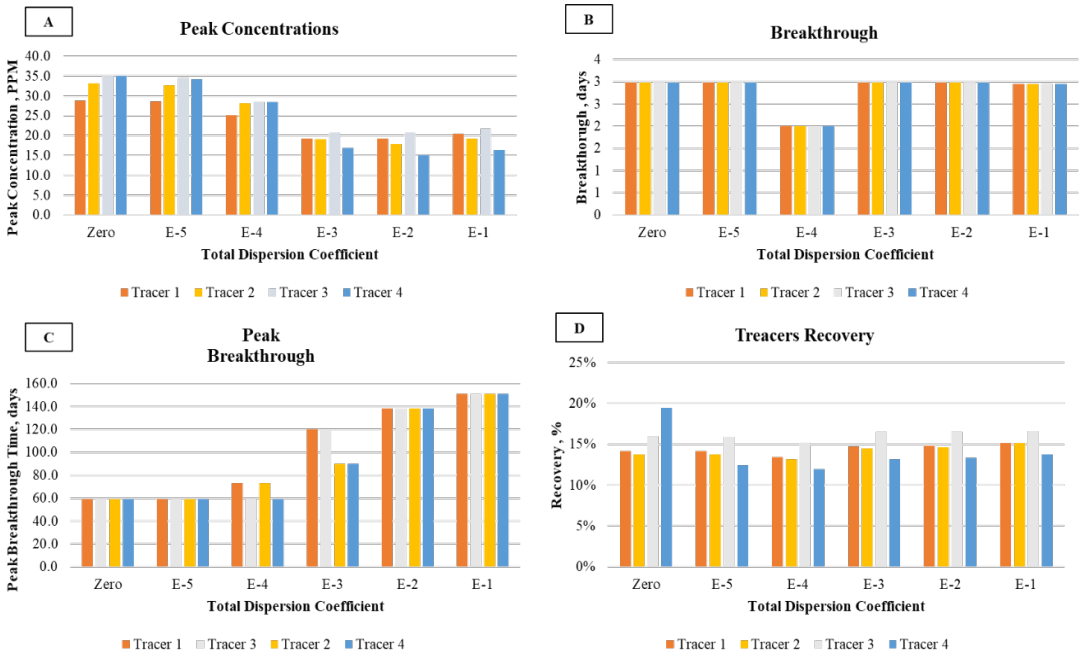

Figure 5-28: Peak Concentrations, Tracer Breakthrough, Peak Breakthrough and Recovery for Dispersion Sensitivity

- **Sensitivity to Pore Volumes Injected:**

The PV mentioned is the pore volume of 5-spot area top layer (36011 m3). In these cases, the tracers are injected for a specific amount and then followed by push water, the total of tracer slug and push water is the PV reported for each case. All the cases in this sensitivity have the same tracer concentration and amounts used, 2000 PPM and 885 kg

per tracer, respectively. The tracer curves for each case are shown in **Figure 5-29** to **Figure 5-34**. The peak concentrations generally reduce with increasing PVs injected, and curves tend to be narrower and to the left with higher PVs. One possible reason to the reduction of concentration could be dilution. The narrower curves at higher PVs are expected since the more you push the tracers the faster they will reach the producer well. Lower concentrations are observed with increasing PVs injected. This could be due to tracers being confined better with lower PVs injected due to less pressurized 5-spot pattern. See **Figure 5-35** which shows pressure areal map of the 5-spot pattern and part of the surrounding region for one of the layers after 15 months since test start. **Figure 5-35A** shows the map for the case with >1 PV injected and **Figure 5-35B** shows the map for the case with 0.1 PV injected. Both figures are in the same pressure scale, and it could be clearly seen that for the 0.1 PVs injected case, the pressure difference between the pattern and outside is less severe than in the >1 PV.

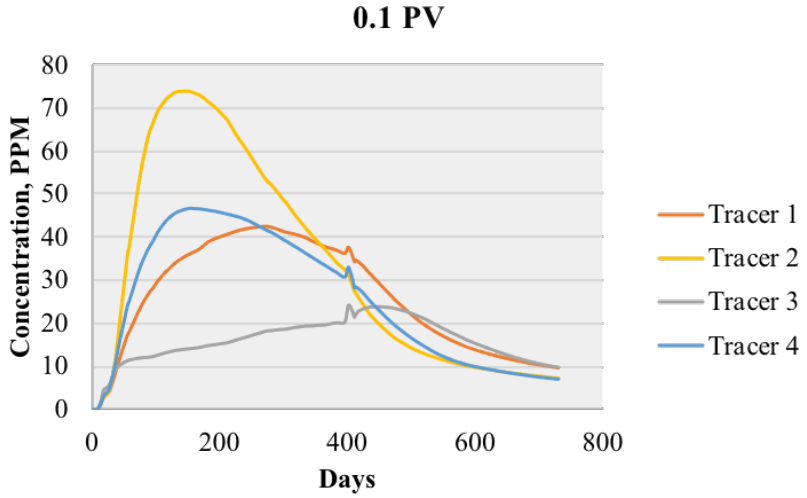

Figure 5-29: Well-222 Producer Tracer Curves for Case Of 0.1 PV Injection

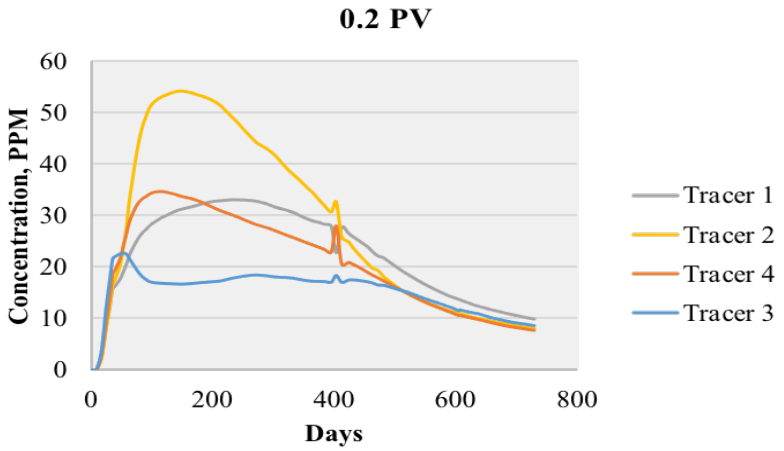

Figure 5-30: Well-222 Producer Tracer Curves for Case Of 0.2 PV Injection

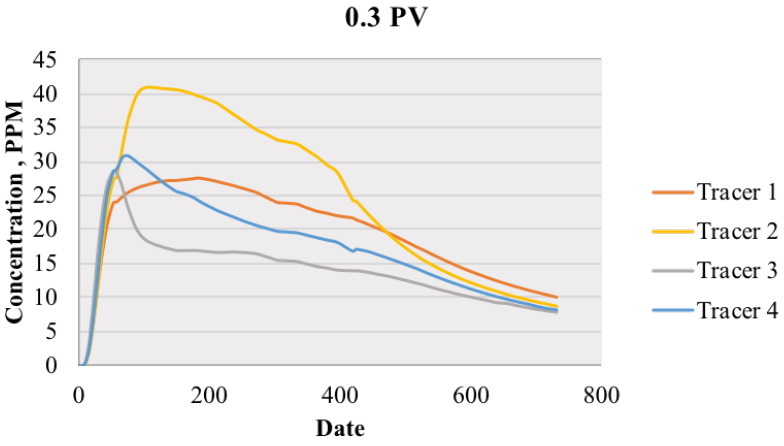

Figure 5-31: Well-222 Producer Tracer Curves for Case Of 0.3 PV Injection

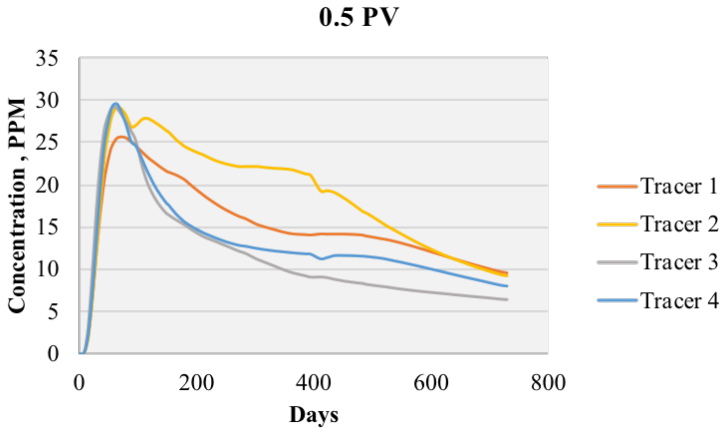

Figure 5-32: Well-222 Producer Tracer Curves for Case Of 0.5 PV Injection

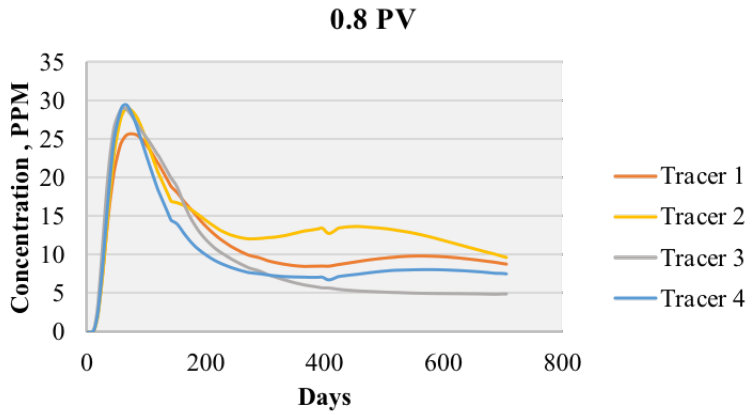

Figure 5-33: Well-222 Producer Tracer Curves for Case Of 0.8 PV Injection

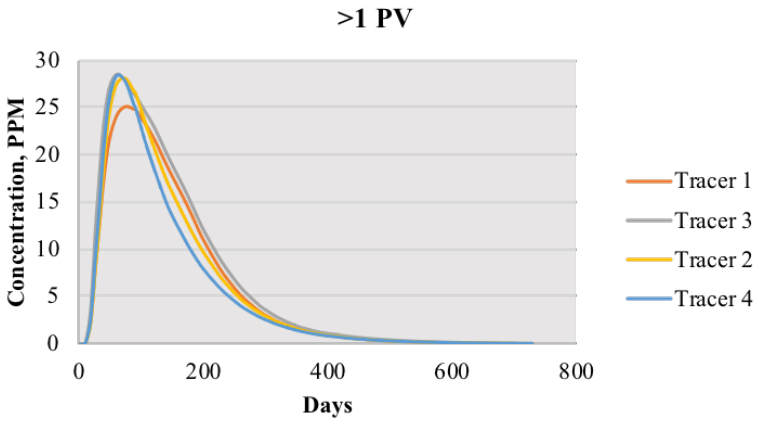

Figure 5-34: Well-222 Producer Tracer Curves for Case Of >1 PV Injection

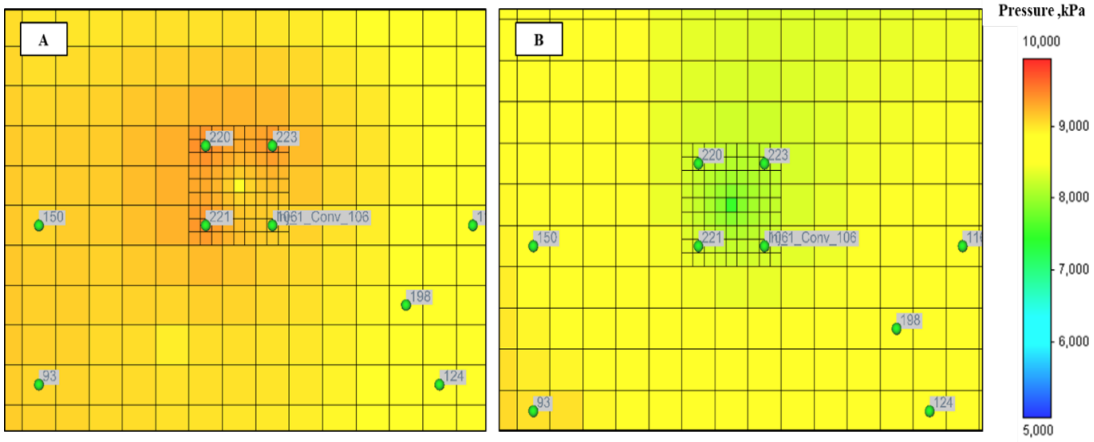

Figure 5-35: Areal View Pressure Map For A) >1 PVs Injected Case And B) 0.1 PVs Injected Case

- **Sensitivity to Polymer Injection:**

To evaluate the need for adding polymer, cases have been simulated with FP2500 PPM, FP5000 PPM and no polymer. The tracer profile curves are shown in **Figure 5-36** to **Figure 5-38** , and details of recovery and peak times are shown in **Table 5-2** and **Table 5-3**. Polymer yields more favorable results as more tracer was recovered, see **Table 5-2.** On the other hand, peak breakthrough times have increased from the no polymer case as shown in **Table 5-3**.

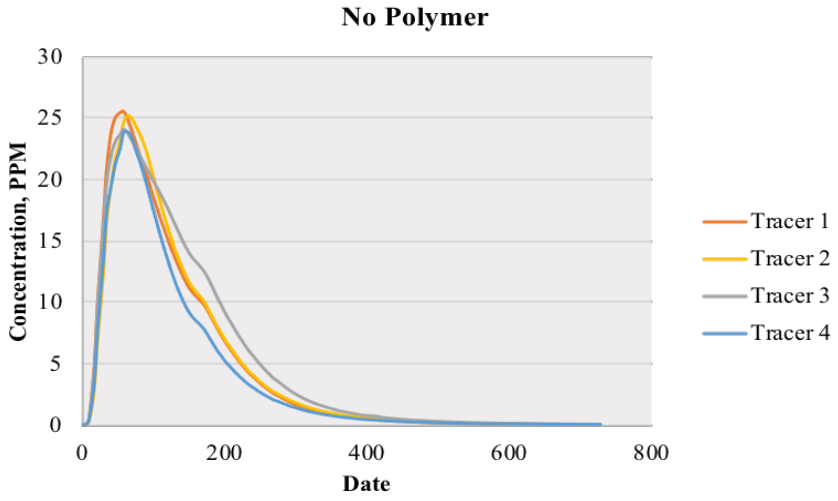

Figure 5-36: Well-222 Producer Tracer Curves for Case of No Polymer

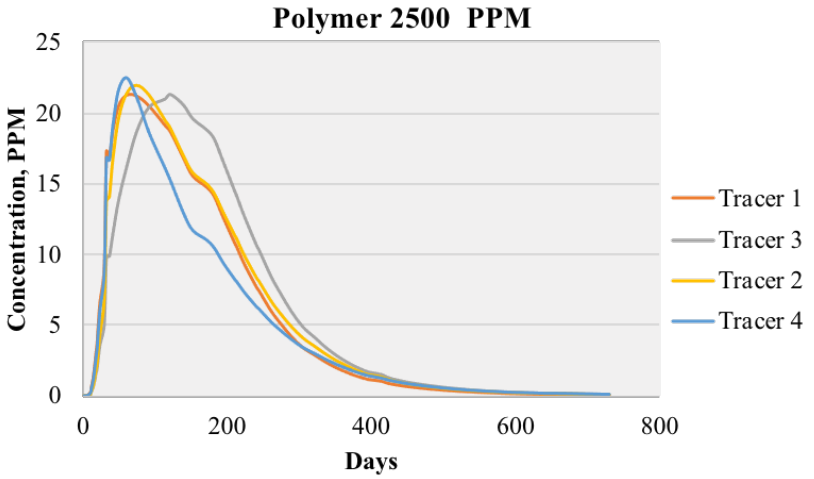

Figure 5-37: Well-222 Producer Tracer Curves for Case of 2500 PPM Polymer

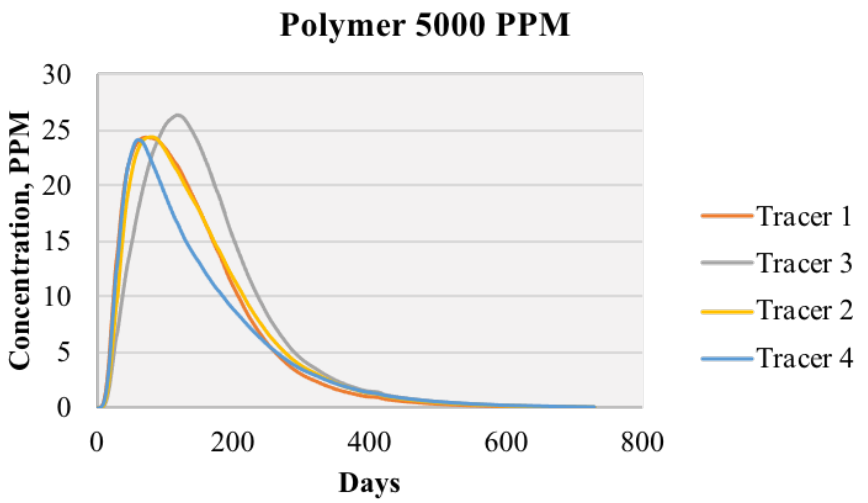

Figure 5-38: Well-222 Producer Tracer Curves for Case of 5000 PPM Polymer

Tracer	Tracer Recovery		
	No Polymer	2500 PPM Polymer	5000 PPM polymer
Tracer 1	10%	13%	14%
Tracer 2	10%	14%	15%
Tracer 3	12%	15%	17%
Tracer 4	9%	12%	13%

Table 5-2: Tracers Recovery Percentages at Each Polymer Concentration

Tracer	Peak BT Time, days	Peak BT Time, days	Peak BT Time, days
	No Polymer	2500 PPM	5000 PPM
Tracer 1	73.00	59	68.00
Tracer 2	73.00	73	80.00
Tracer 3	59.00	120	120.00
Tracer 4	59.00	59	59.00

Table 5-3: Tracer Breakthrough Times for Different Polymer Cases

5.4.3 IWTT Sensitivity Conclusions

Tracer concentrations did not have a significant impact on the results except in the tracer peak arrival times and slightly higher concentration at the peak. This is due to the dilution that occurred at the low tracer concentration injection. 10,000 PPM tracer injection concentrations required < 2 days of injection at 50 m^3/d for the required 885 kg per tracer.

However, for 1000 ppm, it required almost 18 days for injection. Therefore, injecting at high concentrations is preferred.

The amount of tracer injected is the most crucial design parameter. Injecting too little will not yield meaningful results. It is recommended to inject enough so that the peak concentration is at least 100 times the minimum tracer concentration MTC, the minimum detection limit. The 4.5 kg per tracer case did not yield satisfactory results as concentrations at the peaks and recovery were too low. The 40 and 100 kg per tracer showed satisfactory concentrations at the peaks; however, if drift and dispersion are considered, concentrations might be off by around 37% at the peak. Therefore 800 kg per tracer seems to be a safe option and also allows to observe tracers in nearby wells outside the pattern at detectable concentrations.

Highest peak concentrations were observed for low injection rates of 20 m^3/d. at lower rates, lower injection pressures are required and hence the pattern is less pressurized compared to 50 m^3/d case which reduced the amount of tracer traveling outside the pattern. The major drawback is however in the time required to observe peak and tail of the curve, which is around double the time required for 50 m^3/d.

the value of dispersion coefficient is usually used as a history matching parameter for tracer profiles. The sensitivity was conducted evaluate the magnitude of the impact of dispersion. The tracer production curves shift to the later times because more dispersion occurs, and peak times are longer. Also, peak concentrations decrease, the decrease was around 37% between the cases with lowest and highest coefficients.

The sensitivity to pore volumes injected was studied. In all cases, the tracers are injected for a specific amount followed by push water; the total of tracer slug and push water is the PV reported for each case. About 1 PV of tracer and water is favorable since it yields to faster breakthrough times and faster test results.

Adding polymer to the injected tracer water showed favorable results in terms of tracer recoveries. Injection of polymer is beneficial to the IWTT for reducing fingering during viscous oil displacement.

5.4.4 IWTT Design Recommendations

Based on the simulation sensitivity study, the following recommendations for the IWTT design are provided:

- Tracer concentrations: 10,000 PPM per tracer
- Tracer amount: At least 800 kg of tracer
- Well rates: All 5 spot wells at rate 50 m3/d
- Adding polymer: At least 2500 ppm
- Push water: Inject to no more than 1 PV to increase tracer recovery
- Testing/tracer monitoring: At least 7-8 months to observe sufficient amount of tracer in the production well. (If this time period is not available, then it is recommended that tracers be added to the SP slug itself and the effluent water be analyzed for the tracers. The matching of tracers may help the interpretation of the SP pilot)

5.5 SURFACTANT POLYMER SP PILOT DESIGN

5.5.1 SP Pilot Simulation Study Objective and Sensitivities

The effectiveness of the SP formulation in reducing oil-water interfacial tension and mobilizing trapped oil was demonstrated in the corefloods experiments. Numerical scaling-up of the SP process from core to field-pilot scale and sensitivity analysis are essential to the design and success of a pilot project. Conducting an interwell tracer test (IWTT) prior to the SP pilot can further enhance the interpretation of the pilot. The model

used in IWTT simulation studies is used for the simulation of the SP pilot. The objective of the simulation study is to identify suitable choices for key design parameters: SP composition, SP slug size, and polymer drive concentration.

The original oil in place for the 5-spot top layer is 24,648 m^3. The remaining oil in place ROIP by 01/01/2018 is 22,295 m^3 (HCPV); this number is used in the recovery calculations. The PV in the calculations correspond to the PV of the top layer of the 5-spot area; PV=36011 m^3. The initial pressure and oil saturation of the 5-spot is shown in the 3D views in **Figure 5-39a** and **Figure 5-39b**, respectively. The average pressure in the 5-spot is approximately 8695 kPa, and oil saturation is high, ranging from 0.52-0.80. For most of the cases simulated, a 2500 ppm polymer solution is injected before the SP injection. The pre-polymer flooding in the base case is assumed to 0.8 PV and the injection rate is 50 m^3/d in each injection well. Inter-well tracers are also injected along with the polymers.

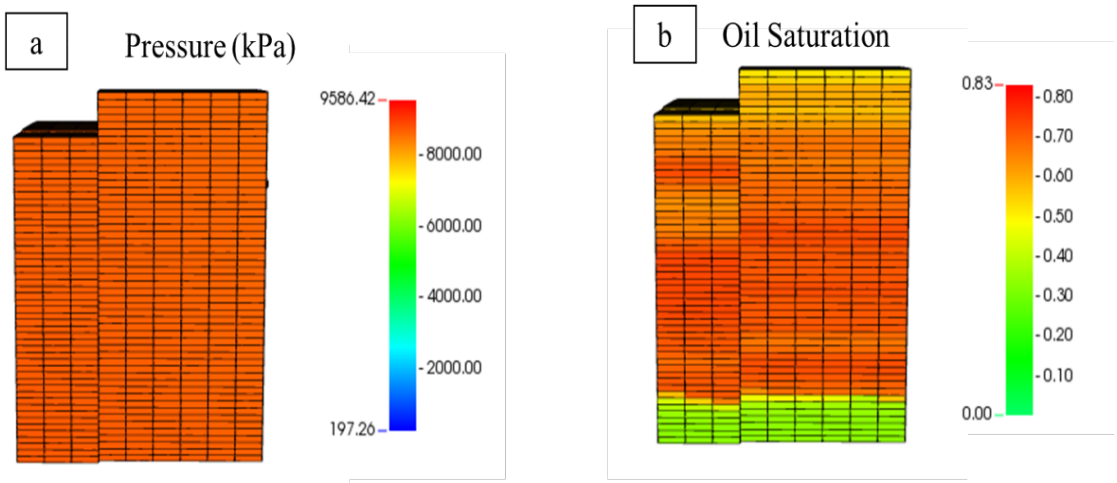

Figure 5-39: a) Pressure And b) Oil Saturation Distribution X-Z View Of The 5-Spot Area On January 2018

The scenarios and sensitivity parameters are summarized in **Table 5-4**. Different parameters were varied to assess their impact on the incremental oil recovery: SP slug size,

polymer concentration in SP slug and polymer drive PD, well rates and injection production ratios (IPR), prior polymer flood PVI, and surfactant concentration. The cases were compared against no-surfactant-water drive only and also a base case that consists of the following: 0.20 PV SP, 1% surfactant concentration, 2500 PPM of polymer SP & PD, 0.8 PV pre-flush, IPR of 4, and well injection rate of 50 m^3/d. The success criteria were chosen to be the incremental oil recovery and the rate of recovery. Oil production was simulated for 2 years; all simulation runs commence on 01/01/2018 and end on 01/01/2020 (to limit simulation run time).

Case. /Parameter	SP Slug, PV	IPR	Injection Wells Rate, m3/d	SP Polymer Concentration, PPM	PD Polymer Concentration, PPM	Pre-polymer size, PV	RRF	Surf. Conc.
1 (Base Case)	0.20	4	50	2500	2500	0.8	1	1%
2	0.20	4	50	2500	2500	0.3	1	1%
3	0.20	4	50	2500	2500	0	1	1%
4	0.20	4	40	2500	2500	0.8	1	1%
5	0.20	4	20	2500	2500	0.8	1	1%
6	0.20	4	10	2500	2500	0.8	1	1%
7	0.20	1	10	2500	2500	0.8	1	1%
8	0.20	2	20	2500	2500	0.8	1	1%
9	0.20	4	50	2500	5000	0.8	1	1%
10	0.20	4	50	5000	5000	0.8	1	1%
11	0.25	4	50	2500	2500	0.8	1	1%

12	0.30	4	50	2500	2500	0.8	1	1%
13	0.40	4	50	2500	2500	0.8	1	1%
14	0.20	4	50	2500	2500	0.8	2	1%
15	0.20	4	50	2500	2500	0.8	3	1%
16	0.20	4	50	2500	2500	0.8	5	1%
17	0.20	4	50	2500	2500	0.8	10	1%
18	0.20	4	50	2500	2500	0.8	20	1%
19	0.20	4	50	2500	2500	0.8	1	0.5%

Table 5-4: Summary of Different Scenarios Setup for the SP Pilot Design

5.5.2 SP Pilot Sensitivity Results

- **Sensitivity to SP Slug Size**

Figure 5-40 shows the results of oil recovery (in terms of % ROIP) as a function of fluid produced from the central well_222 (in terms of the 5-spot PV) for different SP slug sizes (cases 1, 11-13). All the cases have 1% surfactant concentration. As the surfactant slug size increased, oil recovery increased. By the end of the simulation run, which is 19 months after SP injection, the 0.40 SP slug case recovered 11.2% of ROIP, as compared to 9.7% of the base case (0.20 PV SP) and 8.05% of water drive case. The water drive case includes displacement of the injected polymer by water. This displacement which is unstable. CMG does not capture the instability and overestimates oil recovery in this case. The 0.40 SP slug size case resulted in 3.15% of incremental oil, that is considering the period of the simulation run (two years), which might be the period of interest within the SP pilot test timeframe. The incremental recovery could be higher if oil recovery data were to be observed at later years. **Table 5-5** compares the oil recovery after 2.1 PVs (12 months since test start) injected for different surfactant slug sizes; adding 0.40 SP slug

improved the oil recovered by 28% over that of water injection. **Figure 5-41** shows oil saturations inside the 5-spot after 15 months of test start (March 2019) for three slug size cases. It could be seen from the figure that in the case of 0.40 slug size, more oil was mobilized (more blocks below the residual of 0.33 in the grids near the injectors). It is also observed however; the sweep is not ideal (black circled).

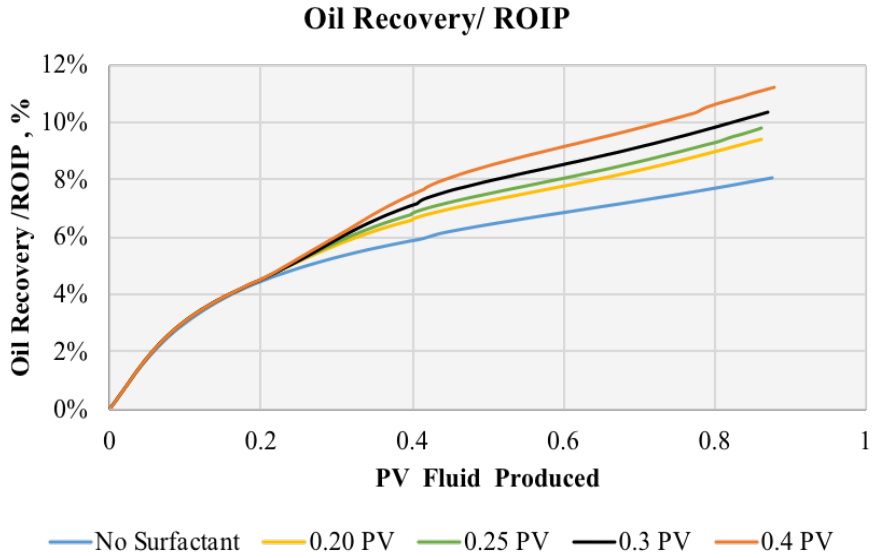

Figure 5-40: Effect of Surfactant Slug Size on The Oil Recovery

SP PV Injected	Recovered Oil after 2.1 PV injected, m^3	Increased oil recovery, % of water drive case
No Surfactant	1292	-
0.20 PV	1431	11%
0.25 PV	1468	14%
0.30 PV	1549	20%
0.40 PV	1655	28%

Table 5-5: Oil Recovery After 2.1 PV Injected (January 2019, 12 Months Since Test Start) And Percent Improvement From Water Drive Case (No Surfactant)

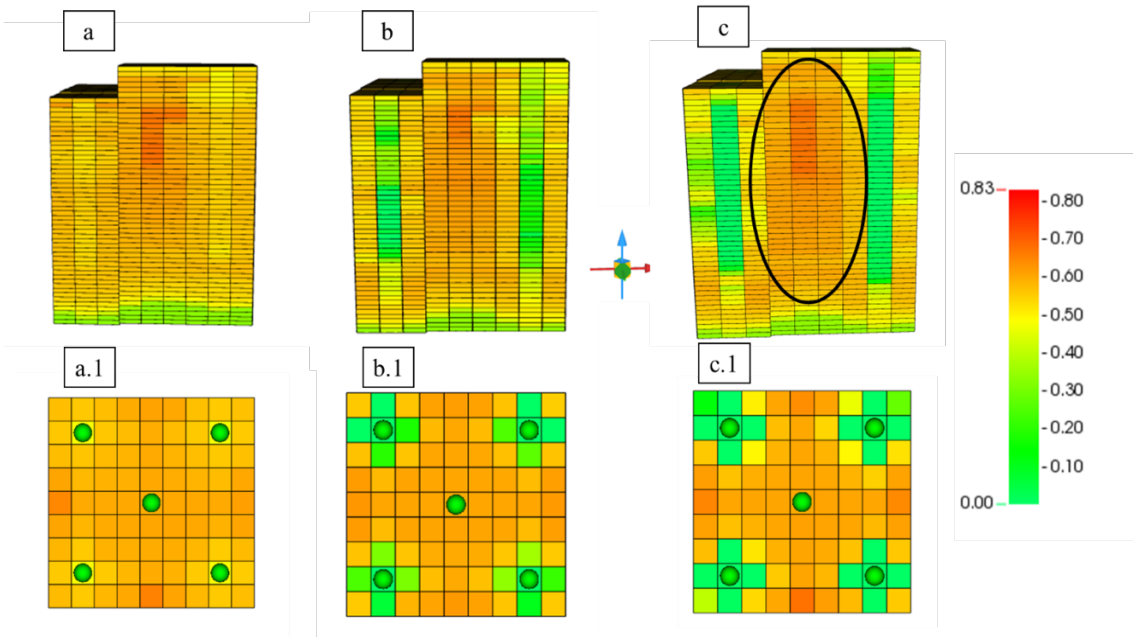

Figure 5-41: Oil Saturation 3D And Aerial View Maps For a) and a.1) No Surfactant b) and b.1) 0.20 PV SP and c) and c.1) 0.40 PV SP at March 2019 (15 Months After Test Start)

- **Sensitivity to Polymer Concentration**

Three cases were run to analyze the effect of polymer concentration during the injection of SP slug, and the concentration of the polymer drive. The base case (case 1) has the same polymer concentration of 2500 PPM in SP slug and PD injection. The other cases include fixing the concentration at 5000 PPM (case 10) and varying it by injecting 2500 PPM polymer with the SP slug and increasing it to 5000 PPM polymer during the PD (Case 9). **Figure 5-42** shows oil recovery with days since pilot starts (including 0.8 PV pre-polymer flush). After 700 days since the beginning of the test, the recovery from the case where polymer concentration was varying (2500- 5000 PPM) was the highest at 13.6% as compared to 9.3% from the base case (2500-2500 PPM). The recovery from the cases that included higher polymer concentrations of 5000 PPM (either during PD, SP or both) was better than the base case due to the better sweep efficiency. **Figure 5-43** shows an aerial oil saturation view inside the 5-spot after 15 months since test start. The figure shows

noticeable improvement from the base case (2500-2500 PPM polymer), it also shows the case of 2500-5000 PPM has better sweep inside the 5-spot as compared with the case of 5000 PPM polymer in SP and PD. The improved recovery at higher concentration is due to the higher polymer viscosity that results in better mobility ratio. The reason behind the better performance for the 2500-5000 PPM case than the 5000-5000 PPM case could be due to higher injection pressure related to the high polymer concentrations during the SP injection and more fluid flow out of the pattern. **Figure 5-44** shows during SP injection, the 5000-5000 PPM case had higher BHP due to reduced injectivity. The reduced injectivity is expected due to the higher viscosities of the polymer at higher concentrations. **Figure 5-45** shows an aerial view of a water phase viscosity of 5000-5000 PPM case in single layer approximately 15 months after test start. Polymer viscosity as a function of concentration (1500-5000 PPM) at a shear rate of 10 s-1 is shown in **Figure 5-46**. The values shown for 1500 and 2500 PPM are model generated based on the model match with viscosity lab measurement at higher concentrations (5000-8000 PPM).

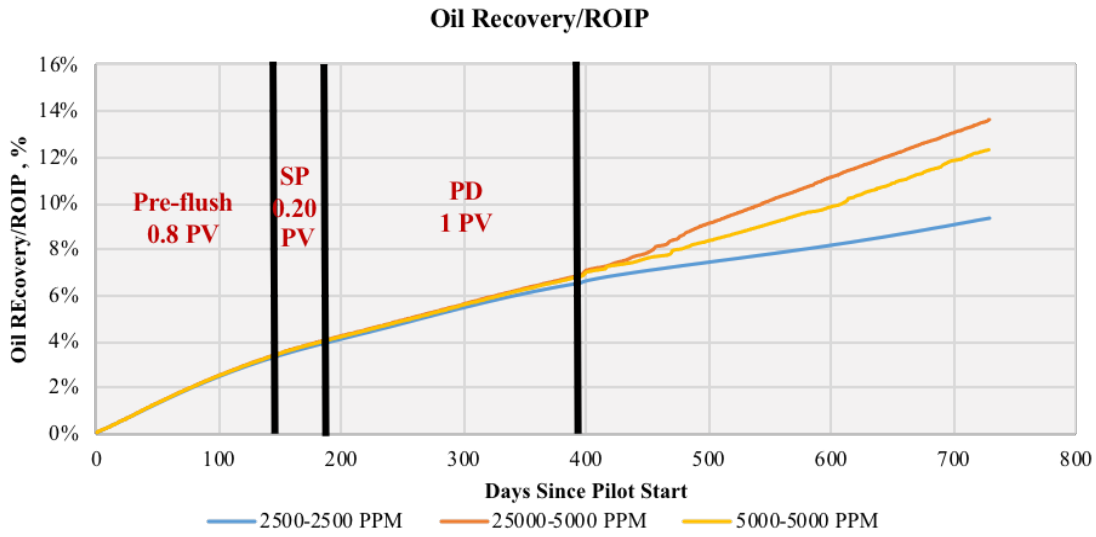

Figure 5-42: Oil Recovery /ROIP Since the Test Start for Cases at Different Polymer Concentrations

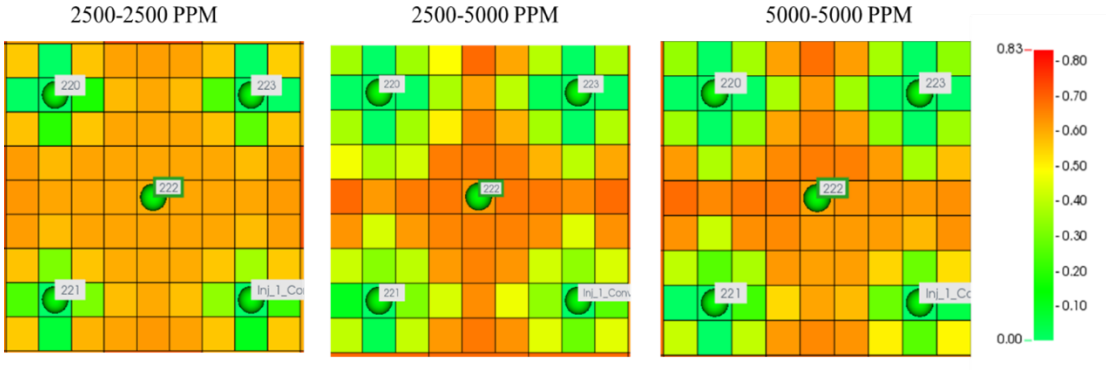

Figure 5-43: Oil Saturation In Layer 27 Inside The 5-Spot For The Three Polymer Concentration Combination Cases At March 2019 (15 Months After Test Start)

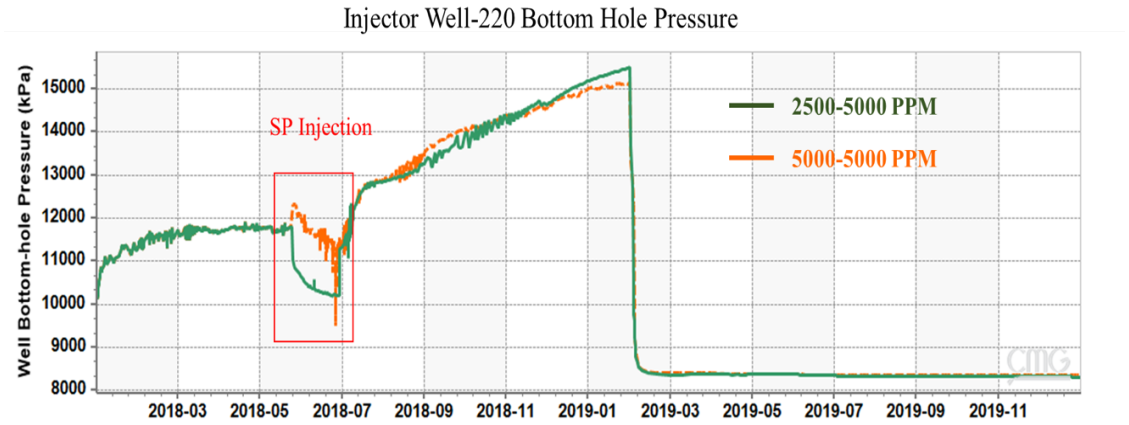

Figure 5-44: Bottom Hole Pressure of Injector Well-220 At Two Different Cases of Polymer Concentrations Combinations

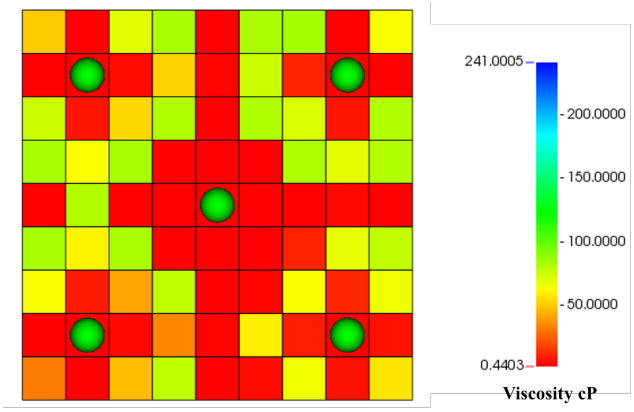

Figure 5-45: Water Phase Viscosity Distribution Of 5000-5000 PPM Case In Layer 19, Approximately 15 Months After Test Start

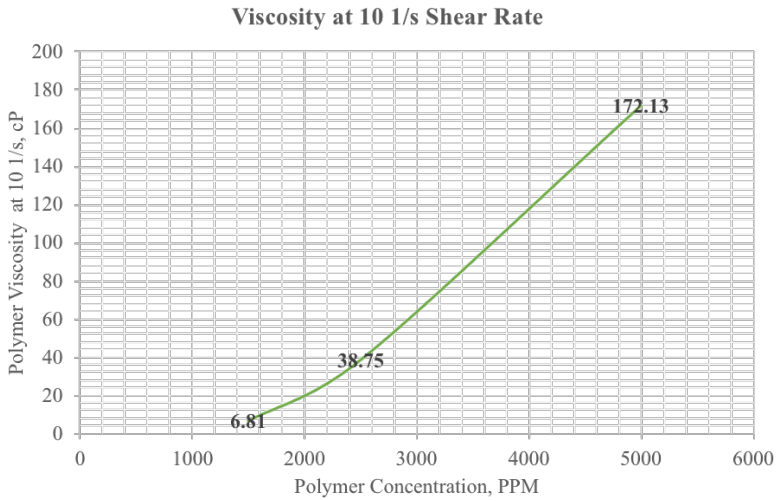

Figure 5-46: Polymer Viscosity At 10 s^{-1} As A Function of Polymer Concentration

- **Sensitivity to Well Rates and Injection Production Ratio IPR**

Figure 5-47 shows the effect of injection rate on the oil recovery from the 5-spot. The higher the rate the faster is the oil recovered, but the 40 m^3/d and 50 m^3/d cases show similar recovery with time. The results are as expected. However, as it could be seen from **Figure 5-4Figure** 5-48 that shows the recovery in terms of PVs injected, the lower the rate the slightly higher amount of oil is recovered at the same PV injected. This is possibly due to lower pressurized 5-spot at lower rates, which resulted in in better confinement of the oil within the 5-spot and hence higher recovery. The lines in **Figure 5-48** do not all extend to the same point because the runs were stopped at the same date instead of same injected pore volume. Based on these results, it could be more appropriate to asses at the impact of the injection production ratio IPR rather than well rates.

Three IPR cases (including the base case) were run: IPR of 1, 2 and 4 (base case). The IPR in this context is the ratio of the total injection inside the pattern to the total production of the pattern (central producer well-222). The base case (IPR 4) consists of same assigned rates for all wells in the pattern including the producer (50 m^3/d), the 2 IPR

case has assigned rate of 20 m^3/d for each injector and 40 m^3/d for the producer, the 1 IPR case has assigned rate of 10 for each injector and 40 m^3/d for each producer. **Figure 5-49** shows the oil recovery as a function of PVs produced for different IPR cases. It could be observed that at the same PV fluid produced, more oil recovered from the case of IPR of 1, at 0.8 PVs produced, the base case recovered 8.3% of the oil, whereas the case of 1 IPR recovered 12.7% of the oil. At IPR 1 the central producer creates a greater pressure sink as compared to the other cases which reduces fluid drifting outside the pattern and hence more oil is produced faster.

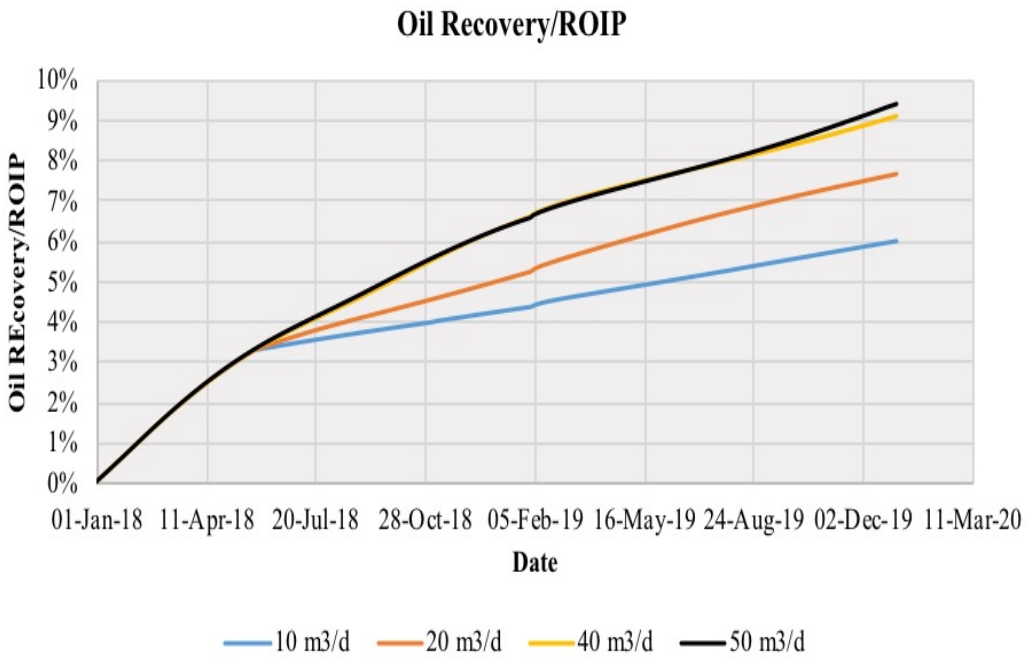

Figure 5-47: Oil Recovery/ROIP at Different Rates

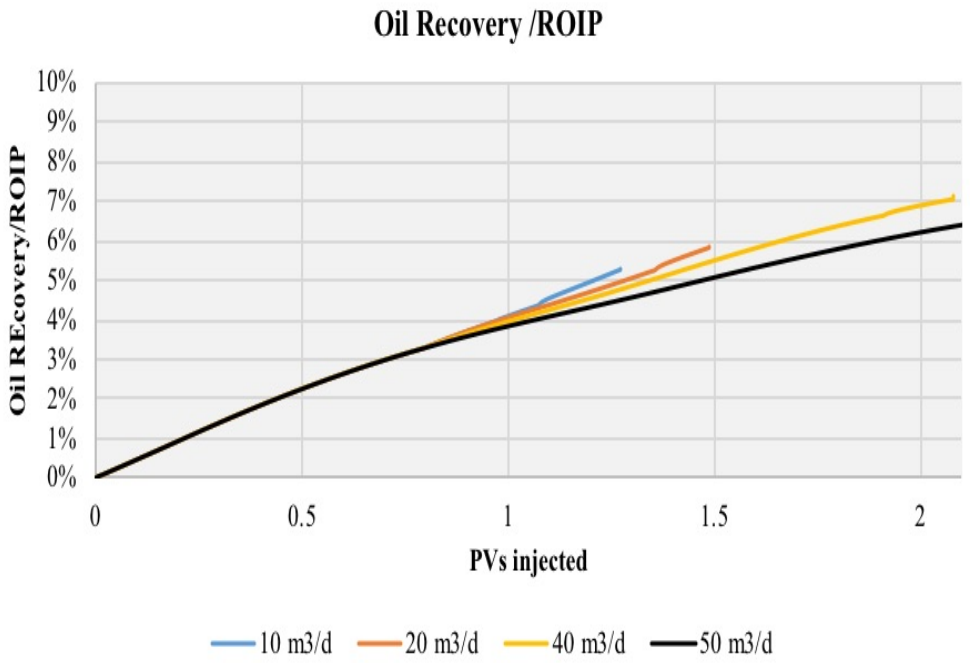

Figure 5-48: Oil Recovery ROIP As A Function of Pore Volumes Injected at Different Well Rates

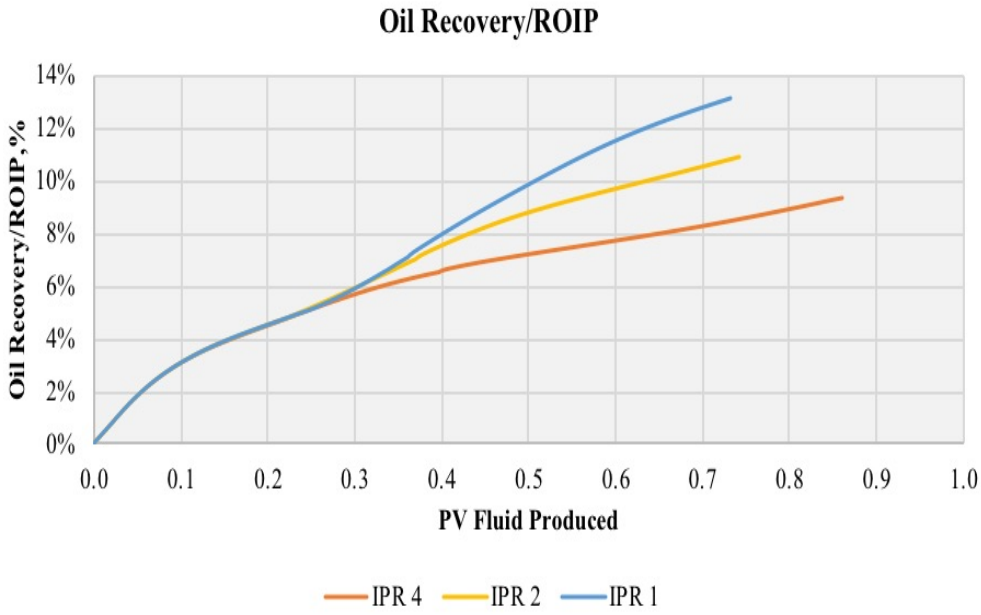

Figure 5-49: Oil recovery (ROIP%) for Different IPRs As A Function of Pore Volumes Produced

- **Sensitivity to Prior Polymer Flood**

Three cases of SP flood were simulated after pre-polymer floods of different PV: No pre-flood, 0.3 PV and 0.8 PV. All the prior polymer floods were at rate of 50 m^3/d for both injectors and the producer. The comparison of oil recovery for these cases is shown in **Figure 5-50.** The results are plotted as a function of days after SP injection start; the y-axis is the oil recovery since SP injection excluding the oil recovered during the pre-flood. The oil recovered during the prior polymer flood was 1.4% ROIP and 3.3% ROIP from the 0.30 PV and 0.8 PV injections, respectively. The case with no pre-flood recovered oil faster, this could be explained by the higher initial remaining oil saturation at the beginning of the SP injection. The lines do not end at the same point because the runs terminated at the same date, but it could be observed from the graph that the slope of the 0.8 PV pre-polymer flush is increasing. **Figure 5-51** shows the recovery as a function of PVs injected and includes the recovery from the pre-flood period. It is observed from the graph that although the case of no-preflood yields initially higher recovery, the recovery rate for the cases start to converge.

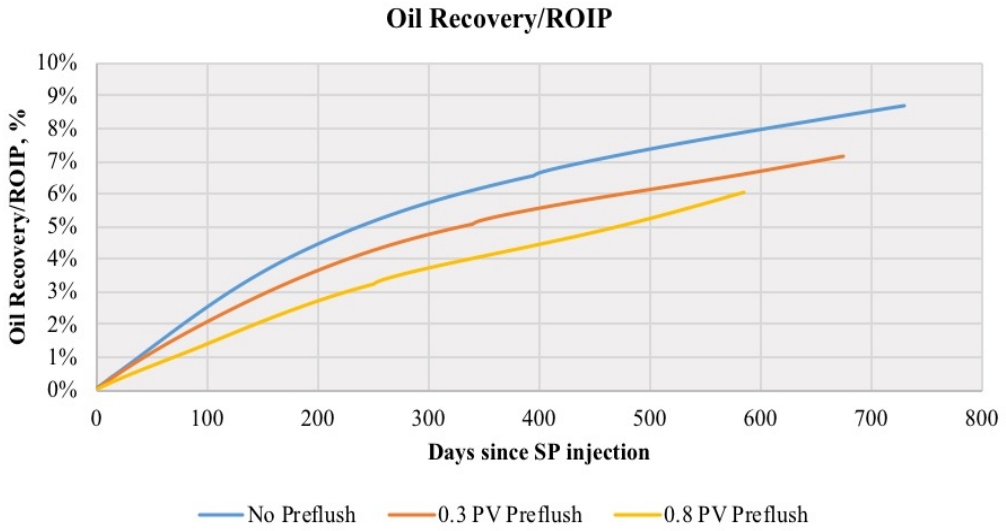

Figure 5-50: Oil Recovery/ROIP Since the Start of SP Injection at Different Pre-Polymer Volumes

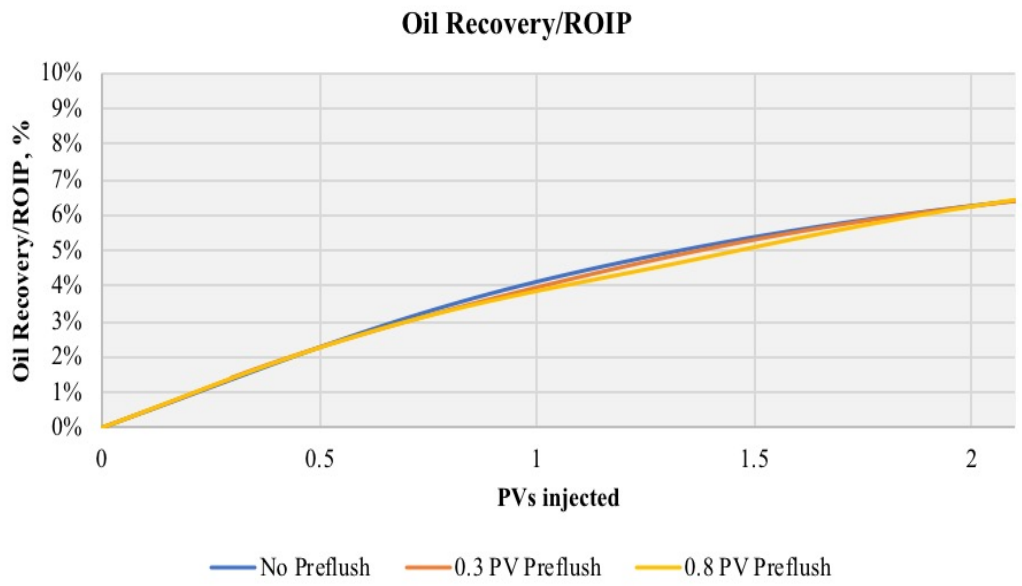

Figure 5-51: Oil Recovery/ROIP at Different Pre-Polymer Volumes as A Function of Injected PVs

- **Sensitivity to Surfactant Concentration**

The effect of surfactant concentration on the recovery is investigated. **Figure 5-52** compares the oil amount recovered from the case of 1% surfactant conc. and 0.5% conc. The case with the lower concentration recovered slightly less than the base case. By the end of simulation run, the recovery from the 1% surfactant recovered 0.14% ROIP more than 0.5 % surf. concentration. However, this result should be taken with caution due to the high uncertainty associated with this case; because the model is set up to match a single point at 1% surfactant concentration (adsorption and oil partitioning) , especially for the oil partitioning, the model is provided two values (at zero surf conc. and at 1% conc.) so the interpolation between these two points could have been overestimated which yields to less residual oil. Reducing surfactant concentration could greatly affect the field performance; When concentration is decreased, the retardation factor will increase as shown in the **Eqn. 5.5.1** below, where $\emptyset$ is porosity, C_{surf} is the surfactant concentration,

$C_{surf_{ads}}$ is the surfactant adsorption, and ρ_{surf} is the surfactant density. This means that more pore volumes are required to be displaced to be able to propagate the surfactant to counteract the adsorption effect.

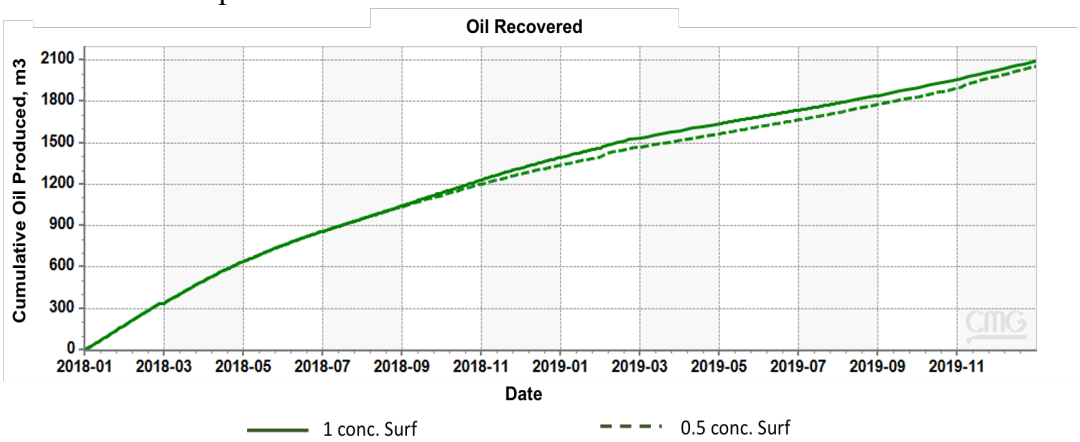

Figure 5-52: Comparison of Oil Recovery Between 0.5% and 1% Surfactant Concentrations

$$Retardation = \frac{(1-\emptyset)\, C_{surf_{ads}}}{\emptyset\, C_{surf}\, \rho_{surf}} \tag{5.5.1}$$

- **Adding Horizontal Wells Scenario**

Two cases have been conducted to examine the efficacy of adding horizontal wells. The cases do not intent to propose new location for horizontal wells, but merely provide a quick insight about horizonal wells' potential and recovery. The cases presented here analyze the recovery from the 5-spot pilot area when 1) the 4 injector wells are replaced by 2 horizontal wells and 2) the 5 wells are replaced with 2 horizontal injectors and 1 horizontal producer. **Figure 5-53** shows an aerial view of the well paths' locations. The length of each horizontal well is approximately 100 m. The horizontal wells are placed in a good permeability zone of the top layer in the 5-spot area as shown in **Figure 5-54**. The petameters used in these cases are the same as the base case parameters. In all the cases, the horizontal wells were constraint by the same constraint of the vertical wells; for

injectors, the wells are constraint by maximum BHP of 20000 kPa, for producers, the wells are constraint by minimum BHP of 3000 kPa and maximum liquid rate by 50 m^3/d.

The cumulative oil recovery from the cases of horizontal wells are compared to the base case in **Figure 5-55.** replacing the 4 injector wells with 2 horizontal injectors improved the recovery by 1% (by end of simulation time), while replacing all the 5 vertical wells with 3 horizontal wells improved the recovery 4.6%.Just by changing the well types, the recovery from the base case increased from 2093 m^3 to 3179 (51.8% increase), and recovery improved from 9.4% ROIP to 14.3% ROIP. The difference between the base case and the 2-horziontal wells case wasn't significant at the beginning of the test, but eventually the horizontal injectors resulted in higher recovery at the end of the simulation run. This possibly due to the pressure exerted by the injectors; horizontal wells are able to inject the required rate (50 m^3/d) at lower pressure, which affected how much fluid traveling outside the pattern, resulting in more oil recovery from the central producer, **Figure 5-56** shows the pressure distribution in one layer in a) horizontal injectors case and b) base vertical producer case . For the 3-horziontal wells case, the producer improvement is evident from the higher oil recovery at the start of the test; similar to the injectors, the increased productivity allowed the producer to recover at the required rate quickly, whereas in the other two cases with vertical producers, the rate was slowly building up to the desired rate as shown in **Figure 5-57.**

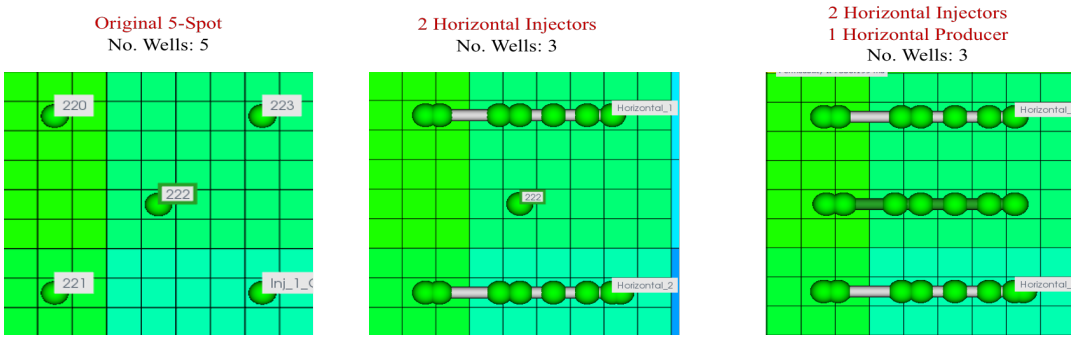

Figure 5-53: Areal View Of Well Paths Locations , Original 5-Spot Layout With All Vertical Wells(Left), 2 Horizontal Injector Wells And One Vertical Producer(Middle), 3 Horizontal Wells(2 Injectors And 1 Producer) (Right)

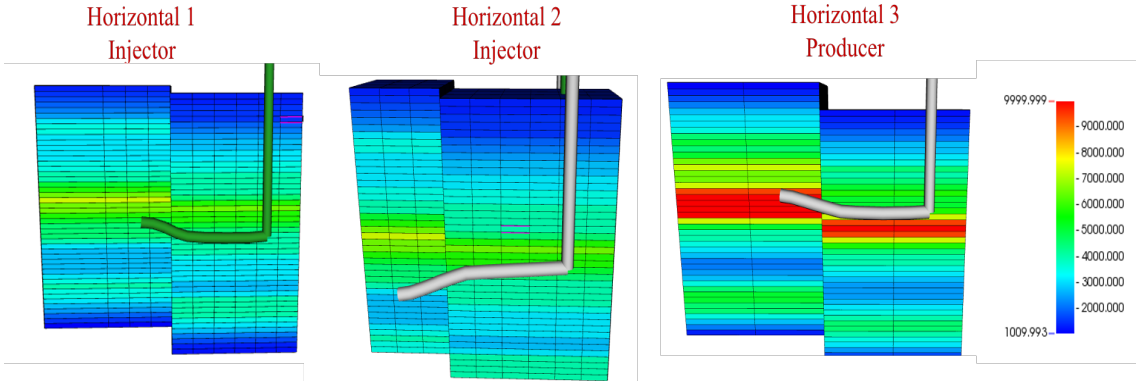

Figure 5-54: Horizontal Wells Placement on an x-k View of Permeability Distribution. Horizontal Injector Well 1 (Left), Horizontal Injector 2 (Middle) Horizontal Producer Well 3(Right)

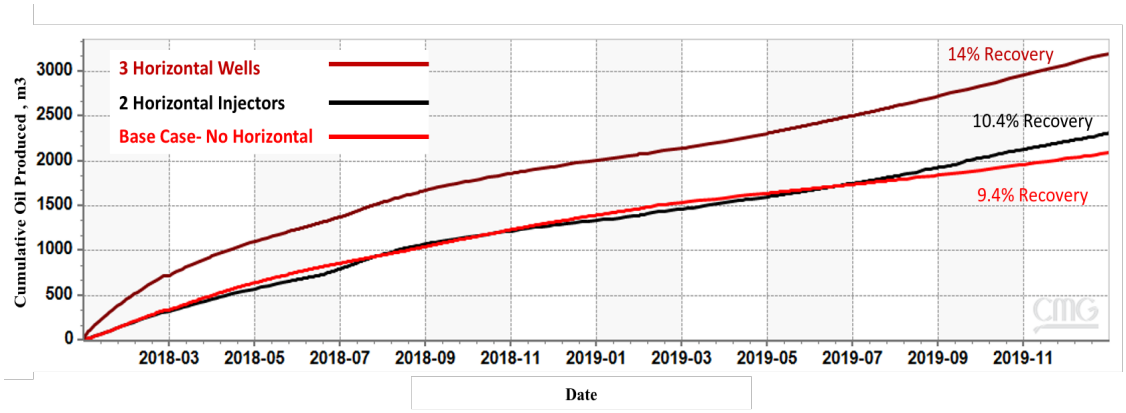

Figure 5-55: Cumulative Oil Produced Comparison Between Base Case and Horizontal Well Cases

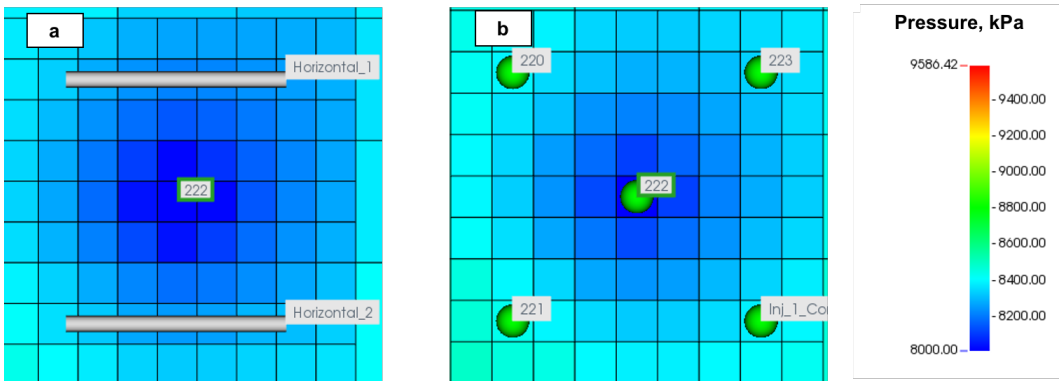

Figure 5-56: Pressure In Layer 33 After 15 Months Of Test Start (March 19) In a) 2-Horizontal Injectors Case And b) Base Case With No Horizontal Wells

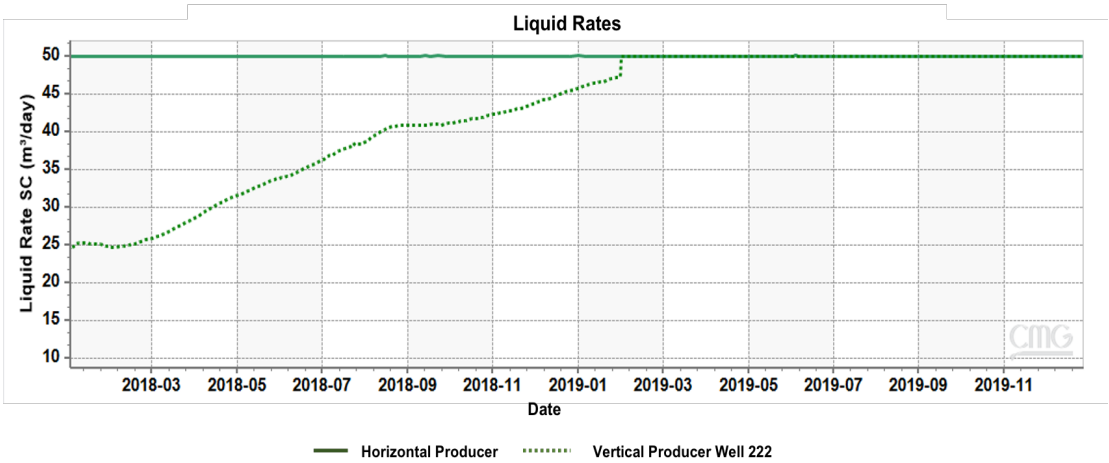

Figure 5-57: Producers Production Rate Comparison Between Vertical Producer Well-222 and Horizontal Producer

5.6 SP Simulation Sensitivity Uncertainties

5.6.1 Residual Resistance Factor RRF

The residual resistance factor for polymer represents the ratio of brine permeability before and after polymer, and it reflects the reduction of the brine permeability caused by adsorbed polymer. Higher values for RRF mean more favorable mobility ratio and higher injection pressure. Different cases were run to assess the impact of the RRF to the oil recovery: 1, 2, 3, 5, 10, and 20. **Figure 5-58** shows the impact of RRF on oil recovery as a function of fluid PVs produced. The recovery at the end of simulation run (24 months after

test including 0.8 PV prior polymer flood) for the most pessimistic case (RRF 1) is 9.4%, while for the case with high RRF value the recovery is 11.1%.

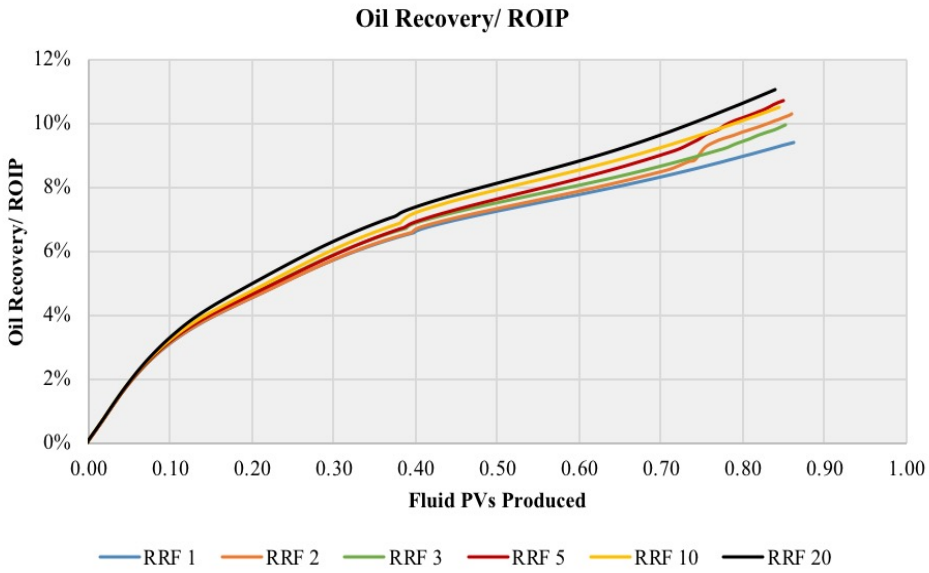

Figure 5-58: Impact of Residual Resistance Factor RRF On Oil Recovery as A Function of Fluid PVs Produced

5.6.2 Surfactant Adsorption

Surfactant adsorption has been measured in the lab for the two different surfactant formulations to be about 0.2 mg/gm of rock. The sensitivity tests the impact of two values of surfactant adsorption: 0.112 mg/g and 0.46 mg/g. CMG take the adsorption in units of gmol/m^3, with appropriate conversions, the values are therefore 2.1 gmol/m^3 and 13.3 gmol/m^3. The results showed the recovery at 19 months after SP injection can vary by +- 1.5%.

5.7 SP Design Optimized Simulation Case

Based on the previous sensitivities, the best scenarios of each parameter were combined in an optimized case. **Figure 5-59** compares the recovery between the optimum

case with a few other cases, including polymer flood only case (2500 PPM Polymer). It could be seen from the figure that there is only a slight improvement of recovery in the polymer only case in comparison with the no-surfactant (water only case). Although oil saturation distribution is slightly better with the polymer flood as shown from **Figure 5-60**, no significant recovery improvement from the central producer is observed. This could be due to the decreased injector injectivity with polymer as could be seen from **Figure 5-61**, which resulted in higher injection pressures that pushed fluids (oil) outside the patter. **Table *5-6*** quantifies the improvement of the SP design based on the sensitivity analysis. The optimum case includes 0.40 SP slug, 1 IPR and 2500-5000 PPM polymer concentration combination. The optimized case increased the total recovery by end of simulation run by 113% and resulted in incremental recovery of 12% (by end of simulation run).

To further understand the potential of the optimized scenario, the waterflood (no-surfactant) and optimized cases were run for an extended simulation period (9 years since test start). The oil recovery from each case is shown in **Figure 5-62**. The oil recovery from the waterflood case yields 12.4% of ROIP by 2027, whereas the optimized case recovers 34.6% of ROIP by 2027; that is 22% of incremental oil.

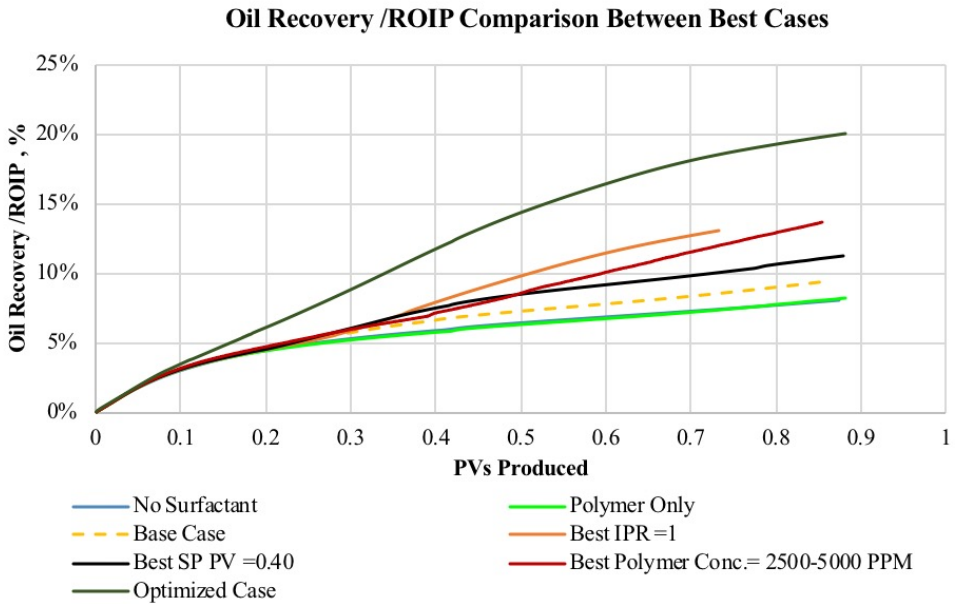

Figure 5-59: Comparison Between the Optimum Case, Water Flood Case And A Few Other Cases

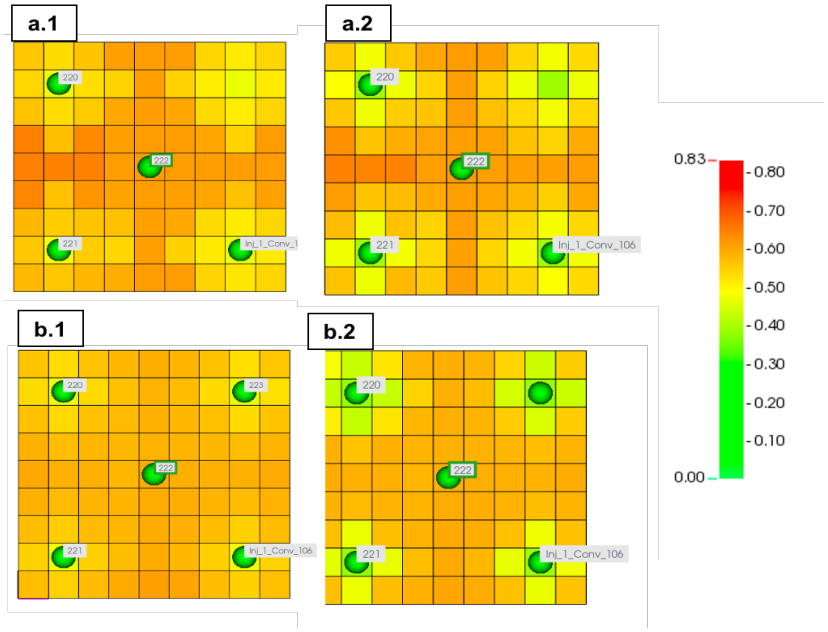

Figure 5-60: Oil Saturation Distribution After 15 Months Of Test Start In Water Case a.1) Layer 15 and b.1) layer 33 and Polymer case in a.2) Layer 15 and b.2) Layer 33

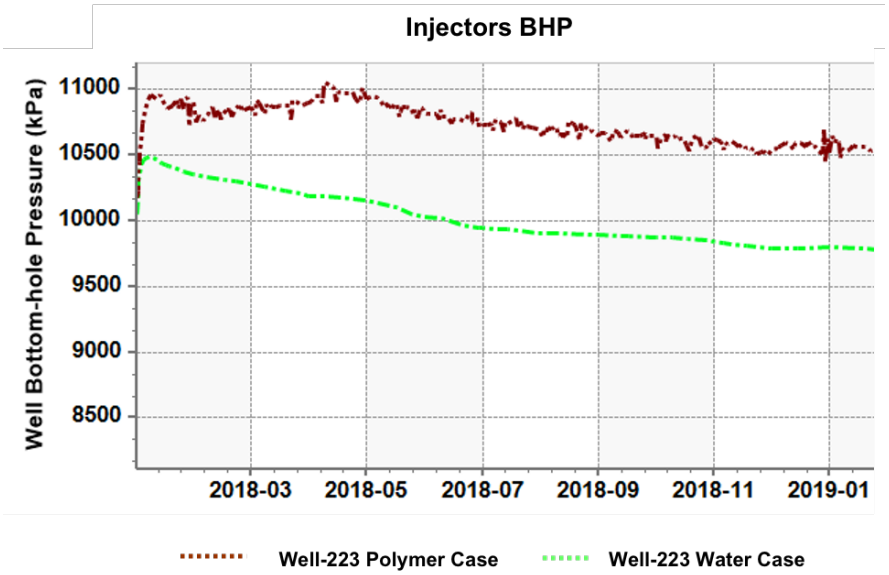

Figure 5-61: Injector Well-223 BHP Comparison Between Polymer and Water Case

Scenario	Oil Produced (By End of Simulation Run), m^3	% ROIP	Incremental oil % (By end of simulation Run)	Incremental to Polymer % (By end of simulation Run)
No- Surfactant	1795	8.1%		-0.23%
Polymer Only	1847	8.3%	0.2%	
Base case	2093	9.4%	1.3%	1.10%
IPR =1	2925	13.1%	5.0%	4.84%
0.40 SP PV	2495	11.2%	3.1%	2.91%
2500-5000 PPM	3036	13.6%	5.5%	5.34%
Optimized Case	4475	20.1%	12.0%	11.79%

Table 5-6: Comparison of Oil Recovery Between Selected Cases

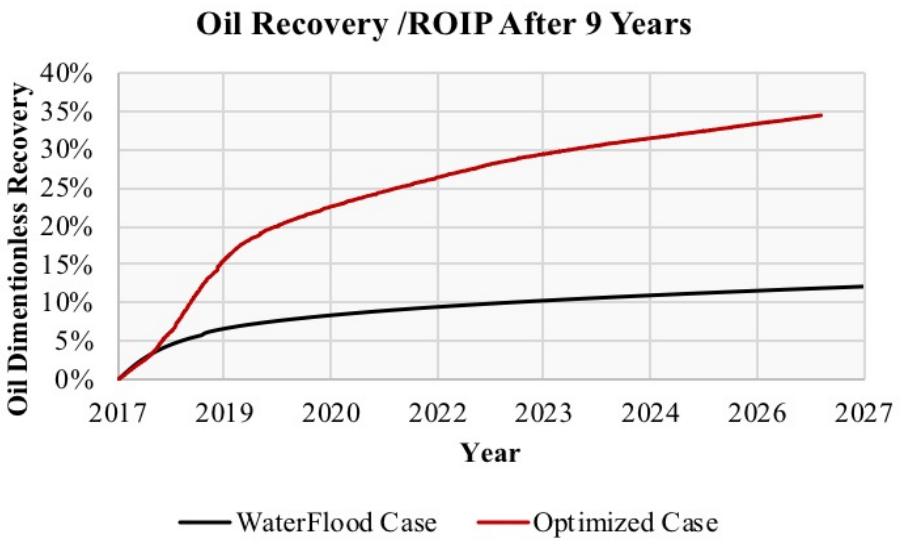

Figure 5-62: Comparison Between Oil Recovery of Waterflood and Optimized Cases

5.8 SP Design Conclusions

The two main parameters that greatly affected the recovery were the IPR value and polymer viscosity. The sensitivity on IPR revealed that lower injection production ratio led to higher oil recovery. When injection rates were reduced keeping the production rate constant, less fluid went outside the 5-spot pattern. The increase in polymer concentration increased oil recovery, but too much increase led to flow out of pattern and the resulting decrease in oil recovery in the central production well. Increase in SP slug size increased oil recovery, as expected. Different pre-polymer flood sizes were tested; the smaller was the pre-polymer flood, the higher was recovery. However, the recovery curves started to converge at a certain point. The higher initial oil saturation led to higher oil recovery in the cases with smaller pre-flood; however, the impact of better sweep eventually increased the oil recovery. There are some uncertainties associated with the simulation including RRF and adsorption. They introduced an uncertainty of +- 2% in recovery.

A brief investigation on well types was conducted to study the potential of horizontal wells implementation in the field. Based on the results, horizontal wells have a promising prospect in the field. More detailed work must be done to realize the full potential of these wells, but what is presented here shows a glimpse of the possible advantages of implementing horizontal wells. Main benefits of implementing horizontal wells include:

- Significant increase in production rates with horizontal producers
- Horizontal injectors to counteract the injectivity decreases associated with polymer injection as they have the capability of injecting higher rates at lower pressures
- Higher injection and production rates capability of the horizontal wells can reduce pilot testing times

5.9 SP DESIGN RECOMMENDATIONS

This design is constrained to the use of only existing wells. Other patterns and horizontal wells should be simulated if new wells are in considerations. The recommended design from this sensitivity study are as follows:

- SP slug size: 0.40 PV
- Polymer concentration: 2500 PPM for SP slug, 5000 PPM for polymer drive
- Injection production ratio IPR: 1 (optimized case used 50 m^3/d for producer and 12.5 m^3/d for each injector)
- Prior polymer flood: Preflush with polymer is recommended, 0.3 PV slug size can be sufficient.

Chapter 6: Summary and Recommendations

This chapter summarizes the main findings of the coreflood modeling, and the simulation studies of SWCT, IWTT and SP pilot.

6.1 Summary and Conclusions

Design of an SP pilot test has been studied for a sandstone viscous oil reservoir. The design workflow started from history matching laboratory scale experiments, followed by an upscaling to single well test, interwell tracer test and finally SP pilot test. Numerical simulation models were developed using CMG-STARS for 7 corefloods and one 2D cell experiment. The models showed a satisfactory agreement with laboratory measured data especially with experimental oil recovery and oil cut. The models did not precisely match the pressure drop in all experiments; the experimental pressure drops indicated polymer degradation which was not included in the coreflood history match models. However, polymer protection package was not used in corefloods and are recommended for field pilots. Despite the differences of the polymer and surfactant models in both simulators, UTCHEM and CMG-STARS yielded similar simulation results in matching coreflood 1.

The surfactant and polymer models developed for the corefloods history matching were used in the SWCT design model. A radial model was constructed based on the static data of a pre-existing 5-spot area in the field. The main objective of conducting SWCT is to determine the residual oil saturation after the SP injection. For 8 m radius of investigation and 302 m^3 pore volume, the model design sensitivities showed the following:

- The error in the S_{or} calculation (analytically calculated against model input) in the SWTT prior to SP injection was up to 20% due to heterogeneity.
- S_{or} in the near-wellbore region dropped to zero when a slug size of 0.2 PV (60 m^3) was used.

- Using high polymer concentrations ($\geq$ 5000 ppm) can alter the relative permeabilities around the wellbore, resulting in lower S_{or} values even before SP injection. The 2500 PPM polymer was demonstrated to be suitable for the test. Even though the 1500 PPM showed satisfactory results, it is important to account for degradation and dilution that could possibly occur in the field.
- The low tracer recovery from low injection rates cases is due to the longer reaction period the Etac before production.
- The larger the tracer push volume (water drive after tracer injection), the higher the analytically calculated S_{or}, this is because larger push volumes cover larger regions so the average saturation increases.

An IWTT using passive tracers is designed to assess the reservoir characteristic of the 5-spot pilot area and the potential of the SP formulation. The criteria for evaluating the design parameters were the produced tracer concentrations, recovery and the testing duration. The following was observed from the model design sensitivities:

- The mass of the injected tracers was the most fundamental variable in the design of the IWTT. About 800 kg of a tracer (per well) resulted in suitable produced tracer concentrations, safely above the detectable limits.
- Higher injected tracer concentrations yielded faster peak concentrations, faster breakthrough time and less time required for tracer injection. A tracer concentration of 10,000 ppm requires less than 2 days of injection at 50 m^3/d.
- High injection rate is beneficial in terms of testing duration time, but it has adverse effects on tracer recovery, as higher rates contribute to higher pressure and consequently more fluid flowing out of the pattern. Therefore, a balance between the two is desired. An injection rate of 50 m^3/d results in a shorter testing period and interpretable tracer curves.

The last step involved the design of an SP pilot that aims to evaluate the efficacy of the formulation and sweep efficiency under reservoir conditions. The goal of the simulation study is to assess the impact of key design parameters: SP slug size, composition and polymer concentrations. The model design sensitivities showed the following:

- Injection production ratio (IPR) and polymer viscosity are the main two parameters affecting the oil recovery.
- Lower IPR values improved the oil recovery mainly because it improved the confinement within the pilot area.
- Higher polymer concentrations resulted in higher oil recovery but increasing the concentrations severely will have an adverse effect on confinement due to the higher injection pressures.
- As expected, the increase in the SP slug size results in an increased recovery.
- The design of the SP has some uncertainties: residual resistance factor and adsorption. The two parameters introduced an uncertainty of +- 2% in recovery.

6.2 RECOMMENDATIONS

The models used in the design of the single well and multi-wells tests include multiple assumptions regarding tracer properties. Screening of available tracers and measuring their partition coefficients, reaction rate (for reactant tracer) and compatibility will validate and further improve the design models. In addition, the field results of the IWTT, ideally conducted prior to SP pilot execution, can provide valuable information about the reservoir characteristics that could further augment the SP pilot design. The design strategy presented herein can therefore be modified if new information is acquired

from field executed IWTT. The recommendations of the SWCT, IWTT and SP pilot are summarized below:

- **SWCT Design Recommendations**

  The pore volume of interest for the SWCT corresponds to 8-meter radius of investigation. Thereby the PV is 302 m^3. Recommendations are provided below:

  - SP slug size of at least 60 m^3 (0.2 PV) is required to reduce S_{or} to less than 10%.
  - Push volume of 50 m^3 (1 day at 50 m^3/day per 6 m pay thickness) is recommended to investigate approximately 5 meters radius.
  - Tracer solution sizes in the range of 8-15 m^3 (0.15 to 0.30 days duration at a rate of 50 m^3/d per 6 m pay thickness) were sufficient for S_{or} determination.
  - A polymer of 2500 ppm with the tracer injection showed good result with analytically calculated S_{or} during the test prior to SP injection.
  - A rate of 50 m^3/d per 6 m pay thickness is recommended for short testing period and easy interpretation of produced tracer curves.

- **IWTT Design Recommendations**

  - Tracer concentrations: 10,000 PPM per tracer
  - Tracer amount: At least 800 kg of tracer
  - Well rates: All 5 spot wells at rate 50 m^3/d
  - Adding polymer: At least 2500 ppm
  - Push water: Inject to no more than 1 PV to increase tracer recovery
  - Testing/tracer monitoring: At least 7-8 months to observe sufficient amount of tracer in the production well. (If this time period is not

available, then it is recommended that tracers be added to the SP slug itself and the effluent water be analyzed for the tracers. The matching of tracers may help the interpretation of the SP pilot)

- **SP Pilot Design Recommendations**
  - SP slug size: 0.40 PV
  - Polymer concentration: 2500 PPM for SP slug, 5000 PPM for polymer drive
  - Injection production ratio IPR: 1 (optimized case used 50 m^3/d for producer and 12.5 m^3/d for each injector)
  - Prior polymer flood: preflush with polymer is recommended, low sizes can be sufficient (e.g. 0.3 PV)
  - This design is constrained to the use of only existing wells. Other patterns and horizontal wells should be simulated if new wells are in considerations.

References

Abbaszadeh-Dehghani, M., & Brigham, W. (1984). Analysis of Well-to-Well Tracer Flow to Determine Reservoir Layering. *Journal of Petroleum Technology, 36*(10), 1753-1762. doi:10.2118/10760-pa

Al-Shalabi, E. W., Luo, H., Delshad, M., & Sepehrnoori, K. (2015). Single-Well Chemical Tracer Modeling of Low Salinity Water Injection in Carbonates. *SPE Western Regional Meeting*. doi:10.2118/173994-ms

Allison, S., Pope, G., & Sepehrnoori, K. (1991). Analysis of field tracers for reservoir description. *Journal of Petroleum Science and Engineering, 5*(2), 173-186. doi:10.1016/0920-4105(91)90066-v

Asakawa, K. (2005). *A generalized analysis of partitioning interwell tracer tests.* (Doctoral dissertation, University of Texas, Austin).

Bhuyan, D., Lake, L. W., & Pope, G. A. (1990). Mathematical Modeling of High-pH Chemical Flooding. *SPE Reservoir Engineering, 5*(02), 213-220. doi:10.2118/17398-pa

Bragg, J., & Shallenberger, L. (1976). In-Situ Determination of Residual Gas Saturation by Injection and Production of Brine. *SPE Annual Fall Technical Conference and Exhibition*. doi:10.2118/6047-ms

Brigham, W., & Smith, D. (1965). Prediction of Tracer Behavior In Five-Spot Flow. *Conference on Production Research and Engineering*. doi:10.2118/1130-ms

Camilleri, D., Engelson, S., Lake, L., Lin, E., Ohnos, T., Pope, G., & Sepehrnoori, K. (1987c). Description of an Improved Compositional Micellar/Polymer Simulator. *SPE Reservoir Engineering, 2*(04), 427-432. doi:10.2118/13967-pa

Camilleri, D., Fil, A., Pope, G., Rouse, B., & Sepehrnoori, K. (1987a). Comparison of an Improved Compositional Micellar/Polymer Simulator with Laboratory Corefloods. *SPE Reservoir Engineering, 2*(04), 441-451. doi:10.2118/12083-pa

Camilleri, D., Fil, A., Pope, G., Rouse, B., & Sepehrnoori, K. (1987b). Improvements in Physical-Property Models Used in Micellar/Polymer Flooding. *SPE Reservoir Engineering, 2*(04), 433-440. doi:10.2118/12723-pa

Cannella, W., Huh, C., & Seright, R. (1988). Prediction of Xanthan Rheology in Porous Media. *SPE Annual Technical Conference and Exhibition*. doi:10.2118/18089-ms

Carlisle, C., Al-Maraghi, E., Al-Saad, B., Britton, C., Fortenberry, R., & Pope, G. (2014). One-Spot Pilot Results in the Sabriyah-Mauddud Carbonate Formation in Kuwait Using a Novel Surfactant Formulation. *SPE Improved Oil Recovery Symposium*. doi:10.2118/169153-ms

Chatzis, I., & Morrow, N. R. (1984). Correlation of Capillary Number Relationships for Sandstone. *Society of Petroleum Engineers Journal, 24*(05), 555-562. doi:10.2118/10114-pa

Cheng, H., Shook, G. M., Malik, T., Varadarajan, D., & Smith, B. R. (2012). Interwell Tracer Tests To Optimize Operating Conditions for a Surfactant Field Trial: Design, Evaluation, and Implications. *SPE Reservoir Evaluation & Engineering, 15*(02), 229-242. doi:10.2118/144899-pa

CMG-STARS Technical Manual, (2019).

Cockin, A., Malcolm, L., Mcguire, P., Giordano, R., & Sitz, C. (2000). Analysis of a Single-Well Chemical Tracer Test To Measure the Residual Oil Saturation to a Hydrocarbon Miscible Gas Flood at Prudhoe Bay. *SPE Reservoir Evaluation & Engineering, 3*(06), 544-551. doi:10.2118/68051-pa

Cooke, C. E., Jr. (1971). *U.S. Patent No. 3590923*. Washington, DC: U.S. Patent and Trademark Office.

Craig, F. F. (1971). *The reservoir engineering aspects of waterflooding*. Henry L. Doherty Memorial Fund of AIME, Society of Petroleum Engineers.

Cubillos, H., Torgersen, H. J., Chatzichristos, C., & Tobio, M. L. (2006). Best Practice and Case Study of Interwell Tracer Program Designs. *International Oil Conference and Exhibition in Mexico*. doi:10.2118/103891-ms

Danckwerts, P. (1953). Continuous flow systems. *Chemical Engineering Science, 2*(1), 1-13. doi:10.1016/0009-2509(53)80001-1

Dashti, G. (2014). *A study of microemulsion viscosity with consideration of polymer and co-solvent additives* (Master dissertation, University of Texas, Austin). Retrieved from https://repositories.lib.utexas.edu/handle/2152/25266

Dean, R. M., Walker, D. L., Dwarakanath, V., Malik, T., & Spilker, K. (2016). Use of Partitioning Tracers to Estimate Oil Saturation Distribution in Heterogeneous Reservoirs. *SPE Improved Oil Recovery Conference*. doi:10.2118/179655-ms

Deans, H. (1978). Using Chemical Tracers To Measure Fractional Flow And Saturation In-Situ. *SPE Symposium on Improved Methods of Oil Recovery*. doi:10.2118/7076-ms

Deans, H. A. (1971). *U.S. Patent No. 3623942*. Washington, DC: U.S. Patent and Trademark Office.

Deans, H. A., & Majoros, S. (1980). *The single-well chemical tracer method for measuring residual oil saturation: Final report*. Washington, D.C.: U.S. Dept. of Energy.

Deans, H., & Carlisle, C. (2006). The Single-Well Chemical Tracer Test - A Method for Measuring Reservoir Fluid Saturations in Situ. In L. W. Lake & E. D. Holstein (Eds.), *Petroleum Engineering Handbook* (Vol. V). Society of Petroleum

Engineers. Retrieved from https://ebookcentral-proquest-com.ezproxy.lib.utexas.edu.

Deans, H., & Ghosh, R. (1994). PH and Reaction Rate Changes During Single-Well Chemical Tracer Tests. *SPE/DOE Improved Oil Recovery Symposium*. doi:10.2118/27801-ms

Deans, H., & Shallenberger, L. (1974). Single-Well Chemical Tracer Method to Measure Connate Water Saturation. *SPE Improved Oil Recovery Symposium*. doi:10.2118/4755-ms

Delshad, M. (1990). *Trapping of micellar fluids in Berea sandstone.* (Doctoral dissertation, University of Texas, Austin).

Delshad, M., Kim, D. H., Magbagbeola, O. A., Huh, C., Pope, G. A., & Tarahhom, F. (2008). Mechanistic Interpretation and Utilization of Viscoelastic Behavior of Polymer Solutions for Improved Polymer-Flood Efficiency. *SPE Symposium on Improved Oil Recovery*. doi:10.2118/113620-ms

Descant, F. J., (1989). *Simulation of Single-Well Tracer Flow* (Master Thesis, University of Texas, Austin). Retrieved from https://repositories.lib.utexas.edu/handle/2152/81164

Ehrlich, R., Hasiba, H., & Raimondi, P. (1974). Alkaline Waterflooding for Wettability Alteration-Evaluating a Potential Field Application. *Journal of Petroleum Technology, 26*(12), 1335-1343. doi:10.2118/4905-pa

Ferreira, L., (1992a). *Reservoir Characterization Using Single-Well Tracer Tests* (Doctoral dissertation, University of Texas, Austin). Retrieved from https://repositories.lib.utexas.edu/handle/2152/80620

Ferreira, L., Descant, F., Delshad, M., Pope, G., & Sepehrnoori, K. (1992b). A Single-Well Tracer Test to Estimate Wettability. *SPE/DOE Enhanced Oil Recovery Symposium*. doi:10.2118/24136-ms

Flory, P. J. (1953). *Principles of Polymer Chemistry*. Ithaca, NY: Cornell University Press.

Fortenberry, R., Suniga, P., Delshad, M., Singh, B., Alkaaoud, H. A., Carlisle, C. T., & Pope, G. A. (2016). Design and Demonstration of New Single-Well Tracer Test for Viscous Chemical Enhanced-Oil-Recovery Fluids. *SPE Journal, 21*(04), 1075-1085. doi:10.2118/178914-pa

Foster, W. (1973). A Low-Tension Waterflooding Process. *Journal of Petroleum Technology, 25*(02), 205-210. doi:10.2118/3803-pa

Gbadamosi, A. O., Junin, R., Manan, M. A., Agi, A., & Yusuff, A. S. (2019). An overview of chemical enhanced oil recovery: Recent advances and prospects. *International Nano Letters, 9*(3), 171-202. doi:10.1007/s40089-019-0272-8

Goudarzi, A., Delshad, M., & Sepehrnoori, K. (2013). A Critical Assessment of Several Reservoir Simulators for Modeling Chemical Enhanced Oil Recovery Processes. *SPE Reservoir Simulation Symposium*. doi:10.2118/163578-ms

Goudarzi, A., Delshad, M., & Sepehrnoori, K. (2016). A chemical EOR benchmark study of different reservoir simulators. *Computers & Geosciences, 94*, 96-109. doi:10.1016/j.cageo.2016.06.013

Green, D. W., & Willhite, G. P. (2018). *Enhanced oil recovery*. Richardson, TX, USA: Society of Petroleum Engineers.

Hand, D. B. (1930). Dineric Distribution. *The Journal of Physical Chemistry, 34*(9), 1961-2000. doi:10.1021/j150315a009

Healy, R. N., & Reed, R. L. (1974). Physicochemical Aspects of Microemulsion Flooding. *Society of Petroleum Engineers Journal, 14*(05), 491-501. doi:10.2118/4583-pa

Healy, R., Reed, R., & Stenmark, D. (1976). Multiphase Microemulsion Systems. *Society of Petroleum Engineers Journal, 16*(03), 147-160. doi:10.2118/5565-pa

Hernandez, C., Chacon, L., Anselmi, L., Angulo, R., Manrique, E., Romero, E., . . . Carlisle, C. (2002). Single Well Chemical Tracer Test to Determine ASP Injection Efficiency at Lagomar VLA-6/9/21 Area, C4 Member, Lake Maracaibo, Venezuela. *SPE/DOE Improved Oil Recovery Symposium*. doi:10.2118/75122-ms

Hirasaki, G. J. (1981). Application of the Theory of Multicomponent, Multiphase Displacement to Three-Component, Two-Phase Surfactant Flooding. *Society of Petroleum Engineers Journal, 21*(02), 191-204. doi:10.2118/8373-pa

Hirasaki, G., Miller, C., & Puerto, M. (2008). Recent Advances in Surfactant EOR. *IPTC 2008: International Petroleum Technology Conference*. doi:10.3997/2214-4609-pdb.148.spe115386

Huh, C. (1979). Interfacial tensions and solubilizing ability of a microemulsion phase that coexists with oil and brine. *Journal of Colloid and Interface Science, 71*(2), 408-426. doi:10.1016/0021-9797(79)90249-2

Huh, C., & Pope, G. A. (2008). Residual Oil Saturation from Polymer Floods: Laboratory Measurements and Theoretical Interpretation. *SPE Symposium on Improved Oil Recovery*. doi:10.2118/113417-ms

Jerauld, G., Mohammadi, H., & Webb, K. J. (2010). Interpreting Single Well Chemical Tracer Tests. *SPE Improved Oil Recovery Symposium*. doi:10.2118/129724-ms

Jin, M. (1995). *A study of non-aqueous phase liquid characterization and surfactant remediation?* (Doctoral dissertation, University of Texas, Austin). Retrieved from https://repositories.lib.utexas.edu/handle/2152/80644

Jin, M., Delshad, M., Dwarakanath, V., Mckinney, D. C., Pope, G. A., Sepehrnoori, K., Tilburg, C., Jackson, R. E. (1995). Partitioning Tracer Test for Detection, Estimation, and Remediation Performance Assessment of Subsurface Nonaqueous Phase Liquids. *Water Resources Research, 31*(5), 1201-1211. doi:10.1029/95wr00174

Lake, L. W., Johns, R. T., Rossen, W. R., & Pope, G. A. (2014). *Fundamentals of enhanced oil recovery*. Richardson, TX: Society of Petroleum Engineers.

Larson, R., Davis, H., & Scriven, L. (1982). Elementary Mechanisms of Oil Recovery by Chemical Methods. *Journal of Petroleum Technology, 34*(02), 243-258. doi:10.2118/8840-pa

Lin, E. (1981). *A study of micellar/polymer flooding using a compositional simulator* (Doctoral dissertation, University of Texas, Austin). Retrieved from https://repositories.lib.utexas.edu/handle/2152/80526

Lorenz, P. B., Donaldson, E. C., & Thomas, R. D. (1974). *The use of centrifugal measurements of wettability to predict oil recovery*. Washington, DC: U.S. Dept. of the Interior, Bureau of Mines.

Maroongroge, V. (1994). *Modeling and Application of Tracers for Reservoir Characterization.* (Doctoral dissertation, University of Texas, Austin).

Mcguire, P., Chatham, J., Paskvan, F., Sommer, D., & Carini, F. (2005). Low Salinity Oil Recovery: An Exciting New EOR Opportunity for Alaska's North Slope. *SPE Western Regional Meeting*. doi:10.2118/93903-ms

Meter, D. M., & Bird, R. B. (1964). Tube flow of non-Newtonian polymer solutions: PART I. Laminar flow and rheological models. *AIChE Journal, 10*(6), 878-881. doi:10.1002/aic.690100619

Moore, T., & Slobod, R. (1955). Displacement of Oil by Water-Effect of Wettability, Rate, and Viscosity on Recovery. *Fall Meeting of the Petroleum Branch of AIME*. doi:10.2118/502-g

Nelson, R., & Pope, G. (1978). Phase Relationships in Chemical Flooding. *Society of Petroleum Engineers Journal, 18*(05), 325-338. doi:10.2118/6773-pa

Ottewill, R., H. (1984). Introduction. In: Tadros, T.F. (Ed.), *Surfactants* (pp.1-18). London: Academic Press

Oyemade, S. N. (2010). Alkaline - Surfactant - Polymer Flood (ASP): Single Well Chemical Tracer Tests - Design, Implementation and Performance. *SPE EOR Conference at Oil & Gas West Asia*. doi:10.2118/130042-ms

Panthi, K., Weerasooriya, U., & Mohanty, K. (2019). Chemical Flood of a Viscous Oil with Novel Surfactants. *SPE Annual Technical Conference and Exhibition*. doi:10.2118/196198-ms

Pope, G. A. (1980). The Application of Fractional Flow Theory to Enhanced Oil Recovery. *Society of Petroleum Engineers Journal, 20*(03), 191-205. doi:10.2118/7660-pa

Pope, G., & Nelson, R. (1978). A Chemical Flooding Compositional Simulator. *Society of Petroleum Engineers Journal, 18*(05), 339-354. doi:10.2118/6725-pa

Pope, G., Wu, W., Narayanaswamy, G., Delshad, M., Sharma, M., & Wang, P. (2000). Modeling Relative Permeability Effects in Gas-Condensate Reservoirs With a New Trapping Model. *SPE Reservoir Evaluation & Engineering, 3*(02), 171-178. doi:10.2118/62497-pa

Prey, E. L. (1973). Factors Affecting Liquid-Liquid Relative Permeabilities of a Consolidated Porous Medium. *Society of Petroleum Engineers Journal, 13*(01), 39-47. doi:10.2118/3039-pa

Prouvost, L., & Pope, G. A. (1986). Modelling of Phase Behavior of Micellar Systems Used for Enhanced Oil Recovery. *Surfactants in Solution,* 473-487. doi:10.1007/978-1-4613-1831-6_38

Prouvost, L., Pope, G. A., & Rouse, B. (1985). Microemulsion Phase Behavior: A Thermodynamic Modeling of the Phase Partitioning of Amphiphilic Species. *Society of Petroleum Engineers Journal, 25*(05), 693-703. doi:10.2118/12586-pa

Prouvost, L., Pope, G.A., and Sepehrnoori, K. (1986). Modeling of Phase Behavior of Micellar Systems Used for EOR. K. L. Mittal and P. Bothorel (Ed.). *Surfactants in Solution* (4, pp. 473-487). Boston, MA: Springer.

Prouvost, L., Satoh, T., Sepehrnoori, K., & Pope, G. (1984). A New Micellar Phase-Behavior Model for Simulating Systems With Up to Three Amphiphilic Species. *SPE Annual Technical Conference and Exhibition*. doi:10.2118/13031-ms

Qi, P., Ehrenfried, D. H., Koh, H., & Balhoff, M. T. (2017). Reduction of Residual Oil Saturation in Sandstone Cores by Use of Viscoelastic Polymers. *SPE Journal, 22*(02), 447-458. doi:10.2118/179689-pa

Reed, R. L., & Healy, R. N. (1984). Contact Angles for Equilibrated Microemulsion Systems. *Society of Petroleum Engineers Journal, 24*(03), 342-350. doi:10.2118/8262-pa

Robinson, B. A., & Tester, J. W. (1984). Dispersed fluid flow in fractured reservoirs: An analysis of tracer-determined residence time distributions. *Journal of Geophysical Research: Solid Earth, 89*(B12), 10374-10384. doi:10.1029/jb089ib12p10374

Rosen, M. (1978). *Surfactants and interfacial phenomena*. New York: Wiley.

Satoh, T. (1984). *Treatment of phase behavior and associated properties used in a micellar-polymer flood simulator* (Master dissertation, University of Texas, Austin). Retrieved from https://repositories.lib.utexas.edu/handle/2152/80561

Serres-Piole, C., Preudhomme, H., Moradi-Tehrani, N., Allanic, C., Jullia, H., & Lobinski, R. (2012). Water tracers in oilfield applications: Guidelines. *Journal of Petroleum Science and Engineering, 98-99*, 22-39. doi:10.1016/j.petrol.2012.08.009

Sharma, A., Shook, G. M., & Pope, G. A. (2014). Rapid Analysis of Tracers for Use in EOR Flood Optimization. *SPE Improved Oil Recovery Symposium*. doi:10.2118/169109-ms

Sharma, A., Shook, G. M., & Pope, G. A. (2014). Rapid Analysis of Tracers for Use in EOR Flood Optimization. *SPE Improved Oil Recovery Symposium*. doi:10.2118/169109-ms

Sheely, C., & Baldwin, D. (1982). Single-Well Tracer Tests for Evaluating Chemical Enhanced Oil Recovery Processes. *Journal of Petroleum Technology, 34*(08), 1887-1896. doi:10.2118/8838-pa

Sheng, J. (2011). *Modern chemical enhanced oil recovery: Theory and practice*. Amsterdam: Gulf Professional Pub.

Sheng, J. J. (2013). *Enhanced Oil Recovery Field Case Studies* (1st ed.). Waltham, MA: Gulf Professional Publishing.

Shook, G. M., Pope, G. A., & Asakawa, K. (2009). Determining Reservoir Properties and Flood Performance From Tracer Test Analysis. *SPE Annual Technical Conference and Exhibition*. doi:10.2118/124614-ms

Shook, G. M., Pope, G. A., & Asakawa, K. (2009). Determining Reservoir Properties and Flood Performance From Tracer Test Analysis. *SPE Annual Technical Conference and Exhibition*. doi:10.2118/124614-ms

Shook, M. G. (2003). A Simple, Fast Method of Estimating Fractured Reservoir Geometry from Tracer Tests. *Geothermal Resources Council, 27*, 407-411.

Shook, M. G., & Forsmann, H. J. (2005). *Tracer Interpretation Using Temporal Moments on a Spreadsheet* (Rep. No. INL/EXT-05-00400). Idaho Falls, Idaho: Idaho National Laboratory (INL). doi:10.2172/910998

Sinha, R., Asakawa, K., Pope, G., & Sepehrnoori, K. (2004). Simulation of Natural and Partitioning Interwell Tracers to Calculate Saturation and Swept Volumes in Oil Reservoirs. *SPE/DOE Symposium on Improved Oil Recovery*. doi:10.2118/89458-ms

Sorbie, K. (1991). *Polymer-improved oil recovery*. Glasgow: Blackie.

Stegemeier, G. (1977). Mechanisms Of Entrapment And Mobilization Of Oil In Porous Media. *Improved Oil Recovery by Surfactant and Polymer Flooding,* 55-91. doi:10.1016/b978-0-12-641750-0.50007-4

Tagavifar, M., Herath, S., Weerasooriya, U. P., Sepehrnoori, K., & Pope, G. (2016). Measurement of Microemulsion Viscosity and Its Implications for Chemical EOR. *SPE Improved Oil Recovery Conference*. doi:10.2118/179672-ms

Tang, J., & Harker, B. (1991). Interwell Tracer Test To Determine Residual Oil Saturation In A Gas-Saturated Reservoir. Part II: Field Applications. *Journal of Canadian Petroleum Technology, 30*(04). doi:10.2118/91-04-01

Tester, J. W., Bivins, R. L., & Potter, R. M. (1982). Interwell Tracer Analyses of a Hydraulically Fractured Granitic Geothermal Reservoir. *Society of Petroleum Engineers Journal, 22*(04), 537-554. doi:10.2118/8270-pa

Tian, W., Wu, X., & Shen, T. (2019). Improved Method of Moment To Determine Mobile-Phase Saturations Using a Single-Well Chemical-Tracer Test. *SPE Reservoir Evaluation & Engineering, 22*(02), 612-627. doi:10.2118/189300-pa

Tomich, J. F., & Deans, H. A. (1975). *U.S. Patent No. 3902362*. Washington, DC: U.S. Patent and Trademark Office.

Tomich, J., Dalton, R., Deans, H., & Shallenberger, L. (1973). Single-Well Tracer Method to Measure Residual Oil Saturation. *Journal of Petroleum Technology, 25*(02), 211-218. doi:10.2118/3792-pa

UTCHEM Technical Documentation. (2019)

Van-Quy, N., Simandoux, P., & Corteville, J. (1972). A Numerical Study of Diphasic Multicomponent Flow. *Society of Petroleum Engineers Journal, 12*(02), 171-184. doi:10.2118/3006-pa

Viig, S. O., Juilla, H., Renouf, P., Kleven, R., Krognes, B., Dugstad, O., & Huseby, O. K. (2013). Application of a New Class of Chemical Tracers To Measure Oil Saturation in Partitioning Interwell Tracer Tests. *SPE International Symposium on Oilfield Chemistry*. doi:10.2118/164059-ms

Wagner, O., Baker, L., & Scott, G. R. (1974). The Design and Implementation of Multiple Tracer Program for Multifluid, Multiwell Injection Projects. *Fall Meeting of the Society of Petroleum Engineers of AIME*. doi:10.2118/5125-ms

Watkins, J. W., & Mardock, E. (1954). Use of Radioactive Iodine as a Tracer in Water-Flooding Operations. *Journal of Petroleum Technology, 6*(09), 117-124. doi:10.2118/349-g

Winsor, P. A. (1954). *Solvent properties of amphiphilic compounds*. London: Butterworth.

Young, L. C., & Stephenson, R. E. (1983). A Generalized Compositional Approach for Reservoir Simulation. *Society of Petroleum Engineers Journal, 23*(05), 727-742. doi:10.2118/10516-pa

Zemel, B. (1995). *Tracers in the oil field* (Vol. 43, Developments in Petroleum Science). Amsterdam: Elsevier.